Received: Added at production | Revised: Added at production | Accepted: Added at production

DOI: xxx/xxxx

RESEARCH ARTICLE

A variational method for analysis of laminates with parallel arrays of intralaminar cracks

Vladimir Vinogradov

School of Engineering,
Newcastle University,
Newcastle upon Tyne, NE1 7RU, U.K.,
Email: v.vinogradov@ncl.ac.uk

The paper presents a robust variational method for prediction of the effective thermoelastic properties of laminates with parallel, but not necessarily coplanar intralaminar cracks. Arbitrary laminate layup, crack patterns, and any in-plane forces and bending moments and temperature change can be treated simultaneously. The method is based on the principle of minimum complementary energy. The admissible in-plane stress components are assumed to be linear through the ply thickness. Simple matrix expressions are derived for the effective compliance matrix, thermal expansions and curvatures and specific heat of a cracked laminate. Predictions for the Young's modulus, Poisson's ratio, shear modulus, flexural rigidity and thermal expansion as functions of crack density for various laminates of symmetric and non-symmetric layups demonstrated excellent agreement with experimental results of seven independently published studies. Accuracy and robustness of the method are complemented by the fact that no experimentally fitted parameters are required. It is shown that the same formalism can be applied to analysis of closed intralaminar cracks, as well as non-uniform and non-symmetrical distributions of cracks.

KEYWORDS:
Solids, Composites, Damage, Variational methods, Linear Solvers

1 | INTRODUCTION

Matrix cracks in the most off-axis plies are usually regarded as the initial type of damage in both cross-ply and general laminates made of fiber reinforced polymers, when subjected to either quasi-static or cyclic, mechanical or thermal loads. Depending on the laminate layup, cracks can initially develop in inner or outer plies, in a symmetric, staggered or random arrangements. Numerous experimental studies reported that these intralaminar cracks multiply with increasing loading or number of cycles, sequentially capturing plies with different orientations. The intralaminar cracks perturb the stress fields in the laminate, affect its effective properties and trigger initiation of other types of damage, such as delamination, or interlaminar, cracks.

Variational analysis (only the stress-based variational analysis is discussed herein) is an accurate analytical method to estimate effective elastic properties of a cracked laminate. The method was originated by Hashin [1], who derived very simple expressions for the effective Young's and shear moduli of a symmetric cross-ply laminate $[0/90]_S$ with the cracked transverse ply. Analysis was based on construction of an admissible stress field within a cracked laminate that satisfies equilibrium, continuity of traction at the interfaces between plies and zero tractions at the external unloaded surfaces of the laminate, as well as on the open crack surfaces, but does not satisfy compatibility conditions. Assumptions that allowed to construct the admissible stress field comprised of the axial stress, in case of longitudinal tension, and the shear stress, in case of in-plane shear loading, being solely

functions of the coordinate in the 0° direction perpendicular to the crack planes, while these functions were determined using the principle of minimum complementary energy. Consequently, the Young's and shear moduli predicted by the method represent the lower bounds, meaning that the exact solution of the elastic problem should lead to higher values of the stiffness parameters. Hashin[2] was also able to extend the original analysis to cross-plies containing symmetric intralaminar cracks in both the middle and outer plies.

The method has been extensively and quite successfully used in conjunction with energy based fracture criteria, both deterministic and probabilistic, to describe progressive transverse cracking in cross-ply laminates with loading[3–5]. There has been considerable interest in recent years in improving its accuracy and generalization for more complex layups.

One of the first extensions of the approach was performed by Nairn and Hu[6], who looked at the effect of staggered arrangement of cracks in the outer plies of cross-ply $[90/0]_S$ laminates under tension on the effective Young's modulus and the energy release rates. The original assumption for the in-plane stresses was employed, which required subdivision of the middle uncracked ply into two sub-plies in order to maintain force and moment equilibrium. Vinogradov and Hashin[7] considered an angle ply laminate with a generic layup of $[\theta_m^{(1)}/\theta_n^{(2)}]_S$ containing cracks in the middle ply and derived closed form expressions for the laminate effective compliance matrix. Prediction for the Young's modulus deterioration as a function of crack density was found in excellent agreement with experimental results of Katerelos et al.[8] for GFRP $[0/45]_S$. Li and Hafeez[9] looked at a general symmetric cross-ply with symmetric periodic arrangement of transverse cracks and introduced the requirement of natural boundary conditions in case physical boundary conditions (zero traction on crack surfaces) and periodicity conditions do not suffice. Several publications followed this approach, keeping the Hashin's assumption of the in-plane stresses being independent of the transverse direction within each ply (e.g. Hajikazemi et al.[10,11]). It is worth noticing that comparison of the variational analysis applied to symmetric laminates assuming piecewise constant in-plane perturbation stress with results of the Generalized Plane Strain approach of McCartney (see, e.g. McCartney[12] and references therein), performed recently by Hajikazemi and McCartney[13], demonstrated almost identical results in terms of both stress and displacement fields when sufficient ply refinement was employed.

Giannadakis and Varna[14] and Katerelos et al.[15], in contrast to the papers mentioned above, introduced a through-the-thickness dependence of the in-plane shear stress when studied the effect of transverse cracks on the shear modulus of a symmetric and balanced $[S/90]_S$. A nonlinear addition to the shear stress distribution was assumed in the outer 'homogenized' sub-laminate. It was shown that the non-uniform (exponential) distribution of the shear stress in the outer plies brings the results for the effective shear modulus closer to FE predictions than the original piecewise constant distribution.

In the paper by Kuriakose and Talreja[16] simple cross-plies ($[0/90]_S$ and $[90/0]_S$) were subjected to bending, and naturally, a linear stress distribution with thickness was introduced. Hajikazemi et al.[17,18] (whose approach is the closest to the one developed in the present paper) considered a generic cross-ply under arbitrary in-plane forces and bending moments, enhancing the formulation of Li and Hafeez[9] by additional linear through the thickness terms in the distribution of the in-plane stress.

In all studies that adopted the generalized variational approach of Li and Hafeez[9], two inherent steps are present: (1) derivation of natural boundary conditions, whose solution together with physical boundary conditions leads to the stress field in a cracked laminate, and (2) application of specific loading and integration of the resultant stress energy density to evaluate the complementary energy and corresponding compliances of the laminate.

Analysis in the present paper addresses the problem of itralaminar cracks in an general laminate, when cracks are in plies with parallel fiber orientation. An admissible stress field is constructed, Section 2, that has a linear with the thickness distribution of the in-plane stress components for any laminate independently of its layup. The admissible stresses satisfy equilibrium and continuity of tractions at the interfaces between plies. Functions that determine the stress in-plane distributions are obtained by applying the principle of minimum complementary energy, while two alternative ways of treating the minimization problem are suggested. The first approach, described in Section 3 clearly shows that some of the unknown functions are dependent and can be eliminated from the analysis. Both physical and natural boundary conditions are derived for a laminate, whose crack arrays satisfy reflection symmetry, which includes, but is not limited to, periodic symmetric and staggered crack patterns. It is shown that for the problem at hand the step of the energy density integration over the laminate volume can be avoided and the closed form expressions for the energy functional are derived. The alternative approach described in Section 4 uses Lagrange multipliers to take into account the symmetry conditions and boundary conditions for the traction free surfaces. It is shown that this approach leads to a very concise solution, making construction of the natural boundary conditions redundant as well. Closed form matrix expressions for the effective compliance, thermal expansions and specific heat of cracked laminates are presented in Section 5 and the asymptotic behavior at low and high crack densities is discussed in Section 6.

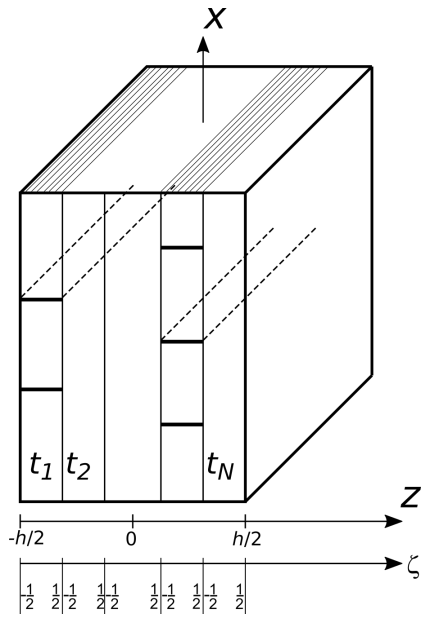

FIGURE 1: Cracked laminate with transverse cracks.

The resultant effective Young's modulus, Poisson's ratio, shear modulus, thermal expansion and flexural rigidity for several laminates are compared to experimental data found in literature; excellent agreement between the model predictions and experimental results are demonstrated in Section 7. In Section 8 several potential extensions/applications of the method are described, namely: improvement of the approximate stress distribution using ply refinement and some compatibility conditions, analysis of fully and partially closed cracks, and analysis of laminates with arbitrary spatial distributions of parallel intralaminar crack.

2 | ADMISSIBLE STRESS FIELD

Consider an N-ply laminate plate under uniform in-plane membrane forces and bending moments and impose an arbitrary state of intralaminar damage in a family of plies defined by a certain fibre orientation θ^*, when the intralaminar cracks are perpendicular to the laminate plane and parallel to the fibre direction θ^*, but not necessarily coplanar. One can then rotate the coordinate system by $(\pi/2 - \theta^*)$ about the out-of-plane z-axis, such that the crack surfaces are normal to the x-axis and the cracked plies become 90° plies (Figure 1). Analysis will be performed in this coordinate system, in which the laminate is subjected to membrane forces N_x, N_y, N_{xy} and bending moments M_x, M_y, M_{xy}.

The compacted index notations of the Classical Laminate Theory will be used. For arbitrary orientation of plies in the laminate and in the case of applied bending moments, when no cracks are present, the in-plane stresses $\sigma_1^{0(m)} \equiv \sigma_{xx}^{0(m)}$, $\sigma_2^{0(m)} \equiv \sigma_{yy}^{0(m)}$ and $\sigma_6^{0(m)} \equiv \sigma_{xy}^{0(m)}$ in any ply (m) are linear function of the transverse coordinate z, which can be evaluated using the classical laminate theory. The rest of the stress tensor components $\sigma_4^0 \equiv \sigma_{yz}^0$, $\sigma_5^0 \equiv \sigma_{xz}^0$ and $\sigma_3^0 \equiv \sigma_{zz}^0$ are equal to zero.

The transverse cracks introduce stress perturbations, which are denoted by $\sigma_i^{(m)}$, where i ranges over 1 to 6, and the total stresses in ply m of the cracked material is given by a superposition of the stresses in the uncracked material (under the same loading) and perturbation stresses due to the presence of the cracks.

$$\sigma_i^{C(m)}(x, z) = \sigma_i^{0(m)}(z) - \sigma_i^{(m)}(x, z). \tag{1}$$

For a cracked laminate subjected to arbitrary membrane forces and bending moments, the total stresses must satisfy the zero traction boundary condition on the open crack surfaces. This implies that the perturbation stresses contributing to the traction vectors in the cracked plies on the crack surfaces must also be linear functions of the z-coordinate.

It is now assumed that the in-plane perturbation stresses $\sigma_1^{(m)}$, $\sigma_2^{(m)}$ and $\sigma_6^{(m)}$ in any ply m are linear functions of z everywhere in the cracked laminate, i.e. for any coordinate x. According to this assumption the in-plane perturbation stresses can be expressed

in the form

$$\sigma_i^{(m)}(\xi,\zeta) = \phi_i^{(m)}(\xi) + \psi_i^{(m)}(\xi)\,\zeta \quad \text{for} \quad i = 1,2,6, \tag{2}$$

where $\xi = x/t_0$ is the dimentionless x-coordinate, t_0 is an arbitrary normalization thickness, which is here taken as thickness of one lamina, ζ is the dimentionless z-coordinate, defined as

$$\zeta = (z - \bar{z}_m)/t_m, \tag{3}$$

and running from $-1/2$ to $1/2$ within each ply (Figure 1). Here t_m is the thickness of ply m and $\bar{z}_m$ is the z-coordinate of the center of the ply. Functions $\phi_i^{(m)}(x)$ and $\psi_i^{(m)}(x)$ represent the average perturbation stresses and their z-gradients, respectively, within the ply.

The resulting stresses must satisfy equilibrium, interface and boundary conditions, forming so-called admissible stress field. Equilibrium differential equations written for the perturbation stresses using the non-dimensional coordinates ξ and ζ read:

$$\begin{aligned}
&\frac{\partial}{\partial\xi}\sigma_1^{(m)}(\xi,\zeta) + \frac{1}{\lambda_m}\frac{\partial}{\partial\zeta}\sigma_5^{(m)}(\xi,\zeta) = 0,\\
&\frac{\partial}{\partial\xi}\sigma_6^{(m)}(\xi,\zeta) + \frac{1}{\lambda_m}\frac{\partial}{\partial\zeta}\sigma_4^{(m)}(\xi,\zeta) = 0,\\
&\frac{\partial}{\partial\xi}\sigma_5^{(m)}(\xi,\zeta) + \frac{1}{\lambda_m}\frac{\partial}{\partial\zeta}\sigma_3^{(m)}(\xi,\zeta) = 0,
\end{aligned} \tag{4}$$

where $\lambda_m = t_m/t_0$ is the normalized thickness of ply m.

Substituting the linear expression (2) for the perturbation into the equilibrium equations (4) and then integrating the equations with respect to ζ one derives the following general expressions for the out-of-plane stresses:

$$\begin{aligned}
\sigma_5^{(m)}(\xi,\zeta) &= -\lambda_m\phi_1'^{(m)}(\xi)\zeta - \lambda_m\psi_1'^{(m)}(\xi)\frac{\zeta^2}{2} + g_5^{(m)}(\xi),\\
\sigma_4^{(m)}(\xi,\zeta) &= -\lambda_m\phi_6'^{(m)}(\xi)\zeta - \lambda_m\psi_6'^{(m)}(\xi)\frac{\zeta^2}{2} + g_4^{(m)}(\xi),\\
\sigma_3^{(m)}(\xi,\zeta) &= \lambda_m^2\phi_1''^{(m)}(\xi)\frac{\zeta^2}{2} + \lambda_m^2\psi_1''^{(m)}(\xi)\frac{\zeta^3}{6} - g_5'^{(m)}(\xi)\zeta + g_3^{(m)}(\xi),
\end{aligned} \tag{5}$$

where $g_3^{(m)}(\xi)$, $g_4^{(m)}(\xi)$ and $g_5^{(m)}(\xi)$ are integration functions. These integration functions can be expressed in terms of the functions $\phi^{(m)}(\xi)$ and $\psi^{(m)}(\xi)$ using the traction-free condition at the external surface of the first ply

$$\sigma_3^{(1)}(\xi,-\tfrac{1}{2}) = \sigma_4^{(1)}(\xi,-\tfrac{1}{2}) = \sigma_5^{(1)}(\xi,-\tfrac{1}{2}) = 0, \tag{6}$$

and traction continuity conditions at the interfaces between plies

$$\begin{aligned}
\sigma_4^{(m)}(\xi,-\tfrac{1}{2}) &= \sigma_4^{(m-1)}(\xi,\tfrac{1}{2}),\\
\sigma_5^{(m)}(\xi,-\tfrac{1}{2}) &= \sigma_5^{(m-1)}(\xi,\tfrac{1}{2}),\\
\sigma_3^{(m)}(\xi,-\tfrac{1}{2}) &= \sigma_3^{(m-1)}(\xi,\tfrac{1}{2}).
\end{aligned} \tag{7}$$

One can start with the external surface of the first ply and iteratively progress toward the opposite external surface to evaluate all the integration functions $g(\xi)$. Equations (6) and (7) applied to $(N-1)$ interfaces between the N plies provide the required constraints. Development of these recursive relations leads to the following rather simple resultant expressions:

$$\sigma_5^{(m)} = -\lambda_m\frac{1}{2}(1+2\zeta)\phi_1'^{(m)} + \lambda_m\frac{1}{8}(1-4\zeta^2)\psi_1'^{(m)} - \sum_{i=1}^{m-1}\lambda_i\phi_1'^{(i)}, \tag{8}$$

$$\sigma_4^{(m)} = -\lambda_m\frac{1}{2}(1+2\zeta)\phi_6'^{(m)} + \lambda_m\frac{1}{8}(1-4\zeta^2)\psi_6'^{(m)} - \sum_{i=1}^{m-1}\lambda_i\phi_6'^{(i)}, \tag{9}$$

$$\begin{aligned}
\sigma_3^{(m)} = {}& \lambda_m^2\frac{1}{8}(1+2\zeta)^2\phi_1''^{(m)} - \lambda_m^2\frac{1}{24}(1+2\zeta)^2(1-\zeta)\psi_1''^{(m)}\\
&+ \frac{1}{2}\sum_{i=1}^{m-1}\lambda_i\left(\lambda_i + 2\sum_{j=i+1}^{m-1}\lambda_j + \lambda_m(1+2\zeta)\right)\phi_1''^{(i)} - \frac{1}{12}\sum_{i=1}^{m-1}\lambda_i^2\psi_1''^{(i)}.
\end{aligned} \tag{10}$$

Similar to equation (6) the traction-free condition on the external surface of the last ply, which is not used in derivation of (8)-(10), reads

$$\sigma_3^{(N)}(\xi,\tfrac{1}{2}) = \sigma_4^{(N)}(\xi,\tfrac{1}{2}) = \sigma_5^{(N)}(\xi,\tfrac{1}{2}) = 0. \tag{11}$$

However, it can be shown that these zero-traction conditions are satisfied automatically if the perturbation membrane forces and moments caused by the perturbation in-plane stresses are equal to zero, meaning that the forces and moments applied to the laminate do not change due to the presence of cracks. This was shown by Li and Hafeez[9] for piece-wise constant in-plane perturbation stresses in a cross-ply. This is also valid in a more general case of any y-independent perturbation stresses as shown in Appendix A. For the perturbation membrane forces the following should hold

$$N_i = \int_{-h/2}^{h/2} \sigma_i dz = 0,$$

which leads to

$$t_0 \sum_{m=1}^{N} \lambda_m \int_{-\frac{1}{2}}^{\frac{1}{2}} \sigma_i^{(m)}(\xi,\zeta)\, d\zeta = 0, \quad \text{for } i = 1,2,6, \tag{12}$$

and for perturbation moments

$$M_i = \int_{-h/2}^{h/2} \sigma_i z\, dz = 0,$$

which in the normalized coordinates reads

$$t_0^2 \sum_{m=1}^{N} \lambda_m^2 \int_{-\frac{1}{2}}^{\frac{1}{2}} \sigma_i^{(m)}(\xi,\zeta) \left(\zeta + \frac{\bar{z}_m}{t_m}\right) d\zeta = 0, \quad \text{for } i = 1,2,6. \tag{13}$$

The ratio $\bar{z}_m/t_m$ can also be written in terms of normalized thicknesses:

$$\frac{\bar{z}_m}{t_m} = \frac{1}{2\lambda_m}\left(\sum_{i=1}^{m-1} \lambda_i - \sum_{i=m+1}^{N} \lambda_i\right).$$

According to the derivation in Appendix A, for (11) to hold, it suffices to set the perturbation forces N_1 and N_6 and perturbation moment M_1 constant, which is part of the more general consideration of force and moment equilibrium (12)-(13).

In to order proceed with the solution, the stresses are now expressed in a matrix form [In this paper bold-face low-case letter refer to column vectors and bold-face capital letters refer to matrices.]

$$\boldsymbol{\sigma}^{(m)}(\xi,\zeta) = \mathbf{A}_0^{(m)}(\zeta)\,\mathbf{f}(\xi) + \mathbf{A}_1^{(m)}(\zeta)\,\mathbf{f}'(\xi) + \mathbf{A}_2^{(m)}(\zeta)\,\mathbf{f}''(\xi), \tag{14}$$

where $\boldsymbol{\sigma} = [\sigma_1, \sigma_2, \sigma_3, \sigma_4, \sigma_5, \sigma_6]^T$ is a (6×1) vector of the stress tensor components, $\mathbf{f}(\xi)$ is a $(6N \times 1)$ vector of all the unknown functions

$$\mathbf{f}(\xi) = [\phi_1^{(1)}, \psi_1^{(1)}, \phi_6^{(1)}, \psi_6^{(1)}, \phi_2^{(1)}, \psi_2^{(1)}, \phi_1^{(2)}, \psi_1^{(2)}, \ldots, \psi_2^{(N)}]^T, \tag{15}$$

and $\mathbf{A}_k^{(m)}$ are $(6 \times 6N)$ matrices of ζ-dependent coefficients of the k-th derivatives of the unknown functions in the stress expressions (2) and (8)-(10). The order of the functions in vector $\mathbf{f}(\xi)$ is arbitrary; it is chosen as presented in (15) due to important contribution of the functions defining σ_1 and σ_6 to the problem solution, as it will be shown later on.

Substitution of (2) into the six constraints in (12) and (13) shows that the constraints are linear in the unknown functions forming $\mathbf{f}$ and after integration over ζ can be written in a matrix form too:

$$\mathbf{B}_{\text{eq}}\,\mathbf{f}(\xi) = 0, \tag{16}$$

where $\mathbf{B}_{\text{eq}}$ is a $(6 \times 6N)$ constant matrix, whose elements are given in Appendix B.

According to the variational approach, employed in the present paper, the unknown functions $\mathbf{f}(\xi)$ are determined from complementary energy minimization. The complementary energy in terms of the perturbation stresses is given as[1]:

$$U_C = U_C^0 + \frac{1}{2}\int_V \boldsymbol{\sigma}^T(\mathbf{x})\mathbf{S}(\mathbf{x})\boldsymbol{\sigma}(\mathbf{x})\, dV, \tag{17}$$

where $\mathcal{U}_C^0$ is the complementary energy of the virgin laminate and $\mathbf{S}(\mathbf{x})$ is the local compliance tensor. Using the non-dimensional coordinates and perturbation stress presentation (14), the energy of a laminate plate of unit width and length L can be written as

$$\begin{aligned}\mathcal{U}_C &= \mathcal{U}_C^0 + \frac{t_0^2}{2}\int_L \sum_{m=1}^{N} \lambda_m \int_{-\frac{1}{2}}^{\frac{1}{2}} \boldsymbol{\sigma}^{(m)T}\mathbf{S}^{(m)}\boldsymbol{\sigma}^{(m)} d\zeta\, d\xi \\ &= \mathcal{U}_C^0 + \frac{t_0^2}{2}\int_L \sum_{p,q=0,1,2} \mathbf{f}^{(p)T}(\xi)\,\mathbf{M}^{pq}\,\mathbf{f}^{(q)}(\xi)\, d\xi,\end{aligned} \tag{18}$$

where $\mathbf{f}^{(p)}(\xi)$ denotes the pth derivative of $\mathbf{f}(\xi)$, $\mathbf{S}^{(m)}$ is the 6×6 compliance matrix of ply m, and

$$\mathbf{M}^{pq} = \sum_{m=1}^{N} \lambda_m \mathbf{P}_{pq}^{(m)}, \qquad \mathbf{P}_{pq}^{(m)} = \int_{-\frac{1}{2}}^{\frac{1}{2}} \mathbf{A}_p^{(m)T}(\zeta)\mathbf{S}^{(m)}\mathbf{A}_q^{(m)}(\zeta)\, d\zeta. \tag{19}$$

Elements of the integrand matrix in (19) represent polynomials of ξ of order up to six and can be calculated numerically with any degree of accuracy. For the sake of completeness, explicit expressions for the nonzero elements of $6N\times 6N$ matrices $\mathbf{P}_{pq}^{(m)}$ are given in Appendix B. It can be seen that for the y-independent perturbation stresses and for monoclinic and higher symmetries of the ply material, the following matrices vanish:

$$\mathbf{P}_{01}^{(m)} = \mathbf{P}_{10}^{(m)} = \mathbf{P}_{12}^{(m)} = \mathbf{P}_{21}^{(m)} = 0.$$

Minimization of the complementary energy reduces to the problem of determining functions $\mathbf{f}$ that minimize the integral in (18):

$$\mathcal{I} = \min_{\mathbf{f}(\xi)} \int_L F(\xi)\, d\xi, \tag{20}$$

with the integrand having the following expanded form

$$F(\xi) = \mathbf{f}^T\,\mathbf{M}^{00}\,\mathbf{f} + \mathbf{f}^T\,\mathbf{M}^{02}\,\mathbf{f}'' + \mathbf{f}''^T\,\mathbf{M}^{20}\,\mathbf{f} + \mathbf{f}'^T\,\mathbf{M}^{11}\,\mathbf{f}' + \mathbf{f}''^T\,\mathbf{M}^{22}\,\mathbf{f}''. \tag{21}$$

and subject to constraints (16) and boundary conditions at the planes of cracks that will be discussed later.

3 | DETAILED SOLUTION

3.1 | Euler-Lagrange equations

The six constraints in (16) can be used to eliminate six unknown functions in (15). A natural choice would be to eliminate 6 unknown functions in one of the plies. It is more convenient to choose an unckracked ply to ease on application of boundary conditions later on. Vector $\mathbf{f}(x)$ can be partitioned in the form $[\mathbf{f}_{\text{ind}}, \mathbf{f}_{\text{dep}}]$ placing first the functions corresponding to the independent plies, followed by the functions corresponding to the dependent ply. For example, for $[\theta^{(1)}/90/\theta^{(3)}]_T$ the last ply can be eliminated from consideration, which for (15) yields $\{\text{ind}\} = \{13, 14, \ldots 18\}$ and $\{\text{dep}\} = \{1, 2, \ldots 12\}$. Constraints (16) can then be written as

$$(\mathbf{B}_{\text{eq}})_{\text{ind}}\mathbf{f}_{\text{ind}} + (\mathbf{B}_{\text{eq}})_{\text{dep}}\mathbf{f}_{\text{dep}} = 0, \tag{22}$$

where $(\mathbf{B}_{\text{eq}})_{\text{ind}}$ is a 6×6 matrix and the subscript index denotes $\{\text{ind}\}$ columns of $\mathbf{B}_{\text{eq}}$. This is now solved for $\mathbf{f}_{\text{dep}}$:

$$\mathbf{f}_{\text{dep}} = -(\mathbf{B}_{\text{eq}})_{\text{dep}}^{-1}(\mathbf{B}_{\text{eq}})_{\text{ind}}\mathbf{f}_{\text{ind}}. \tag{23}$$

The functional (21) is then rewritten in terms of $\mathbf{f}_{\text{ind}}$, while matrices $\mathbf{M}^{pq}$ reduce their size to $6(N-1)\times 6(N-1)$:

$$\widetilde{\mathbf{M}}^{pq} = \begin{bmatrix} \mathbf{I} \\ -(\mathbf{B}_{\text{eq}})_{\text{dep}}^{-1}(\mathbf{B}_{\text{eq}})_{\text{ind}} \end{bmatrix}^T \begin{bmatrix} \mathbf{M}_{\text{ind,ind}}^{pq} & \mathbf{M}_{\text{ind,dep}}^{pq} \\ \mathbf{M}_{\text{dep,ind}}^{pq} & \mathbf{M}_{\text{dep,dep}}^{pq} \end{bmatrix} \begin{bmatrix} \mathbf{I} \\ -(\mathbf{B}_{\text{eq}})_{\text{dep}}^{-1}(\mathbf{B}_{\text{eq}})_{\text{ind}} \end{bmatrix}, \quad p,q = 0,1,2, \tag{24}$$

where $\mathbf{I}$ is the identity matrix of rank $6(N-1)$ and the matrix in the middle of the expression is the partitioned matrix $\mathbf{M}^{pq}$, in which the first subscript index refers to rows and the index after comma refers to columns. Lagrangian (21) becomes

$$F = \mathbf{f}_{\text{ind}}^T\,\widetilde{\mathbf{M}}^{00}\,\mathbf{f}_{\text{ind}} + \mathbf{f}_{\text{ind}}^T\,\widetilde{\mathbf{M}}^{02}\,\mathbf{f}_{\text{ind}}'' + \mathbf{f}_{\text{ind}}''^T\,\widetilde{\mathbf{M}}^{20}\,\mathbf{f}_{\text{ind}} + \mathbf{f}_{\text{ind}}'^T\,\widetilde{\mathbf{M}}^{11}\,\mathbf{f}_{\text{ind}}' + \mathbf{f}_{\text{ind}}''^T\,\widetilde{\mathbf{M}}^{22}\,\mathbf{f}_{\text{ind}}''. \tag{25}$$

The matrix $\widetilde{\mathbf{M}}^{00}$ is in general a full rank matrix. The other matrices in (25), however, demonstrate a simple sparse structure if the function vector $\mathbf{f}_{\text{ind}}$ is partitioned again, placing its elements in the following order: first functions corresponding to σ_1 in all the plies, then σ_6 and then σ_2. Let us denote the list of independent functions defining σ_1, σ_6 and σ_2 by α, β and γ, respectively. For instance, for $[\theta^{(1)}/90/\theta^{(3)}]_{\text{T}}$ after eliminating the last dependent ply $\alpha = \{1,2,7,8\}$, $\beta = \{3,4,9,10\}$ and $\gamma = \{5,6,11,12\}$. The partitioned matrices $\widetilde{\mathbf{M}}$ demonstrate the following structure:

$$\widetilde{\mathbf{M}}^{20} = \begin{bmatrix} \widetilde{\mathbf{M}}^{20}_{\alpha,\alpha} & \widetilde{\mathbf{M}}^{20}_{\alpha,\beta} & \widetilde{\mathbf{M}}^{20}_{\alpha,\gamma} \\ \mathbf{0} & \mathbf{0} & \mathbf{0} \\ \mathbf{0} & \mathbf{0} & \mathbf{0} \end{bmatrix}, \qquad \widetilde{\mathbf{M}}^{11} = \begin{bmatrix} \widetilde{\mathbf{M}}^{11}_{\alpha,\alpha} & \widetilde{\mathbf{M}}^{11}_{\alpha,\beta} & \mathbf{0} \\ \widetilde{\mathbf{M}}^{11}_{\beta,\alpha} & \widetilde{\mathbf{M}}^{11}_{\beta,\beta} & \mathbf{0} \\ \mathbf{0} & \mathbf{0} & \mathbf{0} \end{bmatrix},$$

$$\widetilde{\mathbf{M}}^{02} = (\widetilde{\mathbf{M}}^{20})^T = \begin{bmatrix} \widetilde{\mathbf{M}}^{02}_{\alpha,\alpha} & \mathbf{0} & \mathbf{0} \\ \widetilde{\mathbf{M}}^{02}_{\beta,\alpha} & \mathbf{0} & \mathbf{0} \\ \widetilde{\mathbf{M}}^{02}_{\gamma,\alpha} & \mathbf{0} & \mathbf{0} \end{bmatrix}, \qquad \widetilde{\mathbf{M}}^{22} = \begin{bmatrix} \widetilde{\mathbf{M}}^{22}_{\alpha,\alpha} & \mathbf{0} & \mathbf{0} \\ \mathbf{0} & \mathbf{0} & \mathbf{0} \\ \mathbf{0} & \mathbf{0} & \mathbf{0} \end{bmatrix}.$$

The above matrix structures are independent of the laminate layup and hold for monoclinic and higher symmetries of the ply material.

The next step in the variational solution is to derive the Euler-Lagrange equations, which for the Lagrangian (25) are

$$\frac{\partial F}{\partial \mathbf{f}} - \frac{d}{dx}\frac{\partial F}{\partial \mathbf{f}'} + \frac{d^2}{dx^2}\frac{\partial F}{\partial \mathbf{f}''} = 0. \tag{26}$$

It can be noticed that no derivatives of functions $\mathbf{f}_\gamma$ are present in the functional. This is due to the fact that the axial stresses σ_2 do not contribute to the construction of the admissible perturbation stress field through integration of the differential equilibrium equations. The Euler-Lagrange equations for functions $\mathbf{f}_\gamma$ obtain the form:

$$\widehat{\mathbf{M}}^{00}_{\gamma,\alpha}\mathbf{f}_\alpha + \widehat{\mathbf{M}}^{00}_{\gamma,\beta}\mathbf{f}_\beta + \widehat{\mathbf{M}}^{00}_{\gamma,\gamma}\mathbf{f}_\gamma + \widetilde{\mathbf{M}}^{02}_{\gamma,\alpha}\mathbf{f}''_\alpha = 0. \tag{27}$$

This matrix equation can be solved for $\mathbf{f}_\gamma$ to eliminate all the functions that define the stress σ_2:

$$\mathbf{f}_\gamma = -(\widetilde{\mathbf{M}}^{00}_{\gamma,\gamma})^{-1}\left(\widetilde{\mathbf{M}}^{00}_{\gamma,\alpha}\mathbf{f}_\alpha + \widetilde{\mathbf{M}}^{00}_{\gamma,\beta}\mathbf{f}_\beta\right) - (\widetilde{\mathbf{M}}^{00}_{\gamma,\gamma})^{-1}\widetilde{\mathbf{M}}^{02}_{\gamma,\alpha}\mathbf{f}''_\alpha. \tag{28}$$

The Lagrangian can now be expressed in terms of $\mathbf{f}_{\alpha\beta}$ only ($\mathbf{f}_{\alpha\beta}$ denotes the joined array of α and β functions):

$$F = \mathbf{f}^T_{\alpha\beta}\widehat{\mathbf{M}}^{00}_{\alpha\beta,\alpha\beta}\mathbf{f}_{\alpha\beta} + \mathbf{f}'^T_{\alpha\beta}\widehat{\mathbf{M}}^{11}_{\alpha\beta,\alpha\beta}\mathbf{f}'_{\alpha\beta} + \mathbf{f}^T_{\alpha\beta}\widehat{\mathbf{M}}^{02}_{\alpha\beta,\alpha}\mathbf{f}''_\alpha + \mathbf{f}''^T_\alpha\widehat{\mathbf{M}}^{20}_{\alpha,\alpha\beta}\mathbf{f}_{\alpha\beta} + \mathbf{f}''^T_\alpha\widehat{\mathbf{M}}^{22}_{\alpha,\alpha}\mathbf{f}''_\alpha, \tag{29}$$

where

$$\widehat{\mathbf{M}}^{kl}_{i,j} = \widetilde{\mathbf{M}}^{kl}_{i,j} - \widetilde{\mathbf{M}}^{k0}_{i,\gamma}(\widetilde{\mathbf{M}}^{00}_{\gamma,\gamma})^{-1}\widetilde{\mathbf{M}}^{0l}_{\gamma,j}, \quad i,j = \alpha,\beta \quad \text{and} \quad k,l = 0,2,$$
$$\widehat{\mathbf{M}}^{11}_{i,j} = \widetilde{\mathbf{M}}^{11}_{i,j}, \quad i,j = \alpha,\beta.$$

The Euler-Lagrange equations for the independent functions $\mathbf{f}_\alpha$ and $\mathbf{f}_\beta$ become:

$$\begin{bmatrix} \widehat{\mathbf{M}}^{00}_{\alpha,\alpha} & \widehat{\mathbf{M}}^{00}_{\alpha,\beta} \\ \widehat{\mathbf{M}}^{00}_{\beta,\alpha} & \widehat{\mathbf{M}}^{00}_{\beta,\beta} \end{bmatrix}\begin{bmatrix} \mathbf{f}_\alpha \\ \mathbf{f}_\beta \end{bmatrix} + \begin{bmatrix} \widehat{\mathbf{M}}^{02}_{\alpha,\alpha} + \widehat{\mathbf{M}}^{20}_{\alpha,\alpha} - \widehat{\mathbf{M}}^{11}_{\alpha,\alpha} & \widehat{\mathbf{M}}^{20}_{\alpha,\beta} - \widehat{\mathbf{M}}^{11}_{\alpha,\beta} \\ \widehat{\mathbf{M}}^{02}_{\beta,\alpha} - \widehat{\mathbf{M}}^{11}_{\beta,\alpha} & -\widehat{\mathbf{M}}^{11}_{\beta,\beta} \end{bmatrix}\begin{bmatrix} \mathbf{f}''_\alpha \\ \mathbf{f}''_\beta \end{bmatrix} + \begin{bmatrix} \widehat{\mathbf{M}}^{22}_{\alpha,\alpha} & \mathbf{0} \\ \mathbf{0} & \mathbf{0} \end{bmatrix}\begin{bmatrix} \mathbf{f}^{(\text{iv})}_\alpha \\ \mathbf{f}^{(\text{iv})}_\beta \end{bmatrix} = 0. \tag{30}$$

From the second row of equations one can express the second derivative $\mathbf{f}''_\beta$, substitute it in the first row and express the forth derivative $\mathbf{f}^{(\text{iv})}_\alpha$. The result is now augmented by identity $\mathbf{f}''_\alpha = \mathbf{I}\,\mathbf{f}''_\alpha$ and presented as

$$\begin{bmatrix} \mathbf{0} & \mathbf{0} & \mathbf{I} \\ \mathbf{E}_{21} & \mathbf{E}_{22} & \mathbf{E}_{23} \\ \mathbf{E}_{31} & \mathbf{E}_{32} & \mathbf{E}_{33} \end{bmatrix}\begin{bmatrix} \mathbf{f}_\alpha \\ \mathbf{f}_\beta \\ \mathbf{f}''_\alpha \end{bmatrix} = \begin{bmatrix} \mathbf{f}''_\alpha \\ \mathbf{f}''_\beta \\ \mathbf{f}^{(\text{iv})}_\alpha \end{bmatrix}, \tag{31}$$

where

$$
\begin{aligned}
\mathbf{E}_{21} &= (\widehat{\mathbf{M}}^{11}_{\beta,\beta})^{-1}\widehat{\mathbf{M}}^{00}_{\beta,\alpha},\\
\mathbf{E}_{22} &= (\widehat{\mathbf{M}}^{11}_{\beta,\beta})^{-1}\widehat{\mathbf{M}}^{00}_{\beta,\beta},\\
\mathbf{E}_{23} &= (\widehat{\mathbf{M}}^{11}_{\beta,\beta})^{-1}(\widehat{\mathbf{M}}^{02}_{\beta,\alpha} - \widehat{\mathbf{M}}^{11}_{\beta,\alpha}),\\
\mathbf{E}_{31} &= -(\widehat{\mathbf{M}}^{22}_{\alpha,\alpha})^{-1}\left(\widehat{\mathbf{M}}^{00}_{\alpha,\alpha} + (\widehat{\mathbf{M}}^{20}_{\alpha,\beta} - \widehat{\mathbf{M}}^{11}_{\alpha,\beta})(\widehat{\mathbf{M}}^{11}_{\beta,\beta})^{-1}\widehat{\mathbf{M}}^{00}_{\beta,\alpha}\right),\\
\mathbf{E}_{32} &= -(\widehat{\mathbf{M}}^{22}_{\alpha,\alpha})^{-1}\left(\widehat{\mathbf{M}}^{00}_{\alpha,\beta} + (\widehat{\mathbf{M}}^{20}_{\alpha,\beta} - \widehat{\mathbf{M}}^{11}_{\alpha,\beta})(\widehat{\mathbf{M}}^{11}_{\beta,\beta})^{-1}\widehat{\mathbf{M}}^{00}_{\beta,\beta}\right),\\
\mathbf{E}_{33} &= -(\widehat{\mathbf{M}}^{22}_{\alpha,\alpha})^{-1}\left(\widehat{\mathbf{M}}^{02}_{\alpha,\alpha} + \widehat{\mathbf{M}}^{20}_{\alpha,\alpha} - \widehat{\mathbf{M}}^{11}_{\alpha,\alpha} + (\widehat{\mathbf{M}}^{20}_{\alpha,\beta} - \widehat{\mathbf{M}}^{11}_{\alpha,\beta})(\widehat{\mathbf{M}}^{11}_{\beta,\beta})^{-1}(\widehat{\mathbf{M}}^{02}_{\beta,\alpha} - \widehat{\mathbf{M}}^{11}_{\beta,\alpha})\right).
\end{aligned}
$$

The system of $6(N-1)$ homogeneous ordinary differential equations with constant coefficients (31) can be written in short as

$$
\begin{bmatrix} \mathbf{f}''_{\alpha\beta} \\ \mathbf{f}^{(\mathrm{iv})}_{\alpha} \end{bmatrix} = \mathbf{E} \begin{bmatrix} \mathbf{f}_{\alpha\beta} \\ \mathbf{f}''_{\alpha} \end{bmatrix}. \tag{32}
$$

The standard case when matrix $\mathbf{E}$ is *diagonalizable* implies (32) reduces to the following standard eigenproblem:

$$
\left(\mathbf{E} - r^2\mathbf{I}\right) \begin{bmatrix} \mathbf{f}_{\alpha\beta} \\ \mathbf{f}''_{\alpha} \end{bmatrix} = 0. \tag{33}
$$

Eigenproblem (33) can easily be solved numerically for its eigenvalues and corresponding eigenvectors using standard techniques implemented in either commercial software packages or open source subroutines. As one can observe from the dimensions of the above matrices, the system has $6(N-1)$ eigenvalues for r_i^2 and correspondingly $12(N-1)$ values for $r_i = \pm\sqrt{r_i^2}$. The general solution can be written as

$$
\mathbf{f}_{\alpha\beta} = \sum_i \mathbf{v}_i \exp(r_i\xi)\, c_i = \mathbf{U}(\xi)\, \mathbf{c}, \tag{34}
$$

where

$$
\mathbf{U}(\xi) = [\mathbf{v}_1 e^{r_1\xi}, \mathbf{v}_2 e^{r_2\xi}, \ldots, \mathbf{v}_1 e^{-r_1\xi}, \mathbf{v}_2 e^{-r_2\xi}, \ldots] \tag{35}
$$

is a $4(N-1)\times 12(N-1)$ rectangular matrix, $\mathbf{v}_i$ are column eigenvectors associated with eigenvalue r_i^2 of matrix $\mathbf{E}$, and $\mathbf{c}$ is a $12(N-1)$-element column vector of constant (complex) coefficients yet to be determined. It is convenient to write the matrix of the general solution $\mathbf{U}(\xi)$ in the form:

$$
\mathbf{U}(\xi) = \mathbf{V}\left[\mathbf{\Lambda}^{+}(\xi),\ \mathbf{\Lambda}^{-}(\xi)\right], \tag{36}
$$

where $\mathbf{V} = [\mathbf{v}_1, \mathbf{v}_2, \ldots, \mathbf{v}_{6(N-1)}]$ is the matrix of eigenvectors. The diagonal matrices of eigenfunctions $\mathbf{\Lambda}^{+}$ and $\mathbf{\Lambda}^{-}$ can be chosen in various ways, for instance,

$$
\begin{aligned}
\mathbf{\Lambda}^{+}(\xi) &= \exp(\mathbf{\Lambda}_0\xi),\\
\mathbf{\Lambda}^{-}(\xi) &= \exp(-\mathbf{\Lambda}_0\xi),
\end{aligned} \tag{37}
$$

where $\mathbf{\Lambda}_0 = \mathrm{diag}(\mathbf{r}_{\mathrm{eig}})$, and $\mathbf{r}_{\mathrm{eig}} = [r_1, r_2, \ldots, r_{6(N-1)}]$ is the vector of eigenvalues ($r_i = +\sqrt{r_i^2}$). An alternative form could be:

$$
\begin{aligned}
\mathbf{\Lambda}^{+}(\xi) &= \exp(\mathbf{\Lambda}_0\xi) + \exp(-\mathbf{\Lambda}_0\xi),\\
\mathbf{\Lambda}^{-}(\xi) &= \exp(\mathbf{\Lambda}_0\xi) - \exp(-\mathbf{\Lambda}_0\xi),
\end{aligned} \tag{38}
$$

which clearly indicates that the solution can be written as a superposition of hyperbolic cosines and sines for real eigenvalues and a cross product of hyperbolic and trigonometric cosines and sines for complex eigenvalues, similar to how it was presented in Vinogradov and Hashin[7] for $[\theta/90]_{\mathrm{S}}$.

In Li et al.[19] a variational problem for transversely cracked laminates is formulated in terms of perturbation displacements, leading to a system of second order linear differential equations. The authors pointed out the possibility of having 'defective' eigenvalues in the associated eigenvalue problem and briefly discussed related computational difficulties. Independently on whether matrix $\mathbf{E}$ is diagonalizable or *non-diagonalizable* (when the geometric multiplicity of one or several defective eigenvalues is smaller than the algebraic one, so that the matrix has less than $6(N-1)$ linearly independent eigenvectors), one can write the solution of (31) employing the Schur decomposition of $\mathbf{E}$ in the form

$$
\mathbf{E} = \mathbf{Q}\mathbf{T}\mathbf{Q}^{*}, \tag{39}
$$

where $\mathbf{Q}$ is a unitary matrix, $\mathbf{T}$ is an upper-triangular matrix having the eigenvalues of $\mathbf{E}$ on its main diagonal, and the asterisk denotes conjugate (Hermitian) transpose (also $\mathbf{Q}^{-1} = \mathbf{Q}^*$). The general solution can still be written as

$$\mathbf{f}_{\alpha\beta} = \mathbf{U}(\xi)\mathbf{c} = \mathbf{V}\left[\mathbf{\Lambda}^+(\xi), \mathbf{\Lambda}^-(\xi)\right]\mathbf{c}, \tag{40}$$

where matrix $\mathbf{V}$ is now defined as $\mathbf{V} = \mathbf{Q}_{\alpha\beta}$ (rows of $\mathbf{Q}$ corresponding to functions $\mathbf{f}_{\alpha\beta}$) and the matrix of eigenvalues is replaced with $\mathbf{\Lambda}_0 = \sqrt{\mathbf{T}}$. Procedures for computing the Schur decomposition, matrix (principle) square root, and matrix exponential in (37) or (38) are standard and implemented in any numerical linear algebra package. At the same time, one should expect increased computation times in comparison with the eigenvalue decomposition of the diagonalizable case, where calculation of $\mathbf{U}(\xi)$ only requires evaluation of scalar exponential functions.

It should be noted, however, that the case of repeated eigenvalues and the non-diagonalizable case, in particular, is unlikely to occur (and has never been observed in numerous simulations, including those presented in Sections 7-8), since this would require a very special combination of the material elastic moduli and ply thicknesses, when some of these parameters might need to be either irrational (which would not be a typical input data format) or physically not feasible. In the very unlikely case of a defective eigenvalue, and in view of the fact that the method provides an approximate solution of the elasticity problem, it might be more efficient to split all or some of the plies into subplies keeping the parent fiber orientations or alter the existing ply subdivision, which would separate the eigenvalues (ply refinement is demonstrated in Section 8.1).

Solution (34) requires $12(N-1)$ boundary conditions to determine the constant coefficients c_i.

3.2 | Boundary conditions

In this section crack arrangements will be considered that satisfy mirror reflection symmetry, for which the cracked laminate can be reconstructed by reflecting a single fragment bounded by two adjacent cracks about each crack plane. Examples of such arrangements can be seen in Figure 2a-d, where each dashed line represents a symmetry plane. It can be seen that reflection symmetry implies that the symmetry planes are uniformly distributed along the laminate and cracks in each cracked ply are equally spaced. These symmetry requirements, although lead to some loss of generality, do allow to treat various crack patterns, including but not limited to periodic symmetrically aligned and/or staggered cracks, which often suffice for estimation of the effective laminate properties. In any of the schemes presented in Figure 2a-d elastic energy stored in one fragment between two adjacent planes of symmetry will be equal to energy stored in any other fragment. Thus, it suffices to minimize the complementary energy in a single fragment (unit cell) using appropriate stress boundary conditions at the crack planes that implement the described type of symmetry. The problem, therefore, is restricted to a fragment of normalized length $2\xi_0$ bounded by two adjacent symmetry planes at ξ_0 and $-\xi_0$, while the cracks at ξ_0 and $-\xi_0$ are not necessarily within the same plies (e.g., as in Figures 2c and 2d).

The general case, shown in Figure 2e, will be discussed in Section 8.

3.2.1 | Physical BC

Physical boundary conditions are constructed using information about tractions in the planes containing cracks. Let α^{c} and α^{u} denote the indexes of α functions that belong to the cracked and uncracked plies, and α_+ and α_- those that belong to the surfaces $+\xi_0$ and $-\xi_0$, respectively. Similarly, N_+^c and N_-^c refer to the number of cracked plies at $+\xi_0$ and $-\xi_0$, and $N_+^u = N - N_+^c$ and $N_-^u = N - N_-^c$ refer to the number of uncracked plies at $+\xi_0$ and $-\xi_0$, respectively.

The traction free conditions on the open crack surfaces assume the following constraints for the perturbation in-plane stresses:

$$\sigma_1^{(m_{\mathrm{cr}})}(\pm\xi_0) + \sigma_1^{0(m_{\mathrm{cr}})} = 0, \qquad \sigma_6^{(m_{\mathrm{cr}})}(\pm\xi_0) + \sigma_6^{0(m_{\mathrm{cr}})} = 0, \tag{41}$$

which in terms of the unknown functions becomes

$$\mathbf{f}_{\alpha_\pm^{\mathrm{c}}\beta_\pm^{\mathrm{c}}}(\pm\xi_0) = \mathbf{f}^0_{\alpha_\pm^{\mathrm{c}}\beta_\pm^{\mathrm{c}}}. \tag{42}$$

Here the right-hand side represents the average and gradients of stresses $\sigma_1^{0(m_{cr})}$ and $\sigma_6^{0(m_{cr})}$ in the virgin laminate within plies that contain cracks, determined by the Classical Laminate Theory (see also Appendix D). Using the general solution of the

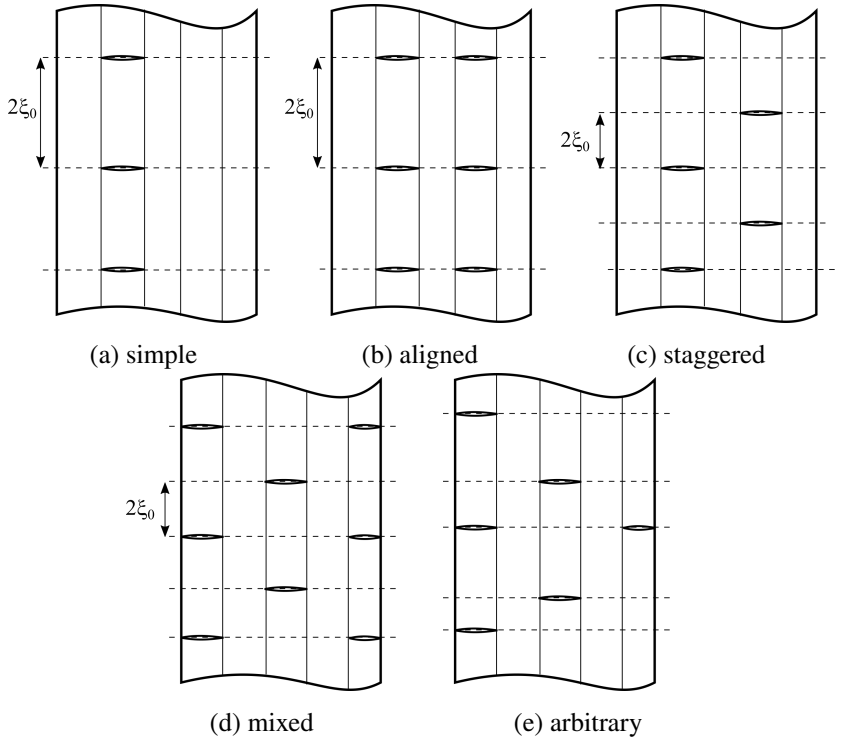

FIGURE 2: Schematic presentation of cracking patterns with reflection symmetry (a)-(d) and arbitrary distribution of cracks (e).

Euler-Lagrange equations (34) these boundary conditions can be written as

$$\begin{bmatrix} \mathbf{U}_{\alpha_+^c}(+\xi_0) \\ \mathbf{U}_{\beta_+^c}(+\xi_0) \\ \mathbf{U}_{\alpha_-^c}(-\xi_0) \\ \mathbf{U}_{\beta_-^c}(-\xi_0) \end{bmatrix} \mathbf{c} = \begin{bmatrix} \mathbf{f}^0_{\alpha_+^c} \\ \mathbf{f}^0_{\beta_+^c} \\ \mathbf{f}^0_{\alpha_-^c} \\ \mathbf{f}^0_{\beta_-^c} \end{bmatrix}. \tag{43}$$

Conditions (43) contain $4(N_+^c + N_-^c)$ equations.

Reflection symmetry implies that the shear stress $\sigma_5^{(m)}$ vanishes in every ply at $\pm\xi_0$, not only on the open crack surfaces:

$$\sigma_5(\pm\xi_0) = 0. \tag{44}$$

To keep the boundary conditions linearly independent, only independent plies should be taken into account and the shear stress in the eliminated ply will automatically vanish due to constraint (16) applied earlier. In terms of the unknown functions this becomes

$$\mathbf{f}'_\alpha(\pm\xi_0) = 0, \tag{45}$$

which represents $4(N-1)$ equations:

$$\begin{bmatrix} \mathbf{U}'_\alpha(+\xi_0) \\ \mathbf{U}'_\alpha(-\xi_0) \end{bmatrix} \mathbf{c} = 0. \tag{46}$$

Appending (46) to (43) yields a system of physical boundary conditions that can be written in the form:

$$\mathbf{B}_{\text{bc}}\mathbf{c} = \mathbf{b}. \tag{47}$$

3.2.2 | Natural BC

Similar to what was demonstrated by Li and Hafeez[9], the physical boundary conditions are generally insufficient to determine the unknown constants and so-called 'natural boundary conditions' are required, which in the variational calculus result from

integration by parts of the perturbed functional. For the quadratic Lagrangian (29) these natural boundary conditions are given by

$$\frac{dF}{d\mathbf{f}'} - \frac{d}{d\xi}\frac{dF}{d\mathbf{f}''} = 0, \quad \text{at} \quad \xi = \pm\xi_0, \tag{48}$$

and

$$\frac{dF}{d\mathbf{f}''} = 0, \quad \text{at} \quad \xi = \pm\xi_0. \tag{49}$$

The first natural boundary condition should be evaluated for the functions, whose values are unknown at $\pm\xi_0$, i.e. those α and β functions that define stresses in the independent uncracked plies. The second natural boundary condition applies to functions, whose derivatives are unknown at $\pm\xi_0$, namely $\mathbf{f}_\beta$, since the first derivatives of $\mathbf{f}_\alpha$ vanish at the crack planes due to symmetry conditions (45). However the energy functional does not involve the second derivatives of $\mathbf{f}''_\beta$, therefore only the first natural boundary condition survives.

For $2(N^u_+ + N^u_- - 2)$ independent functions $\mathbf{f}_{\alpha^u}$ equation (48) reads:

$$\left(\widehat{\mathbf{M}}^{11}_{\alpha^{\mathrm{u}}_\pm,\alpha\beta} - \widehat{\mathbf{M}}^{20}_{\alpha^{\mathrm{u}}_\pm,\alpha\beta}\right)\mathbf{f}'_{\alpha\beta} - \widehat{\mathbf{M}}^{22}_{\alpha^{\mathrm{u}}_\pm,\alpha}\mathbf{f}'''_\alpha = 0, \quad \text{at} \ \pm\xi_0, \tag{50}$$

which in view of (45) reduces to

$$\left(\widehat{\mathbf{M}}^{11}_{\alpha^{\mathrm{u}}_\pm,\beta} - \widehat{\mathbf{M}}^{20}_{\alpha^{\mathrm{u}}_\pm,\beta}\right)\mathbf{f}'_{\beta} - \widehat{\mathbf{M}}^{22}_{\alpha^{\mathrm{u}}_\pm,\alpha}\mathbf{f}'''_\alpha = 0, \quad \text{at} \ \pm\xi_0. \tag{51}$$

For functions $\mathbf{f}_{\beta^{\mathrm{u}}}$ the natural boundary conditions (48) reduce to $2(N^u_+ + N^u_- - 2)$ equations:

$$\frac{dF}{d\mathbf{f}'_{\beta^u_\pm}} = 0, \quad \text{at} \ \pm\xi_0,$$

which after evaluating the derivatives become

$$\widehat{\mathbf{M}}^{11}_{\beta^{\mathrm{u}}_\pm,\alpha\beta}\mathbf{f}'_{\alpha\beta} = 0, \quad \text{at} \ \pm\xi_0, \tag{52}$$

and again in view of reflection symmetry (45)

$$\widehat{\mathbf{M}}^{11}_{\beta^{\mathrm{u}}_\pm,\beta}\mathbf{f}'_{\beta} = 0, \quad \text{at} \ \pm\xi_0. \tag{53}$$

Boundary conditions (51) and (53) complement the physical boundary conditions (43) and (46) and form together $12(N-1)$ equations for the vector of unknown coefficients $\mathbf{c}$. It should be noticed that since different plies can be cracked at $+\xi_0$ and $-\xi_0$ the natural boundary equations are written for different functions at these locations. For instance, (53) should be interpreted as

$$\widehat{\mathbf{M}}^{11}_{\beta^{\mathrm{u}}_+,\beta}\mathbf{f}'_{\beta} = 0, \quad \text{at} \ +\xi_0,$$
$$\widehat{\mathbf{M}}^{11}_{\beta^{\mathrm{u}}_-,\beta}\mathbf{f}'_{\beta} = 0, \quad \text{at} \ -\xi_0.$$

Li and Hafeez[9] suggested a slightly different set of natural boundary conditions: since they considered only periodic and aligned crack arrangement, periodicity for tractions and natural boundary conditions was imposed. The present formulation allows for any crack pattern, i.e. cracks in any plies at $+\xi_0$ and $-\xi$ independently; the resultant stress field automatically becomes symmetric (about the central yz plane of the fragment) in case of symmetric geometry.

3.3 | Evaluation of the minimum complementary energy

The resultant stress field can be substituted into the energy functional and integrated over the volume of a fragment. In order to derive a simple expression for the minimum complementary energy, one can multiply the equations in the first row of the Euler-Largange equation (30) by $\mathbf{f}^T_\alpha$, the second row by $\mathbf{f}^T_\beta$, combine the results and integrate from $-\xi_0$ to ξ_0:

$$\int_{-\xi_0}^{\xi_0}\left[\mathbf{f}^T_{\alpha\beta}\widehat{\mathbf{M}}^{00}_{\alpha\beta,\alpha\beta}\mathbf{f}_{\alpha\beta} + \mathbf{f}^T_{\alpha\beta}\widehat{\mathbf{M}}^{02}_{\alpha\beta,\alpha}\mathbf{f}''_\alpha + \mathbf{f}^T_\alpha\widehat{\mathbf{M}}^{20}_{\alpha,\alpha\beta}\mathbf{f}''_{\alpha\beta} - \mathbf{f}^T_{\alpha\beta}\widehat{\mathbf{M}}^{11}_{\alpha\beta,\alpha\beta}\mathbf{f}''_{\alpha\beta} + \mathbf{f}^T_\alpha\widehat{\mathbf{M}}^{22}_{\alpha,\alpha}\mathbf{f}^{(\mathrm{iv})}_\alpha\right]d\xi = 0. \tag{54}$$

The fourth term is now integrated by parts:

$$-\int_{-\xi_0}^{\xi_0}\mathbf{f}^T_{\alpha\beta}\widehat{\mathbf{M}}^{11}_{\alpha\beta}\mathbf{f}''_{\alpha\beta}\,d\xi = \int_{-\xi_0}^{\xi_0}\mathbf{f}'^T_{\alpha\beta}\widehat{\mathbf{M}}^{11}_{\alpha\beta,\alpha\beta}\mathbf{f}'_{\alpha\beta}\,d\xi - \left[\mathbf{f}^T_{\alpha\beta}\widehat{\mathbf{M}}^{11}_{\alpha\beta,\alpha\beta}\mathbf{f}'_{\alpha\beta}\right]_{-\xi_0}^{\xi_0}, \tag{55}$$

and the third and the fifth terms are integrated by parts twice:

$$\int_{-\xi_0}^{\xi_0} \mathbf{f}_\alpha^T \widehat{\mathbf{M}}_{\alpha,\alpha\beta}^{20} \mathbf{f}_{\alpha\beta}'' \, d\xi = \int_{-\xi_0}^{\xi_0} \mathbf{f}_\alpha''^T \widehat{\mathbf{M}}_{\alpha,\alpha\beta}^{20} \mathbf{f}_{\alpha\beta} \, d\xi + \left[\mathbf{f}_\alpha^T \widehat{\mathbf{M}}_{\alpha,\alpha\beta}^{20} \mathbf{f}_{\alpha\beta}' \right]_{-\xi_0}^{\xi_0} - \left[\mathbf{f}_\alpha'^T \widehat{\mathbf{M}}_{\alpha,\alpha\beta}^{20} \mathbf{f}_{\alpha\beta} \right]_{-\xi_0}^{\xi_0}, \tag{56}$$

$$\int_{-\xi_0}^{\xi_0} \mathbf{f}_\alpha^T \widehat{\mathbf{M}}_{\alpha,\alpha}^{22} \mathbf{f}_\alpha^{(\mathrm{iv})} \, d\xi = \int_{-\xi_0}^{\xi_0} \mathbf{f}_\alpha''^T \widehat{\mathbf{M}}_{\alpha,\alpha}^{22} \mathbf{f}_\alpha'' \, d\xi + \left[\mathbf{f}_\alpha^T \widehat{\mathbf{M}}_{\alpha,\alpha}^{22} \mathbf{f}_\alpha''' \right]_{-\xi_0}^{\xi_0} - \left[\mathbf{f}_\alpha'^T \widehat{\mathbf{M}}_{\alpha,\alpha}^{22} \mathbf{f}_\alpha'' \right]_{-\xi_0}^{\xi_0}. \tag{57}$$

Substitution of these results into (54) and identification of terms contributing to Lagrangian (29) yields

$$\mathcal{I} + \left[-\mathbf{f}_{\alpha\beta}^T \widehat{\mathbf{M}}_{\alpha\beta,\alpha\beta}^{11} \mathbf{f}_{\alpha\beta}' + \mathbf{f}_\alpha^T \widehat{\mathbf{M}}_{\alpha,\alpha\beta}^{20} \mathbf{f}_{\alpha\beta}' - \mathbf{f}_\alpha'^T \widehat{\mathbf{M}}_{\alpha,\alpha\beta}^{20} \mathbf{f}_{\alpha\beta} + \mathbf{f}_\alpha^T \widehat{\mathbf{M}}_{\alpha,\alpha}^{22} \mathbf{f}_\alpha''' - \mathbf{f}_\alpha'^T \widehat{\mathbf{M}}_{\alpha,\alpha}^{22} \mathbf{f}_\alpha'' \right]_{-\xi_0}^{\xi_0} = 0, \tag{58}$$

which in view of boundary conditions (45) can be simplified to

$$\mathcal{I} = \left[\mathbf{f}_{\alpha\beta}^T \widehat{\mathbf{M}}_{\alpha\beta,\beta}^{11} \mathbf{f}_\beta' - \mathbf{f}_\alpha^T \widehat{\mathbf{M}}_{\alpha,\beta}^{20} \mathbf{f}_\beta' - \mathbf{f}_\alpha^T \widehat{\mathbf{M}}_{\alpha,\alpha}^{22} \mathbf{f}_\alpha''' \right]_{-\xi_0}^{\xi_0}, \tag{59}$$

or equivalently

$$\mathcal{I} = \left[\mathbf{f}_\alpha^T \left\{ (\widehat{\mathbf{M}}_{\alpha,\beta}^{11} - \widehat{\mathbf{M}}_{\alpha,\beta}^{20}) \mathbf{f}_\beta' - \widehat{\mathbf{M}}_{\alpha,\alpha}^{22} \mathbf{f}_\alpha''' \right\} + \mathbf{f}_\beta^T \left\{ \widehat{\mathbf{M}}_{\beta,\beta}^{11} \mathbf{f}_\beta' \right\} \right]_{-\xi_0}^{\xi_0}. \tag{60}$$

One can observe that the expressions in the figure brackets are identical to the natural boundary conditions (51) and (53) that vanish in the uncracked plies. Therefore, the sum is reduced to over the cracked plies only:

$$\mathcal{I} = \left[\mathbf{f}_{\alpha^c}^T \left\{ (\widehat{\mathbf{M}}_{\alpha^c,\beta}^{11} - \widehat{\mathbf{M}}_{\alpha^c,\beta}^{20}) \mathbf{f}_\beta' - \widehat{\mathbf{M}}_{\alpha^c,\alpha}^{22} \mathbf{f}_\alpha''' \right\} + \mathbf{f}_{\beta^c}^T \left\{ \widehat{\mathbf{M}}_{\beta^c,\beta}^{11} \mathbf{f}_\beta' \right\} \right]_{-\xi_0}^{\xi_0}. \tag{61}$$

The transposed function vectors are defined by the physical boundary conditions (42) and therefore known. Expression (61) is a generalization of the scalar analogue derived by Vinogradov and Hashin[7] for symmetric $[\theta/90]_S$.

4 | SOLUTION USING LAGRANGE MULTIPLIERS

Instead of eliminating the dependent functions using constraints (16), they are now accommodated in minimization of functional (20) using the method of Lagrange multipliers. The constraints are added to the Lagrangian forming the new augmented functional

$$\mathcal{I} = \int_{-\xi_0}^{\xi_0} \left\{ F(\xi) + 2\boldsymbol{\omega}_{\mathrm{eq}}^T(\xi) \mathbf{B}_{\mathrm{eq}} \mathbf{f}(\xi) \right\} d\xi, \tag{62}$$

where $2\boldsymbol{\omega}_{\mathrm{eq}}(\xi)$ is the 6×1 vector of Lagrange multipliers and

$$F(\xi) = \mathbf{f}^T \mathbf{M}^{00} \mathbf{f} + \mathbf{f}^T \mathbf{M}^{02} \mathbf{f}'' + \mathbf{f}''^T \mathbf{M}^{20} \mathbf{f} + \mathbf{f}'^T \mathbf{M}^{11} \mathbf{f}' + \mathbf{f}''^T \mathbf{M}^{22} \mathbf{f}''. \tag{63}$$

The Euler-Lagrange equations for this augmented functional follow from (26) and lead to the system:

$$\mathbf{M}^{00}\mathbf{f} + \left(\mathbf{M}^{02} + \mathbf{M}^{20} - \mathbf{M}^{11} \right) \mathbf{f}'' + \mathbf{M}^{22} \mathbf{f}^{(\mathrm{iv})} + \mathbf{B}_{\mathrm{eq}}^T \boldsymbol{\omega}_{\mathrm{eq}} = 0, \tag{64}$$

$$\mathbf{B}_{\mathrm{eq}} \mathbf{f} = 0, \tag{65}$$

or using a matrix representation:

$$\begin{bmatrix} \mathbf{M}^{00} & \mathbf{B}_{\mathrm{eq}}^T \\ \mathbf{B}_{\mathrm{eq}} & \mathbf{0} \end{bmatrix} \begin{bmatrix} \mathbf{f} \\ \boldsymbol{\omega}_{\mathrm{eq}} \end{bmatrix} + \begin{bmatrix} \mathbf{M}^{02} + \mathbf{M}^{20} - \mathbf{M}^{11} & \mathbf{0} \\ \mathbf{0} & \mathbf{0} \end{bmatrix} \begin{bmatrix} \mathbf{f}'' \\ \boldsymbol{\omega}'' \end{bmatrix} + \begin{bmatrix} \mathbf{M}^{22} & \mathbf{0} \\ \mathbf{0} & \mathbf{0} \end{bmatrix} \begin{bmatrix} \mathbf{f}^{(\mathrm{iv})} \\ \boldsymbol{\omega}^{(\mathrm{iv})} \end{bmatrix} = 0. \tag{66}$$

The vector of Lagrange multipliers can be eliminated from matrix equation (66) to express the functions $\mathbf{f}$ in terms of their derivatives:

$$\mathbf{f} = (\mathbf{M}^{00})^{-1} \mathbf{H} \left[\left(\mathbf{M}^{11} - \mathbf{M}^{02} - \mathbf{M}^{20} \right) \mathbf{f}'' - \mathbf{M}^{22} \mathbf{f}^{(\mathrm{iv})} \right], \tag{67}$$

where $\mathbf{H}$ is the projection matrix given by

$$\mathbf{H} = \mathbf{I} - \mathbf{B}_{\mathrm{eq}}^T \left(\mathbf{B}_{\mathrm{eq}} \left(\mathbf{M}^{00} \right)^{-1} \mathbf{B}_{\mathrm{eq}}^T \right)^{-1} \mathbf{B}_{\mathrm{eq}} \left(\mathbf{M}^{00} \right)^{-1}. \tag{68}$$

Thus, an eigenvalue problem can be formulated for the reciprocals of r^2 in the form:

$$\left(\begin{bmatrix} (\mathbf{M}^{00})^{-1}\mathbf{H}\left(\mathbf{M}^{11}-\mathbf{M}^{20}-\mathbf{M}^{02}\right) & -(\mathbf{M}^{00})^{-1}\mathbf{H}\,\mathbf{M}^{22} \\ \mathbf{I} & \mathbf{0} \end{bmatrix} - \frac{1}{r^2}\mathbf{I} \right) \begin{bmatrix} \mathbf{f} \\ \mathbf{f}'' \end{bmatrix} = 0. \tag{69}$$

The matrix in the eigenvalue problem is obviously singular, because the dependent functions are not eliminated; it has the same $6(N-1)$ nonzero eigenvalues r_i^{-2} as in (33) and $6(N+1)$ zero eigenvalues. Equation (69) is just an alternative form of the above treated nonsingular eigenvalue problem (33). Numerical implementations of the eigenvalue problem solution may introduce small nonzero values for the eigenvalues that should be equal to zero exactly. However, knowing the number of nonzero eigenvalues, it is not difficult to eliminate the rest, for example by sorting the eigenvalues by their absolute values.

Similar to the previous section, the general solution is constructed by selecting the nonzero eigenvalues and corresponding eigenvectors.

$$\mathbf{f} = \mathbf{U}(\xi)\mathbf{c} = \mathbf{V}\left[\mathbf{\Lambda}^{+}(\xi), \mathbf{\Lambda}^{-}(\xi)\right]\mathbf{c} \tag{70}$$

where $\mathbf{U}(\xi)$ is now a $6N \times 12(N-1)$ matrix, which includes functions for all the stress components in all the plies, and $\mathbf{c}$ is the vector of yet unknown constants to be determined using boundary conditions on the planes with cracks.

Multiplying the Euler-Lagrange equation (64) by $\mathbf{f}^{\mathrm{T}}$, or (67) by $\mathbf{f}^{\mathrm{T}}\mathbf{M}^{00}$, using the fact that the general solution satisfies constraints (65), and integrating over the fragment length, similar to how it was done in the previous section, the following expression for the functional is obtained:

$$\mathcal{I} = \left[\mathbf{f}^{\mathrm{T}}(\mathbf{M}^{11}-\mathbf{M}^{20}+\mathbf{M}^{02})\mathbf{f}' - \mathbf{f}^{\mathrm{T}}\mathbf{M}^{22}\mathbf{f}''' + \mathbf{f}'^{\mathrm{T}}\mathbf{M}^{22}\mathbf{f}''\right]_{-\xi_0}^{\xi_0}. \tag{71}$$

In order to avoid the cumbersome process of constructing natural boundary conditions, the physical boundary conditions of Section 3.2.1 and the Lagrange multipliers technique can again be employed to minimize the energy functional. Substitution of (70) into (71) leads to the following quadratic form in terms of independent constants $\mathbf{c}$:

$$\min_{\mathbf{c}}\{\mathcal{I} = \mathbf{c}^{\mathrm{T}}\mathbf{W}\,\mathbf{c}\}, \tag{72}$$

where

$$\mathbf{W} = \left[\mathbf{U}^{\mathrm{T}}\left(\mathbf{M}^{11}-\mathbf{M}^{20}+\mathbf{M}^{02}\right)\mathbf{U}' - \mathbf{U}^{\mathrm{T}}\mathbf{M}^{22}\mathbf{U}''' + \mathbf{U}'^{\mathrm{T}}\mathbf{M}^{22}\mathbf{U}''\right]_{-\xi_0}^{\xi_0}, \tag{73}$$

subject to boundary condition constraints at the crack planes, such as (43) and (46), written together as

$$\mathbf{B}_{\mathrm{bc}}\mathbf{c} = \mathbf{b}. \tag{74}$$

It should be noticed, that (73) does not depend on which of the 90° plies are cracked; the same matrix once constructed can be used for any crack pattern. It can also be shown that in case the general solution of the Euler-Lagrange equations is chosen according to (38), matrix $\mathbf{W}$ assumes a rather simple form:

$$\mathbf{W} = 2\begin{bmatrix} \mathbf{W}_{11} & \mathbf{0} \\ \mathbf{0} & \mathbf{W}_{22} \end{bmatrix}, \tag{75}$$

where

$$\begin{aligned} \mathbf{W}_{11} =& \mathbf{\Lambda}^{+}\mathbf{V}^{\mathrm{T}}\left(\mathbf{M}^{11}-\mathbf{M}^{20}+\mathbf{M}^{02}\right)\mathbf{V}\mathbf{\Lambda}_0\mathbf{\Lambda}^{-} - \mathbf{\Lambda}^{+}\mathbf{V}^{\mathrm{T}}\mathbf{M}^{22}\mathbf{V}\mathbf{\Lambda}_0^3\mathbf{\Lambda}^{-} + \mathbf{\Lambda}^{-}\mathbf{\Lambda}_0\mathbf{V}^{\mathrm{T}}\mathbf{M}^{22}\mathbf{V}\mathbf{\Lambda}_0^2\mathbf{\Lambda}^{+}, \\ \mathbf{W}_{22} =& \mathbf{\Lambda}^{-}\mathbf{V}^{\mathrm{T}}\left(\mathbf{M}^{11}-\mathbf{M}^{20}+\mathbf{M}^{02}\right)\mathbf{V}\mathbf{\Lambda}_0\mathbf{\Lambda}^{+} - \mathbf{\Lambda}^{-}\mathbf{V}^{\mathrm{T}}\mathbf{M}^{22}\mathbf{V}\mathbf{\Lambda}_0^3\mathbf{\Lambda}^{+} + \mathbf{\Lambda}^{+}\mathbf{\Lambda}_0\mathbf{V}^{\mathrm{T}}\mathbf{M}^{22}\mathbf{V}\mathbf{\Lambda}_0^2\mathbf{\Lambda}^{-}, \end{aligned}$$

and

$$\begin{aligned} \mathbf{\Lambda}^{+} &= \mathrm{diag}\left[(\exp(\mathbf{r}_{\mathrm{eig}}\xi_0) + \exp(-\mathbf{r}_{\mathrm{eig}}\xi_0)\right] = \exp(\mathbf{\Lambda}_0\xi_0) + \exp(-\mathbf{\Lambda}_0\xi_0), \\ \mathbf{\Lambda}^{-} &= \mathrm{diag}\left[(\exp(\mathbf{r}_{\mathrm{eig}}\xi_0) - \exp(-\mathbf{r}_{\mathrm{eig}}\xi_0)\right] = \exp(\mathbf{\Lambda}_0\xi_0) - \exp(-\mathbf{\Lambda}_0\xi_0), \\ \mathbf{\Lambda}_0 &= \mathrm{diag}(\mathbf{r}_{\mathrm{eig}}) \end{aligned}$$

Introducing Lagrange multipliers $2\boldsymbol{\omega}_{\mathrm{bc}}$ the new functional becomes

$$\mathcal{I} = \mathbf{c}^{\mathrm{T}}\mathbf{W}\mathbf{c} + 2\boldsymbol{\omega}_{\mathrm{bc}}^{\mathrm{T}}(\mathbf{B}_{\mathrm{bc}}\mathbf{c} - \mathbf{b}), \tag{76}$$

with the Euler-Lagrange equations for the unknown constants $\mathbf{c}$ having the form

$$\begin{bmatrix} \mathbf{W}_{\mathrm{sym}} & \mathbf{B}_{\mathrm{bc}}^{\mathrm{T}} \\ \mathbf{B}_{\mathrm{bc}} & \mathbf{0} \end{bmatrix} \begin{bmatrix} \mathbf{c} \\ \boldsymbol{\omega}_{\mathrm{bc}} \end{bmatrix} = \begin{bmatrix} \mathbf{0} \\ \mathbf{b} \end{bmatrix}, \tag{77}$$

where $\mathbf{W}_{\text{sym}} = \frac{1}{2}(\mathbf{W} + \mathbf{W}^{\text{T}})$ is the symmetric part. The solution of the system is given by

$$\begin{aligned} \mathbf{c} &= \mathbf{W}_{\text{sym}}^{-1}\mathbf{B}_{\text{bc}}^{\text{T}}(\mathbf{B}_{\text{bc}}\mathbf{W}_{\text{sym}}^{-1}\mathbf{B}_{\text{bc}}^{\text{T}})^{-1}\mathbf{b}, \\ \boldsymbol{\omega}_{\text{bc}} &= -(\mathbf{B}_{\text{bc}}\mathbf{W}_{\text{sym}}^{-1}\mathbf{B}_{\text{bc}}^{\text{T}})^{-1}\mathbf{b}. \end{aligned} \tag{78}$$

Since $\mathcal{I}$ is a scalar, the following identity holds

$$\mathcal{I} = \mathbf{c}^{\text{T}}\mathbf{W}\mathbf{c} = \mathbf{c}^{\text{T}}\mathbf{W}_{\text{sym}}\mathbf{c}, \tag{79}$$

and substituting the vector of constants $\mathbf{c}$ given in (78) the functional becomes

$$\mathcal{I} = \mathbf{b}^{\text{T}}\boldsymbol{\Xi}(\xi_0)\mathbf{b}, \tag{80}$$

where matrix $\boldsymbol{\Xi}(\xi_0)$ is defined as

$$\boldsymbol{\Xi}(\xi_0) = (\mathbf{B}_{\text{bc}}\mathbf{W}_{\text{sym}}^{-1}\mathbf{B}_{\text{bc}}^{\text{T}})^{-1}. \tag{81}$$

Finally, the complementary energy of the cracked laminate obtains the following concise expression:

$$\mathcal{U}_C = \mathcal{U}_C^0 + \frac{t_0^2}{2}\mathbf{b}^{\text{T}}\boldsymbol{\Xi}(\xi_0)\,\mathbf{b}. \tag{82}$$

It should be noticed the matrix $\mathbf{W}$ can be significantly simplified in case the boundary conditions assume reflection symmetry. The first row of the eigenvalue problem (69) implies the following relation holds:

$$(\mathbf{M}^{00})^{-1}\mathbf{H}\left(\mathbf{M}^{11} - \mathbf{M}^{20} - \mathbf{M}^{02}\right)\mathbf{V} - (\mathbf{M}^{00})^{-1}\mathbf{H}\,\mathbf{M}^{22}\mathbf{V}\boldsymbol{\Lambda}_0^2 - \mathbf{V}\boldsymbol{\Lambda}_0^{-2} = 0. \tag{83}$$

Multiplying this by $\mathbf{V}^{\text{T}}\mathbf{M}^{00}$ from the left and by $\boldsymbol{\Lambda}_0$ from the right and using the fact that $\mathbf{V}^{\text{T}}\mathbf{H} = \mathbf{V}^{\text{T}}$, which follows from (65), yields

$$\mathbf{V}^{\text{T}}\left(\mathbf{M}^{11} - \mathbf{M}^{20} - \mathbf{M}^{02}\right)\mathbf{V}\boldsymbol{\Lambda}_0 - \mathbf{V}^{\text{T}}\mathbf{M}^{22}\mathbf{V}\boldsymbol{\Lambda}_0^3 - \mathbf{V}^{\text{T}}\mathbf{M}^{00}\mathbf{V}\boldsymbol{\Lambda}_0^{-1} = 0. \tag{84}$$

With help of (84) the matrix $\mathbf{W}_{11}$, for instance, can be written as

$$\mathbf{W}_{11} = 2\boldsymbol{\Lambda}^{+}\mathbf{V}^{\text{T}}\mathbf{M}^{02}\mathbf{V}\boldsymbol{\Lambda}_0\boldsymbol{\Lambda}^{-} + \boldsymbol{\Lambda}^{+}\mathbf{V}^{\text{T}}\mathbf{M}^{00}\mathbf{V}\boldsymbol{\Lambda}_0^{-1}\boldsymbol{\Lambda}^{-} + \boldsymbol{\Lambda}^{-}\boldsymbol{\Lambda}_0\mathbf{V}^{\text{T}}\mathbf{M}^{22}\mathbf{V}\boldsymbol{\Lambda}_0^2\boldsymbol{\Lambda}^{+}. \tag{85}$$

One can realize that after multiplication by the constant vector $\mathbf{c}$ from the right, the first term will contain the factor $\mathbf{M}^{02}\mathbf{V}\boldsymbol{\Lambda}_0\boldsymbol{\Lambda}^{-}\mathbf{c}$, which is associated with $\mathbf{M}^{02}\mathbf{f}'$, and hence vanishes, since the only nonzero columns of matrix $\mathbf{M}^{02}$ are those that are multiplied by perturbation stress functions $\phi_1^{(m)}$ and $\psi_1^{(m)}$, whose first derivatives vanish on the crack planes for all the plies due to symmetry conditions. The third term vanishes after multiplying it by $\mathbf{c}^{\text{T}}$ from the left for the same reason. Thus, the first and the third terms in $\mathbf{W}_{11}$ do not contribute to the value of the functional. Matrix $\mathbf{W}_{22}$ is treated similarly, reducing $\mathbf{W}$ to

$$\mathbf{W} = 2\begin{bmatrix} \boldsymbol{\Lambda}^{+}\,\mathbf{V}^{\text{T}}\mathbf{M}^{00}\mathbf{V}\boldsymbol{\Lambda}_0^{-1}\boldsymbol{\Lambda}^{-} & \mathbf{0} \\ \mathbf{0} & \boldsymbol{\Lambda}^{-}\,\mathbf{V}^{\text{T}}\mathbf{M}^{00}\mathbf{V}\boldsymbol{\Lambda}_0^{-1}\boldsymbol{\Lambda}^{+} \end{bmatrix}. \tag{86}$$

This formulation is obviously equivalent to (60), when all the function dependencies, explicitly eliminated in (60), are now taken into account through the eigenvectors, whose elements forming the dependent functions necessarily satisfy (23) and (28). While the two representations are equivalent, unlike (60), the new formulation requires no excessive matrix manipulations and is advantageous for numerical implementations.

It should be noted that the two applications of the method of Lagrange multipliers (62) and (76) are independent of each other. All the above expressions for $\mathbf{W}$ still hold if the dependent functions are first eliminated as in Section 3. If this route is pursued, matrices $\widehat{\mathbf{M}}$ with the eigenvectors of (33) should be used instead. The expressions for $\mathbf{W}$ also hold if one chooses to use the Schur decomposition as described in Section 3.1 using the corresponding definitions of $\mathbf{V}$ and $\boldsymbol{\Lambda}_0$.

5 | EFFECTIVE THERMOELASTIC PROPERTIES

The complementary energy of a linear elastic material with internal stress field $\boldsymbol{\sigma}(\mathbf{x})$ and temperature change ΔT subjected to applied tractions on its surfaces is defined as

$$\mathcal{U}_C = \int_V \left(\frac{1}{2}\boldsymbol{\sigma}^{\text{T}}\mathbf{S}\,\boldsymbol{\sigma} + \boldsymbol{\sigma}^{\text{T}}\boldsymbol{\alpha}\,\Delta T - \frac{1}{2}c_p\frac{\Delta T^2}{T_0}\right)dV, \tag{87}$$

where T_0 is a reference temperature and c_p is the specific heat at constant stress. For a laminate of length L, thickness h and unit width, (87) can be expressed in terms of the effective properties, which for the undamaged laminate has the form (Appendix C)

$$\mathcal{U}_C^0 = \frac{1}{2}\mathbf{t}^{\mathrm{T}}\mathbf{S}^0\mathbf{t}\,L + \mathbf{t}^{\mathrm{T}}\boldsymbol{\alpha}^0\Delta T\,L - \frac{1}{2}c_p^0\frac{\Delta T^2}{T_0}L, \tag{88}$$

and for the cracked laminate

$$\mathcal{U}_C = \frac{1}{2}\mathbf{t}^{\mathrm{T}}\mathbf{S}^*\mathbf{t}\,L + \mathbf{t}^{\mathrm{T}}\boldsymbol{\alpha}^*\Delta T\,L - \frac{1}{2}c_p^*\frac{\Delta T^2}{T_0}L, \tag{89}$$

where $\mathbf{t}$ is the vector of membrane forces and moments $\mathbf{t} = [N_1, N_2, N_6, M_1, M_2, M_6]^{\mathrm{T}}$, $\mathbf{S}$ represents the effective 6×6 compliance matrix $\mathbf{ABD}'$ of the laminate, $\boldsymbol{\alpha}$ is the 6×1 vector of in-plane thermal expansions and curvatures $\boldsymbol{\alpha} = [\alpha_1, \alpha_2, \alpha_6, \kappa_1, \kappa_2, \kappa_6]^{\mathrm{T}}$, and c_p is the specific heat of the laminate of thickness h per unit length and width.

Hashin[4] showed that in the thermoelastic case the complementary energy assumes exactly the same form as in (17):

$$\mathcal{U}_C = \mathcal{U}_C^0 + \frac{1}{2}\int_V \boldsymbol{\sigma}^{\mathrm{T}}\mathbf{S}\boldsymbol{\sigma}\,dV, \tag{90}$$

where $\boldsymbol{\sigma}$ are the perturbation stresses due to cracks. Therefore, independently of whether the temperature change is present or not, minimization of the volume integral of perturbation stresses in (90) is exactly the same as presented above. In order to adapt the derivation in the previous section, one has to simply replace the vector of boundary conditions $\mathbf{b}$ in (74) with

$$\mathbf{b} = \mathbf{K}_{\mathrm{mech}}\mathbf{t} + \mathbf{k}_{\mathrm{th}}\Delta T, \tag{91}$$

introducing linear dependency of the stresses on the applied loads and temperature change, where matrix $\mathbf{K}_{\mathrm{mech}}$ and vector $\mathbf{k}_{\mathrm{th}}$ can be seen as ply stress concentration factors in the virgin laminate due to mechanical and thermal loadings, respectively. A procedure for assembly of matrices $\mathbf{B}_{\mathrm{bc}}$, $\mathbf{K}_{\mathrm{mech}}$ and $\mathbf{k}_{\mathrm{th}}$ that solely comprise the physical boundary conditions is suggested in Appendix D.

Substituting (91) into (82) one derives the following quadratic form for the complementary energy

$$\begin{aligned}\mathcal{U}_C &\le \mathcal{U}_C^0 + \frac{t_0^2}{2}(\mathbf{K}_{\mathrm{mech}}\mathbf{t} + \mathbf{k}_{\mathrm{th}}\Delta T)^{\mathrm{T}}\boldsymbol{\Xi}(\xi_0)(\mathbf{K}_{\mathrm{mech}}\mathbf{t} + \mathbf{k}_{\mathrm{th}}\Delta T)\\ &= \mathcal{U}_C^0 + \frac{t_0^2}{2}\left(\mathbf{t}^{\mathrm{T}}\mathbf{K}_{\mathrm{mech}}^{\mathrm{T}}\boldsymbol{\Xi}(\xi_0)\mathbf{K}_{\mathrm{mech}}\mathbf{t} + 2\mathbf{t}^{\mathrm{T}}\mathbf{K}_{\mathrm{mech}}^{\mathrm{T}}\boldsymbol{\Xi}(\xi_0)\mathbf{k}_{\mathrm{th}}\Delta T + \mathbf{k}_{\mathrm{th}}^{\mathrm{T}}\boldsymbol{\Xi}(\xi_0)\mathbf{k}_{\mathrm{th}}\Delta T^2\right).\end{aligned} \tag{92}$$

A straightforward comparison of (92) with (88) and (89) yields:

$$\mathbf{S}^* \le \mathbf{S}^0 + \frac{t_0}{2\xi_0}\mathbf{K}_{\mathrm{mech}}^{\mathrm{T}}\boldsymbol{\Xi}(\xi_0)\mathbf{K}_{\mathrm{mech}}, \tag{93}$$

$$\boldsymbol{\alpha}^* \le \boldsymbol{\alpha}^0 + \frac{t_0}{2\xi_0}\mathbf{K}_{\mathrm{mech}}^{\mathrm{T}}\boldsymbol{\Xi}(\xi_0)\mathbf{k}_{\mathrm{th}}, \tag{94}$$

$$-c_p^*/T_0 \le -c_p^0/T_0 + \frac{t_0}{2\xi_0}\mathbf{k}_{\mathrm{th}}^{\mathrm{T}}\boldsymbol{\Xi}(\xi_0)\mathbf{k}_{\mathrm{th}}. \tag{95}$$

In case the initial laminate had inclined cracks and was transformed to the coordinate system associated with the cracks (Section 2), the resultant compliance and thermal expansions can be rotated back to the original coordinate system.

The remarkable aspect of the expressions (93)-(95) is that based on the same solution of the energy minimization problem and simply modifying the vector of boundary conditions they instantaneously provide the full compliance matrix $\mathbf{ABD}'$ of a cracked laminate, its thermal expansions and curvatures and specific heat.

An alternative method of estimating the thermal expansion coefficients of cracked laminates suggested by Hashin[20] is based on an extension of the well-known theorem of Levin[21] and requires evaluation of the average mechanical stresses in the plies. The advantage of (94) is that it eliminates the need for additional integration of the stress functions over the laminate volume and also gives the curvatures (per unit temperature change) of a thermally loaded cracked laminate in non-symmetric cases.

Changes in the specific heat of a laminate due to intralaminar cracks, although have not attracted attention in the past, can be used in conjunction with an energy based fracture criterion for prediction of cracking due to temperature changes. In the thermal case the change in the magnitude of the specific heat with crack density is the only parameter that determines the complementary energy change and, consequently, the energy release rate during crack formation, which can easily be seen from (89) if no mechanical loading $\mathbf{t} = 0$ is applied.

6 | ASYMPTOTIC BEHAVIOR AT LOW AND HIGH CRACK DENSITIES

In this section the special cases of low and high crack densities are considered, which might be of practical interest in some applications.

It can be seen from (93)-(95) that for high crack densities ($\xi_0 \to 0$), matrix $\mathbf{\Xi}(\xi_0)$ and then the complementary energy change due to the cracks should be proportional to the length of a fragment ξ_0. This implies that all the perturbation stresses should be independent of the x-coordinate, which yields zero total stresses σ_1 and σ_6 in the cracked plies and zero stresses σ_3, σ_4 and σ_5 everywhere in the laminate. The solution in this case can then be obtained using the Classical Laminate Theory, when the effective stiffness matrix **ABD** of the cracked laminate is calculated with the stiffness of the cracked ply replaced with

$$\mathbf{Q}^{(90^\circ)} = \begin{bmatrix} 0 & 0 & 0 \\ 0 & E_A & 0 \\ 0 & 0 & 0 \end{bmatrix}, \tag{96}$$

where it is written in the coordinate system of analysis (the cracks in 90° ply are normal to axis x) and E_A is the Young's modulus of the ply material in the fiber direction (in the direction of the cracks).

The low crack density case ($\xi_0 \to \infty$) is of a higher importance, since it corresponds to the stage of initial cracking. In this case the stress perturbations are developed in the vicinity of a crack and decay with distance. The energy addition due to the stress perturbations close to non-interacting cracks on the two ends of a fragment can be calculated as a sum of the two additional energies, when the two ends are considered independently.

It is convenient to locate the origin of the coordinate system at one end of the fragment and request that the perturbations stresses satisfy the condition

$$\boldsymbol{\sigma}(\xi \to \infty) = 0, \tag{97}$$

implying that only the eigenfunctions decaying at large x survive. The general solution of this problem can be written in the form:

$$\mathbf{f} = \mathbf{U}(x)\mathbf{c} \equiv [\mathbf{v}_1 e^{-r_1\xi}, \mathbf{v}_2 e^{-r_2\xi}, ...]\mathbf{c} = \mathbf{V}\,\mathrm{diag}(e^{-\mathbf{r}_{\mathrm{eig}}\xi})\mathbf{c}, \tag{98}$$

where eigenvalues $\mathbf{r}_{\mathrm{eig}}$ have a positive real part. Correspondingly, all elements of $\mathbf{W}(\xi_0 \to \infty)$ vanish, meaning

$$\mathbf{W} = -\left[\mathbf{U}^{\mathrm{T}}\left(\mathbf{M}^{11} - \mathbf{M}^{20} + \mathbf{M}^{02}\right)\mathbf{U}' - \mathbf{U}^{\mathrm{T}}\mathbf{M}^{22}\mathbf{U}''' + \mathbf{U}'^{\mathrm{T}}\mathbf{M}^{22}\mathbf{U}''\right]_{\xi=0}, \tag{99}$$

The diagonal matrix of eigenfunctions becomes an identity matrix and reflection symmetry conditions hold at $\xi = 0$. Then $\mathbf{W}$ can be expressed in terms of the matrices of eigenvectors and eigenvalues:

$$\mathbf{W} = \mathbf{V}^{\mathrm{T}}\mathbf{M}^{00}\mathbf{V}\,\mathbf{\Lambda}_0^{-1}. \tag{100}$$

The physical boundary conditions $\mathbf{B}_{\mathrm{bc}}\mathbf{c} = \mathbf{b}$ should be applied at $\xi = 0$, yielding

$$\begin{bmatrix} \mathbf{V}_{\alpha^c} \\ \mathbf{V}_{\beta^c} \\ \mathbf{V}_{\alpha}\mathbf{\Lambda}_0 \end{bmatrix}\mathbf{c} = \begin{bmatrix} \mathbf{f}^0_{\alpha^c} \\ \mathbf{f}^0_{\beta^c} \\ \mathbf{0} \end{bmatrix}, \tag{101}$$

which defines the matrix $\mathbf{B}_{\mathrm{bc}}$ and the vector $\mathbf{b}$ in the case of low crack density. The coefficients $\mathbf{c}$ should be evaluated independently for each cracked plane if the non-interacting cracked planes along the laminate have different cracked plies. The contribution of each cracked plane to the complementary energy increase should be combined:

$$\mathcal{U}_C = \mathcal{U}_C^0 + \frac{t_0^2}{2}\sum_i 2\mathbf{c}_i^{\mathrm{T}}\mathbf{W}\mathbf{c}_i, \tag{102}$$

where the factor 2 under the sum reflects the same energy stored on both sides of a crack plane vicinity. In case the cracked plies are the same at each crack plane, when the contribution of each crack plane is the same, the effective properties can be explicitly written as functions of the crack density. For instance, for a laminate of length L having N_{cr} cracked planes along L define the crack density parameter $c = N_{cr}/L$. Then in absence of the temperature change the energy is

$$\frac{L}{2}\mathbf{t}^{\mathrm{T}}\mathbf{S}^*\mathbf{t} \approx \frac{L}{2}\mathbf{t}^{\mathrm{T}}\mathbf{S}^0\mathbf{t} + t_0^2 N_{cr}\mathbf{t}^{\mathrm{T}}\mathbf{K}^{\mathrm{T}}_{\mathrm{mech}}(\mathbf{B}_{\mathrm{bc}}\mathbf{W}^{-1}_{\mathrm{sym}}\mathbf{B}^{\mathrm{T}}_{\mathrm{bc}})^{-1}\mathbf{K}_{\mathrm{mech}}\mathbf{t}, \tag{103}$$

implying the following linear in terms of the crack density expression for the effective compliance:

$$\mathbf{S}^* \approx \mathbf{S}^0 + \left[2t_0^2\mathbf{K}^{\mathrm{T}}_{\mathrm{mech}}(\mathbf{B}_{\mathrm{bc}}\mathbf{W}^{-1}_{\mathrm{sym}}\mathbf{B}^{\mathrm{T}}_{\mathrm{bc}})^{-1}\mathbf{K}_{\mathrm{mech}}\right]c, \tag{104}$$

where the matrix $\mathbf{W}$ is defined by (100), $\mathbf{B}_{bc}$ follows from (101) and the concentration matrix $\mathbf{K}_{mech}$ is as previously described, $\mathbf{K}_{mech}\mathbf{t} = \mathbf{b}$. Similarly, changes in the thermal expansions and specific heat of a cracked laminate due to small crack density can be obtained from (104) by appropriate replacement of $\mathbf{K}_{mech}$ with $\mathbf{k}_{th}$, as in (93)-(95). The derived simple explicit relations for the effective properties in terms of the crack density parameter might be very useful, since the low crack density approximation is accurate up to quite high values of the crack density, as demonstrated in the next Section.

7 | VALIDATION

In order to assess the model's capability to accurately account for the effects of intralaminar cracks on the effective elastic properties of cracked laminates, seven independent experimental works have been selected where engineering constants were reported as functions of crack densities for different laminates and materials. Table 1 summarizes the list of references that contain results of the experimental studies used for comparison, the laminate property being compared, figures where the results of comparison can be seen and the corresponding material properties of the unidirectional laminae used in calculations. In this section the focus is on the effective engineering properties. For several laminates the stress field distribution is also shown to illustrate some unique features of the presented variational stress analysis. It should be noted that the main goal of the section is to demonstrate the robustness of the developed approach and its ability to deal with laminates of any general layups, rather than study each of the considered cases in detail.

TABLE 1: Source of experimental data and lamina proprties used in analysis.

Source	Material/layup	Parameter	Figures	E_A	E_T	G_A	G_T	ν_A
Joffe et al.[22]	GFRP $[\pm\theta/0_4]_S$	E_x, ν_{xy}	3,5,7	44.73	12.76	5.8	4.49	0.297
Tsai and Daniel[23]	CFRP $[0/90_n]_S$	G_{xy}	8	145	10	6.9	3.7	0.27
Kim et al.[24]	CFRP $[0_2/90_2]_S$	α_x	10	138	10.3	5.5	3.6[a]	0.3
Varna et al.[25]	GFRP $[0/90_8/0_{1/2}]_S$	E_x	12a	44.7	12.7	5.8	4.49[a]	0.297
Tong et al.[26]	GFRP $[0/90/\mp45]_S$	E_x	12b	46	13	5	4.49[a]	0.3
Schmitz and Horst[27,b]	GFRP $[0/90]_S$	D_{11}	15	44.73	12.76	5.8	4.49	0.297
Hoover et al.[28,c]	GFRP $[\pm\theta/90_6/0_2]_T$	E_x	17	41.7	13	3.4	4.49[a]	0.3

[a]Assumed in here
[b]Material properties are assumed as in Ref.[22]
[c]Material properties are assumed as in Ref.[29]

7.1 | Symmetric laminates with one family of transverse cvracks

As the first example, the effective properties of symmetric $[\pm\theta/90]_S$ GFRP laminates with transverse cracks in 90° ply are estimated. The experimental results published in Joffe et al.[22] are used for comparison. The thickness of one cured prepreg lamina was reported to be $t_0 = 0.144$ mm.

Comparison of the model prediction for the effective Young's modulus and Poisson's ratio with the experimental data for $\theta = 0°$, 15° and 30° is shown in Figures 3, 5 and 7, respectively. It can be seen that the model predictions are in excellent agreement with the test measurements. It is noteworthy that the variational approach provides the lower bound for the effective Young's modulus. While most of the experimental points are on or just above the curve of the calculated Young's modulus, a few points fell below it. This can be attributed to randomness in the mechanical properties of the tested specimens. Predictions for the Poisson's ratio are also in good agreement with the experimental data, but being determined as the ratio of two elements of the extensional compliance matrix $\nu_{xy} = -A'_{12}/A'_{11}$, the prediction does not represent a rigorous bound and should be regarded as an estimate. In Figures 3, 5 and 7 the dashed lines correspond to the small crack density asymptotes, derived in Section 6. It is interesting that for these layups the small density approximation is accurate up to quite high crack densities.

The distribution for the axial stress σ_{xx} normilized with respect to the average axial tensile stress in $[0_2/90_4]_S$ calculated for different fragment lengths is shown in Figure 4. Analysis is performed for a laminate comprising three plies symmetrically placed with respect to the centerline of the transverse ply. It can be seen that the stress field that corresponds to minimum complimentary

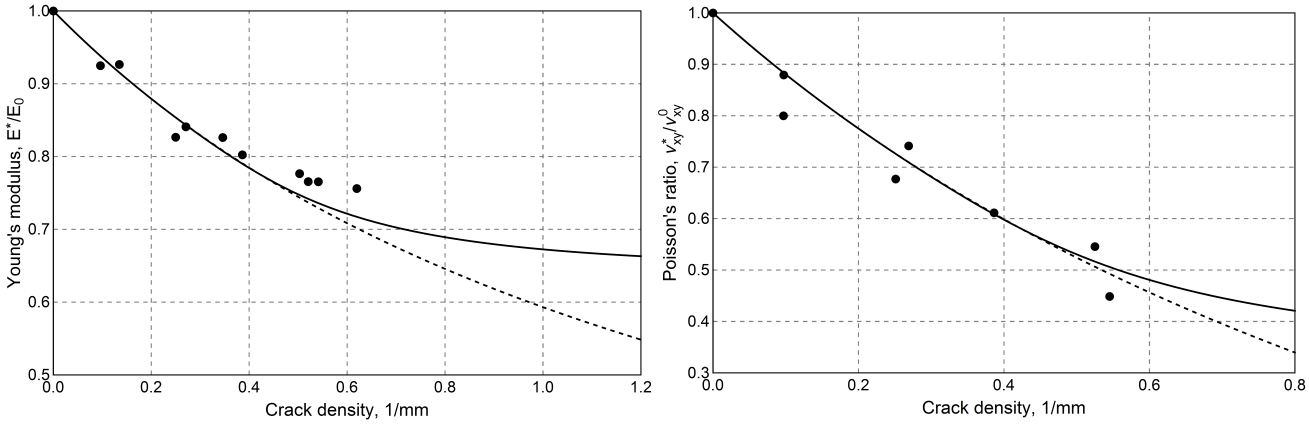

(a) (b)

FIGURE 3: Normalized Young's modulus (a) and Poisson's ratio (b) of $[0_2/90_4]_S$ as a function of crack density. Experimental data: Joffe et al.[22].

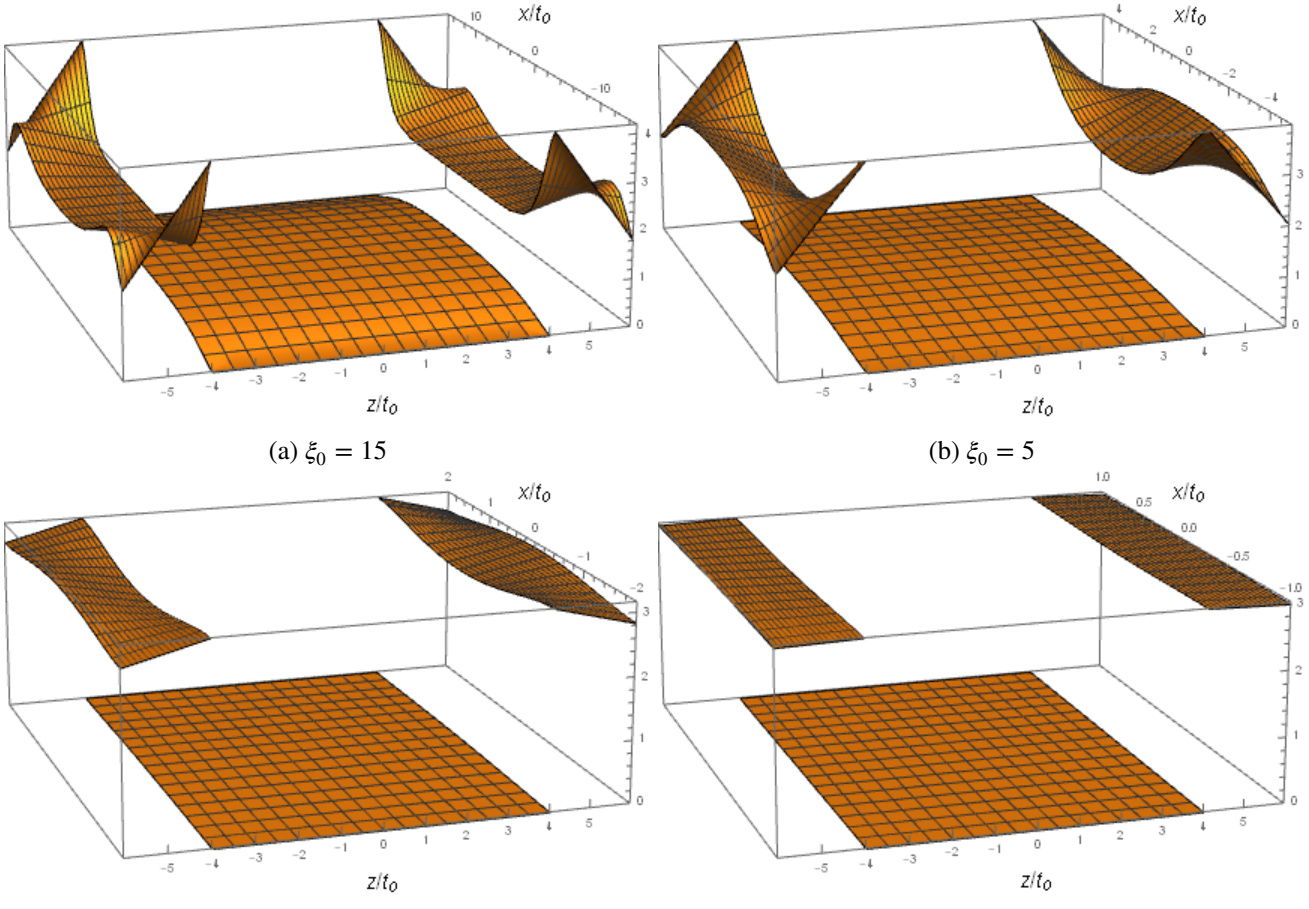

(a) $\xi_0 = 15$ (b) $\xi_0 = 5$

(c) $\xi_0 = 2$ (d) $\xi_0 = 1$

FIGURE 4: Normalized stress σ_{xx} distribution in $[0_2/90_4]_S$ under axial tension for different inter crack spacing.

energy exhibits stress concentrations in the uncracked plies close to the transverse crack tips, which are determined by the non-zero gradient terms in the resultsnt stress field. The gradient terms assymptotically vanish when the crack density becomes large.

The stresses become x-independent, whilest the effective properties approach the assymptotic solution for the infinite crack density described in Section 6. The stress in the transverse ply is uniform along the thickness direction: the gradient term in this ply vanished because of the symmetric layup used for analysis.

An illustration of the stress field in a laminate with out-of-plane plies can be seen in Figure 6 for $[\pm 15/90_4]_S$. It can be seen that all three inplane stresses develop concentrations at the transverse crack tips. Figure 6c shows the different inplane shear stress in the plies with alternating signs whith highier stress concentations in the $-45°$ plies, which are closeer to the cracked transverse ply. This would be overlooked if the outer $\pm 30°$ sublaminate is homogenized prior to analysis.

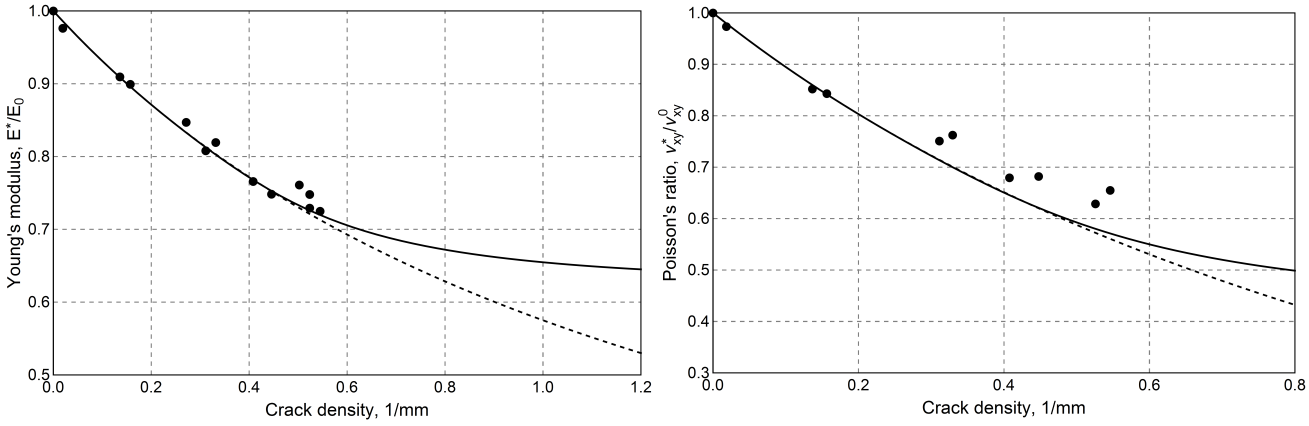

(a) (b)

FIGURE 5: Normalized Young's modulus (a) and Poisson's ratio (b) of $[\pm 15/90_4]_S$ as a function of crack density. Experimental data: Joffe et al.[22].

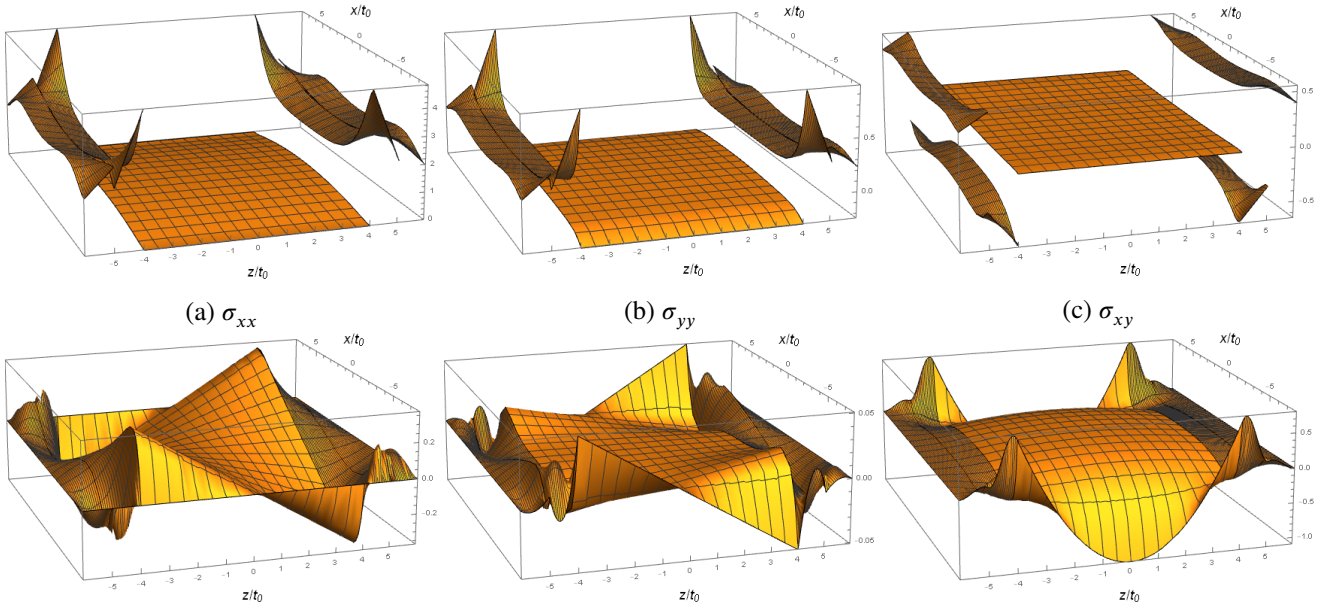

(a) σ_{xx} (b) σ_{yy} (c) σ_{xy}

(d) σ_{xz} (e) σ_{yz} (f) σ_{zz}

FIGURE 6: Stress tensor components in $[\pm 15/90_4]_S$ under axial tension for $\xi_0 = 8$.

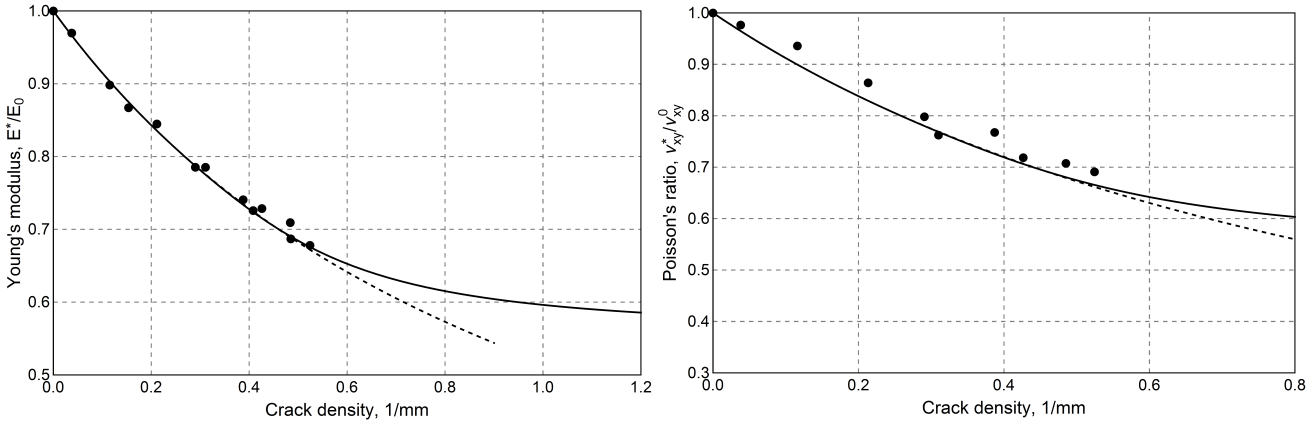

(a) (b)

FIGURE 7: Normalized Young's modulus (a) and Poisson's ratio (b) as a function of crack density for $[\pm 30/90_4]_S$. Experimental data: Joffe et al.[22].

The in-plane shear modulus of cracked laminates has received significantly less attention in experimental studies than the Young's modulus and Poisson's ratio. One of the main reasons for that would be technical difficulties with creating the state of pure shear in a coupon manufactured for a tensile test, in which intralaminar cracks are typically induced. Although various experimental techniques have been developed[23,30,31], more systematic, well documented and reliable experimental data is required.

Figure 8 shows prediction of the shear modulus degradation compared to the experimental results for CFRP cross-ply laminates of Tsai and Daniel[23]. The experimental measurements were reported for the crack density normalized by the thickness of the cracked transverse ply, which eliminates the dependency on the lamina thickness t_0. Although excellent agreement can be observed for $[0/90_4]_S$, the experimental points for $[0/90_2]_S$ are systematically below the analytical curve, which in principle represents the lower bound for the shear modulus. Some discussions regarding accuracy of the experimental data can be found in Katerelos et al.[15].

An example of the shear stress distribution in the later cross-ply is shown in Figure 9. It can be seen that for a long fragment with non-interacting transverse cracks (Figure 9a), the shear stress is almost uniform in the middle of the fragment and complies with the uniform shear stress distribution in an uncracked cross-ply. As the crack density increases both the stress in the transverse ply and the stress gradients in the outer plies decrease.

7.2 | Thermal expansion and temperature induced stresses

As shown in Section 5 and Appendix D, the same analysis provides the thermal expansion coefficients of a cracked laminate when the vector of boundary conditions is replaced with the temperature induced stresses in the cracked plies. Equation (94) is used to estimate the thermal expansion coefficient of a carbon/epoxy AS4/3501-6 laminates having $[0_2/90_2]_S$ layup with cracks in 90° ply. The laminate was a subject of experiments carried out by Kim et al.[24]. In addition to the elastic properties listed in Table 1, the thermal expansion coefficients of the unidirectional lamina are $\alpha_L = 0.43\times10^{-6}\,°C^{-1}$ and $\alpha_T = 25.8\times10^{-6}\,°C^{-1}$. The lamina thickness is assumed here to be $t_0 = 0.125$mm. Very good agreement between the calculated results and the experimental data can be seen in Figure 10. Although expression (94) gives strictly speaking the upper bound for the thermal expansion, it should be noticed that Kim et al.[24] reported a large scatter in the values of the thermal expansion coefficient of the UD ply with a coefficient of variance of 31% for the longitudinal α_L. For illustration purposes the stress σ_{xx} for different values of the fragment length is shown in Figure 11. For high crack densities the stress in the transverse ply approaches zero, leaving the uncracked 0° plies to expand freely.

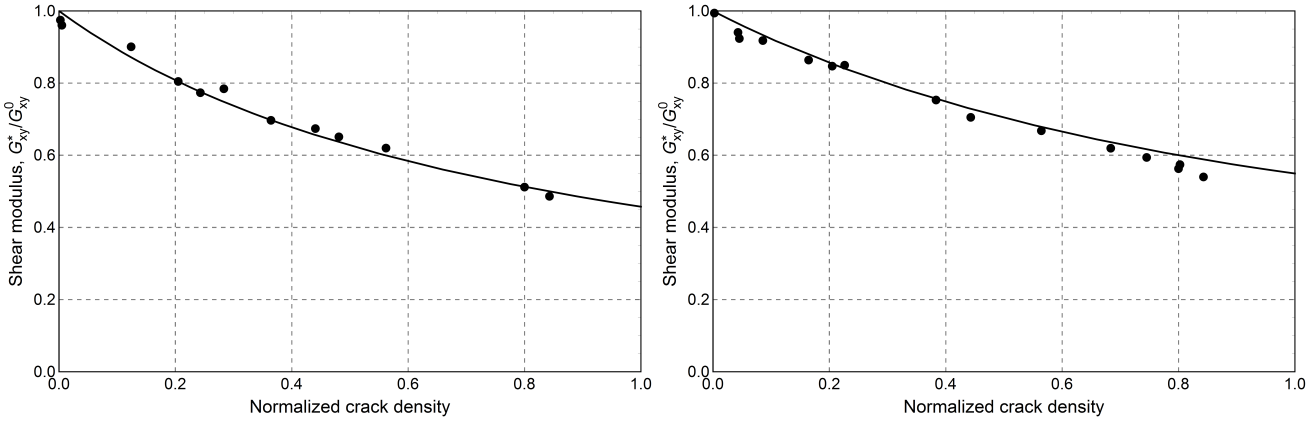

(a) (b)

FIGURE 8: Normalized shear modulus of $[0/90_4]_S$ (a) and $[0/90_2]_S$ (b) as a function of normalized crack density. Experimental data is of Tsai and Daniel[23].

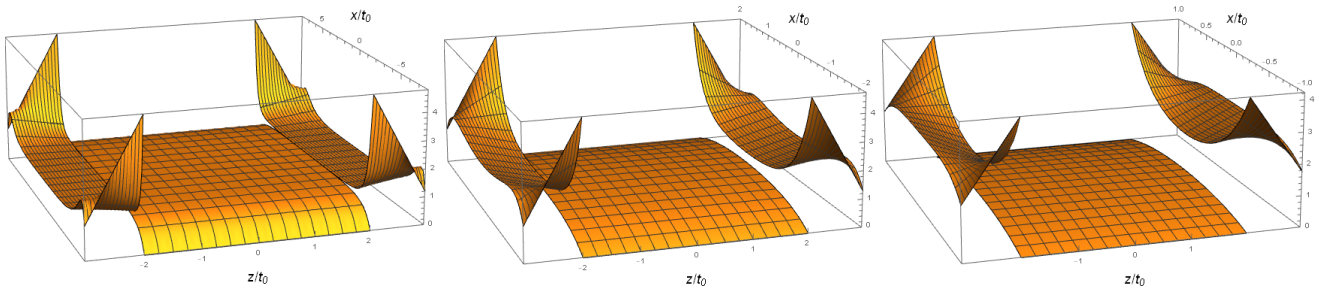

(a) $\xi_0 = 8$ (b) $\xi_0 = 2$ (c) $\xi_0 = 1$

FIGURE 9: Shear stress distribution in $[0/90_2]_S$ under shear force for different fragment lengths.

7.3 | Two families of transverse cracks

The unique ability of the presented model is to analyze both symmetric and non-symmetric laminates with symmetric and/or non-symmetric crack arrays using the same framework. Following the previous examples, symmetric laminates with two parallel arrays of cracks in 90° plies separated by uncracked plies represent the next level of complexity. Comparison of the model prediction for the Young's modulus of GFRP $[0/90_8/0_{1/2}]_S$ with experimental data reported in Varna et al.[25] is shown in Figure 12a. Thickness of an individual lamina was not reported in that paper, but $t_0 = 0.125$ mm was mentioned in Singh and Talreja[32], where the test data was compared to FE predictions.

The reported data and the computational results are plotted versus crack density in each family of the transverse plies, assuming the same crack density in the symmetrically placed transverse plies. The two 90°_8 plies separated by a thin 0° ply do not necessarily form an aligned crack pattern. Since no specific observed crack arrangement was described in the reference, and typically some randomness would be expected in the inter-crack spacing along the coupon, two calculations were performed for staggered and aligned cracks, represented by a dashed and solid curves in Figure 12a, respectively, in accordance with the schemes in Figures 2b and 2c. It can be seen that for this particular material the difference between the two predictions is marginal; both curves can serve as a good estimate of its effective Young's modulus.

Experimental results of Tong et al.[26] for the Young's modulus reduction of GFRP $[0/90/\mp 45]_S$ with crack density in 90° ply and the corresponding model predictions are shown in Figure 12b. The thickness of each lamina is $t_0 = 0.5$mm, according to the measured data. The two curves for the aligned and staggered crack patterns, overlapping in this case, are in excellent agreement with the experiments. The fact that the two crack arrangements give almost indistinguishable results is related to the thicker sub-laminate $[\mp 45]_S$, which significantly reduces the effect the stress perturbations in one transverse ply on the other.

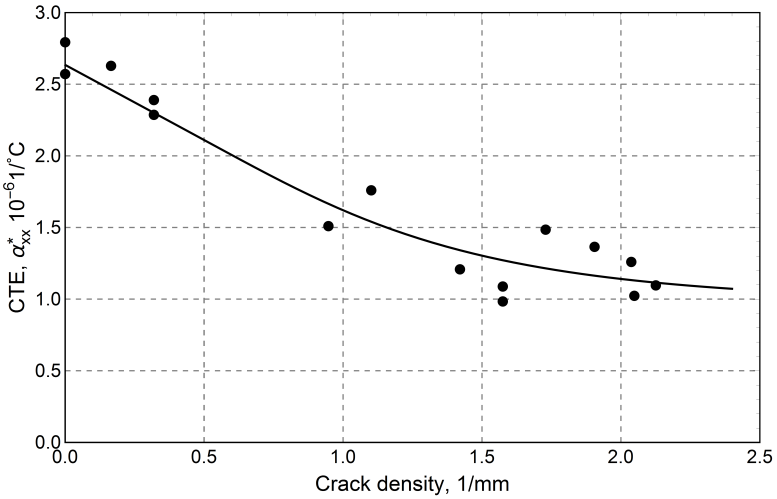

FIGURE 10: Coefficient of thermal expansion as a function of crack density for $[0_2/90_2]_S$. Experimental data is of Kim et al.[24].

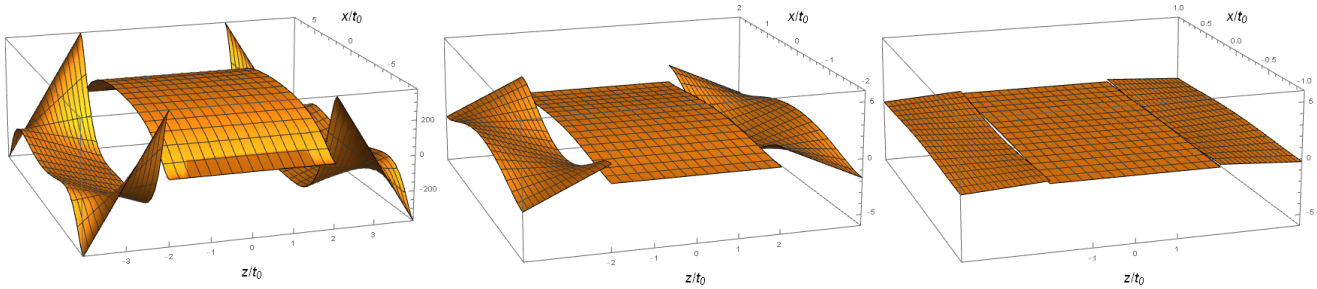

(a) $\xi_0 = 8$ (b) $\xi_0 = 2$ (c) $\xi_0 = 1$

FIGURE 11: Normalized axial stress $\sigma_{xx}/(E_1\alpha_1)$ in $[0_2/90_2]_S$ due to a unit temperature change (cooling) for different fragment lengths.

In Figure 12b the experimental points are shown for the values of the crack density up to about 0.7mm^{-1}, since cracks in the off-axis plies start forming at this stage, leading to a faster degradation of the effective Young's modulus.

Stress distribution in these laminates are shown in Figure 13 and 14 for both aligned and staggered crack patterns. The much thicker transverse plies in $[0/90_8/0_{1/2}]_S$ are subdivided into four sub-plies to see the stress distribution in more detail and to demonstrate this capability. The snapshots of the aligned case show one half of the fragment, in which both the transverse cracks are at the lowest values of x. In the staggered cases, the right transverse ply has a crack on the opposite side of the fragment, leading to an antisymmetric distribution of σ_{xx}. For the two laminates, the length of the fragment is chosen such that the normalized crack density is the same: $t_{90^\circ}/(2\xi_0) = 1$. As expected, the longer transverse cracks in $[0/90_8/0_{1/2}]_S$ create a higher crack intensity in the adjacent outer plies. Comparison of the two crack patterns in $[0/90/\mp 45]_S$ indicates that the stress distribution in the left half of the laminate is insensitive to the crack location in the right transverse ply: the gradient in the middle +45° ply is small and the stress to the right of it is just a mirror reflection of the stress in the aligned case. This supports the previous conclusion that interaction between the cracks in the two transverse plies is negligible.

7.4 | Non-symmetric cracked laminates

Very limited experimental data is available for laminates and loadings that induce curvatures and linear through the thickness in-plane stresses in the undamaged laminate. Schmitz and Horst[27] carried out bending experiments on symmetric $[90/0]_s$ laminates and reported reduction in the flexural rigidity of the laminate as a function of crack density in the outer 90° ply subjected to tension. Although the lamina elastic properties were not reported in the paper, it is assumed here that for GFRP they should not

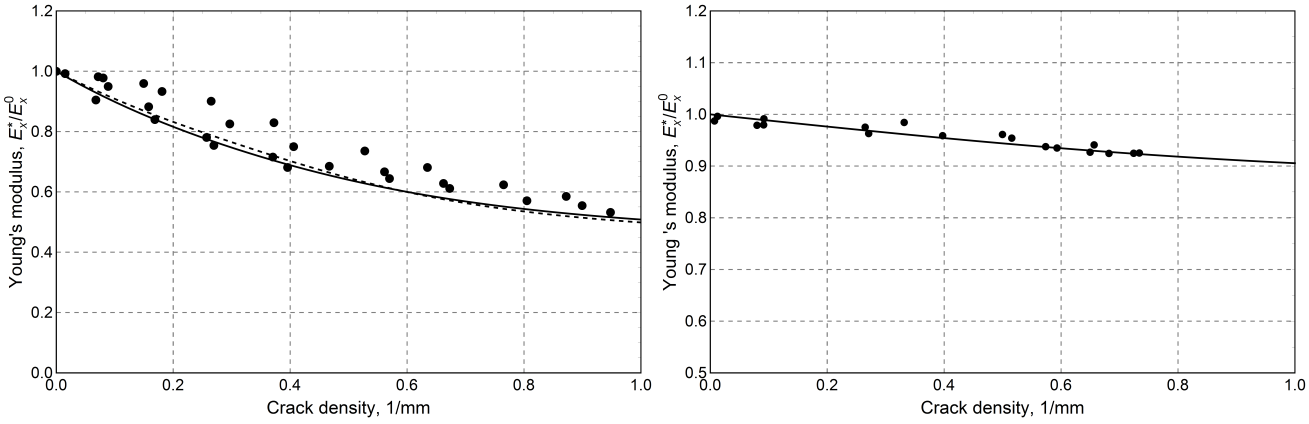

(a) (b)

FIGURE 12: Normalized Young's modulus as a function of crack density for (a) $[0/90_8/0_{1/2}]_S$; experimental data is of Varna et al.[25], (b) $[0/90/\mp 45]_S$; experimental data is of Tong et al.[26]. Dashed lines correspond to staggered crack arrays, the solid lines are for aligned cracks.

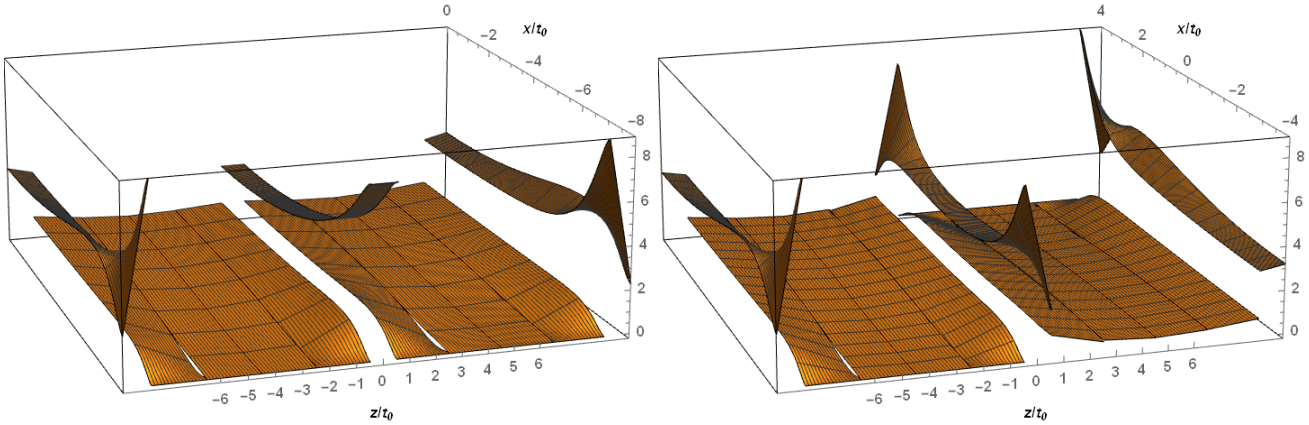

(a) symmetric (b) staggered

FIGURE 13: Normalized stress σ_{xx} in $[0/90_8/0_{1/2}]_S$

deviate significantly from the ones in Ref.[22], see the first row in Table 1. The thickness of each lamina in the experiments was $t_0 = 0.42$mm. Defining the flexural rigidity of the cracked laminate as reciprocal to the first entry in the bending compliance matrix $\mathbf{D}'$, the results for $(D'_{11}/D^0_{11})^{-1}$ are calculated and presented in Figure 15, demonstrating an excellent agreement with the experimental data.

Axial stress distribution in the case of bending of the non-symmetrically cracked cross-ply is shown in Figure 16 for different crack densities. Other nonzero stress components for a specific fragment length are also shown for illustration purposes.

Similar to the example of a symmetric laminate under bending, analysis of non-symmetric laminates, for which the in-plane stresses are linear through the thickness in the undamaged state, requires nonzero boundary condition for the stress gradient terms in the cracked plies even when the laminate is subjected to unidirectional tension, which is impossible with the assumption of piecewise constant through the thickness stress perturbation. Analysis is performed for the Young's modulus reduction of $[\pm 25/90_6/0_2]_T$ and $[\pm 45/90_6/0_2]_T$ with increasing crack density in 90° ply. These layups fabricated from 3M Scotchply type 1003 continuous E-glass-fibre/epoxy-resin-reinforced plastic were tested by Hoover et al.[28]. The lamina properties were not reported, but the same material was used in Highsmith and Reifsnider[29], where the lamina properties are taken from. The lamina thickness of 0.25mm is calculated from the reported total thickness of the tested coupons of 2.5mm. Figure 17 shows very good

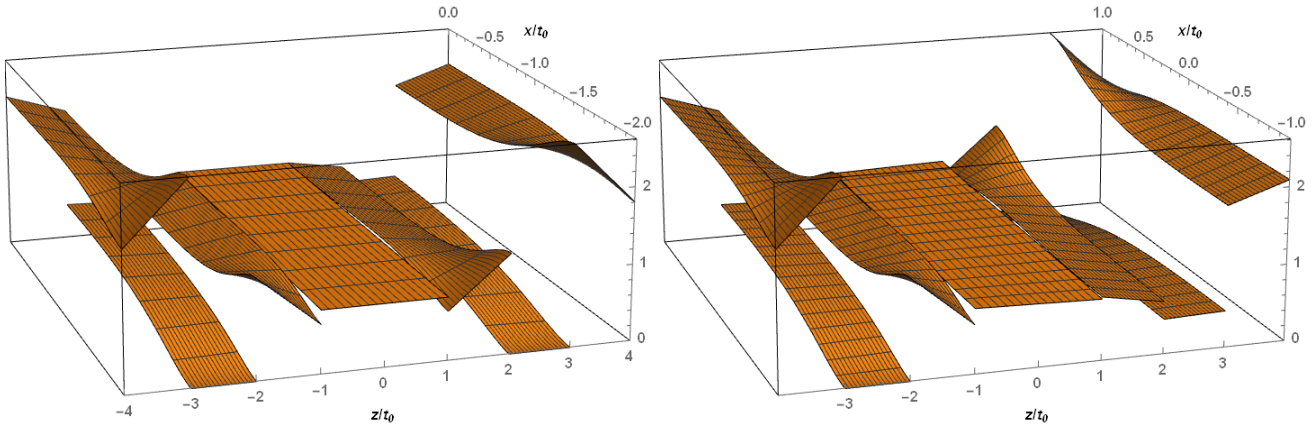

(a) symmetric (b) staggered

FIGURE 14: Normalized stress σ_{xx} in $[0/90/\mp 45]_S$

agreement with the experimental data of Hoover et al.[28] for both the laminates, except the measurements for very small crack densities, which fall markedly below the low bound curve. Whilst experimental measurements for non-symmetric laminates is difficult to interpret in general, it is especially hindered in the low crack density range where the relative location of the few existing cracks and the extensometer can introduce additional error in the test results.

8 | ADDITIONAL APPLICATIONS

8.1 | Ply refinement and compatibility

When experimental data is limited, FE simulations can be referred to as a benchmark for an analytical model. Although it does not necessarily implies good agreement between the results of the model and experimental measurements, comparison to FE could aim at demonstration of robustness of an analytical approach, gain in clarity of the results, reduced computational efforts, etc. Results of FE simulations for the effective stiffness can be seen as the upper bound and would approach the exact solution if a sequentially finer mesh is used.

In the present approach, the analogue of mesh size decrease is the ply refinement technique, when all the plies in a laminate or plies of a certain orientation are subdivided into several sub-plies (as it is done in Section 7.3). Although this increases the dimensions of the matrices one has to operate with, more detailed field description within the cracked material would emerge. Whilst the admissible stress field becomes more accurate and closer to the exact solution of the elasticity problem, a reduction in the value of the complementary energy would be expected with corresponding increase in the effective stiffness, leading to a better lower bound for the stiffness values.

In order to demonstrate this convergence (from below), predictions of the variational approach are compared to numerical FE results of Katerelos et al.[15] for the effective shear modulus of GFRP $[\pm 45/90_2]_S$ laminate, Figure 18. The bottom dashed line in the Figure corresponds to an analysis performed without ply refinement, when all adjacent laminae with the same fiber orientation are modeled as a single ply, as it is done in all the previous examples, except one in Figure 13. For the result represented by the middle dashed line, all plies were split into two sub-plies of the same thickness (total of 10 plies). The upper solid line corresponds to a model, when the plies are subdivided into four sub-plies each (total 20 plies), each sub-ply having different stress perturbation functions. It can be seen that the values of the effective shear modulus increase and approach the FE results of Katerelos et al.[15] when ply subdivision is employed. At the same time, the results without ply refinement are already quite close to the ones of FE and the effect of ply refinement is quite minor in this case, although this effect might be more noticeable if some plies are significantly thick.

The effect of ply refinement on the stress field for this laminate is illustrated in Figure 19a-c, where the in-plane shear stress distribution is plotted for a fragment length of $2\xi_0 = 4$. The laminate is subjected to a unit in-plane shear stress. It can be seen that the stress concentrations in the sub-plies adjacent to the cracked transverse ply increase and resemble stress singularities (Figure 19b,c) that should emerge at the crack tips in the exact solution. At the same time, it is interesting to emphasize that

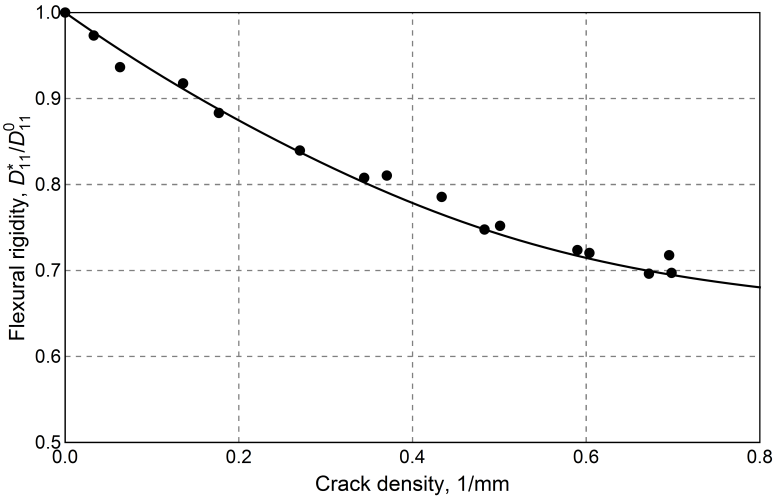

FIGURE 15: Flexural rigidity of $[90/0]_S$ as a function of crack density. Experimental data of Schmitz and Horst[27].

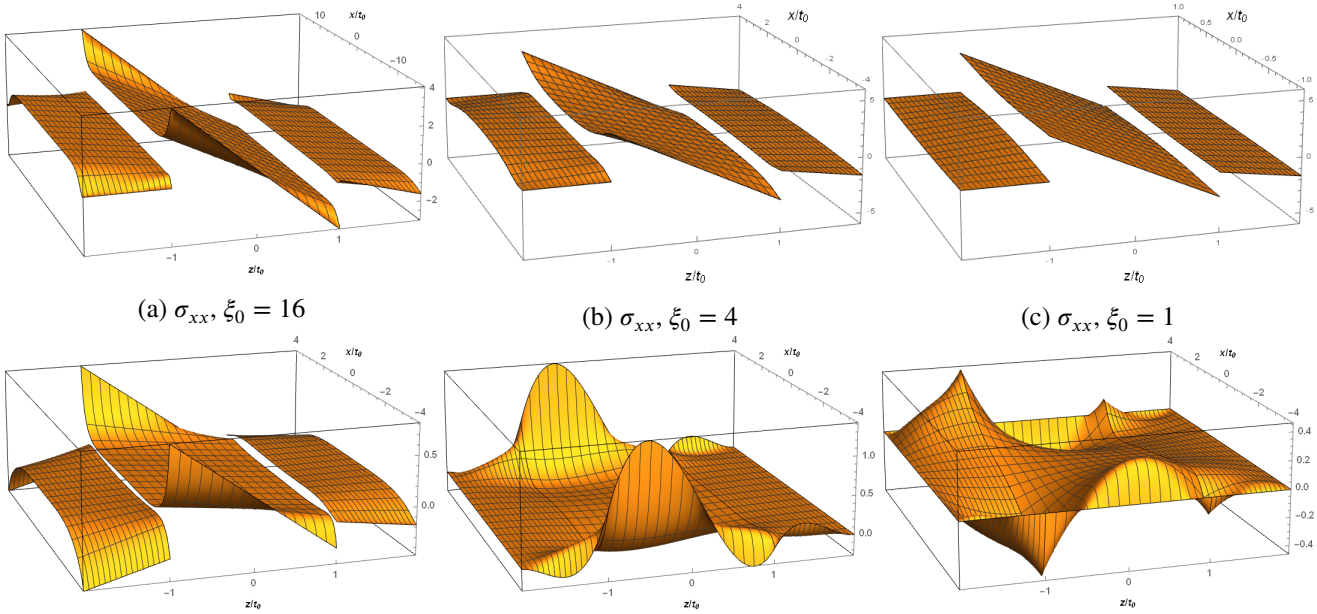

(a) σ_{xx}, $\xi_0 = 16$ (b) σ_{xx}, $\xi_0 = 4$ (c) σ_{xx}, $\xi_0 = 1$

(d) σ_{yy}, $\xi_0 = 4$ (e) σ_{zz}, $\xi_0 = 4$ (f) σ_{xz}, $\xi_0 = 4$

FIGURE 16: (a)-(c): Axial stress σ_{xx} in $[90/0]_S$ subjected to bending for different fragment lengths. (d)-(f) Other nonzero stress components for $\xi_0 = 4$.

comparison with experimental data in most of the examples above demonstrated a good agreement without employing refinement. A potential reason for this might be that the localized severe gradients do not necessarily reflect the realistic stress field in the material (see Hashin[2] for discussion on this matter).

Both in the example of Section 7.3 (Figure 13) and in the present example (Figure 19b,c), discontinuities in the stress distribution can be observed at the artificially introduced interfaces between the sub-plies. This is due to the fact that the admissible stress field is derived without the requirement of compatibility constraints. Further refinement would diminish the gaps, leading to a smoother stress transition over the interfaces. However, the method presented herein allows to incorporate some of the compatibility equations without significant hindrances. Continuity of displacements at the artificial interfaces requires continuity of the in-plane strains, and consequently, in-plane stresses, since the stiffnesses on the both sides of such an interface are the same

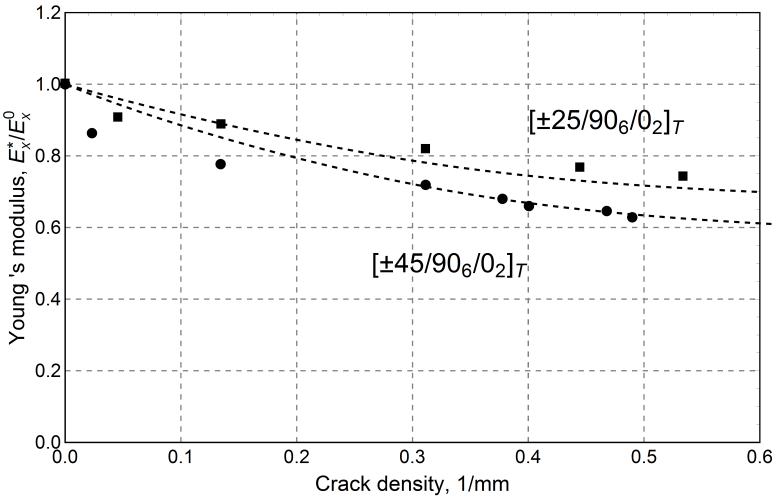

FIGURE 17: Young's modulus as a function of transverse crack density for non-symmetric laminates. Experimental data: Hoover et al.[28].

and the out-of-plane stresses are continuous. These stress continuity criteria for an interface between sub-plies i and $i+1$

$$\sigma^i_{1,2,6}\left(\xi, \zeta = \tfrac{1}{2}\right) - \sigma^{i+1}_{1,2,6}\left(\xi, \zeta = -\tfrac{1}{2}\right) = 0, \tag{105}$$

can be written in the form similar to (16):

$$\mathbf{B}_{\text{comp}}\mathbf{f}(\xi) = 0, \tag{106}$$

where matrix $\mathbf{B}_{\text{comp}}$ is obtained by substituting (14) into (105). Constraints (106) can simply be appended to (16). The method of Lagrange multipliers is a great convenience in this case, as the analysis does not change because of the increased number of constraints, with the exception of a reduced number of eigenvalues due to the additional constraints, which can easily be evaluated. The number of independent physical boundary conditions in (74) decreases as well, since some of the functions become linearly dependent through (106). Since the aim of the section is solely to demonstrate this additional capability of ply refinement and compatibility at the interfaces between sub-plies, the details will be explored elsewhere.

Figure 19d shows the continuous shear stress distribution calculated with the compatibility constraints at the interfaces between the sub-plies. In principle, displacement continuity at the interfaces between sub-plies also implies continuity of the interface in-plane curvatures, which are expressed in terms of strain derivatives and cannot be satisfied using the same approach. It is worth mentioning that the effect of the compatibility conditions on the effective shear modulus in the presented example is negligible. It is also worth noting that no compatibility criteria can be satisfied with a piece-wise constant through-the-thickness admissible stress field and that finer ply refinement would be required to achieve the same accuracy as with the present model.

8.2 | Closed cracks

When a laminate with existing intralaminar cracks is subjected to loadings that impose compression in the direction normal to the crack planes, crack closure should be expected. This might occur, for instance, when a cyclic load in alternating directions is applied and the accumulation of damage is to be assessed based on the varying with time stress field. Assuming frictionless contact between the crack surfaces, when the normal component of tractions does not vanish, but becomes continuous over the crack surfaces, the approach can easily be implemented in this case. The method of Lagrange multipliers is very convenient here, as the only alteration to be done is removal of the rows related to the normal component of the traction vector σ_1 while building the physical boundary conditions (74).

To illustrate the method applicability in this case, the effect of crack closure on the Young's and shear moduli is predicted for two GFRP angle-ply laminates having layups of $[\pm 75]_S$ and $[\pm 45]_S$ with mid-ply transverse cracks. It can be seen in Figure 20a that a significant increase in the Young's modulus occurs when the laminate is subjected to compression. Since the intralaminar cracks are inclined to the load direction, the crack surfaces will experience both normal and shear opening (sliding). It is clear that for this layup with the mid-ply being oriented close to 90 degrees, the normal component of the crack opening has a larger

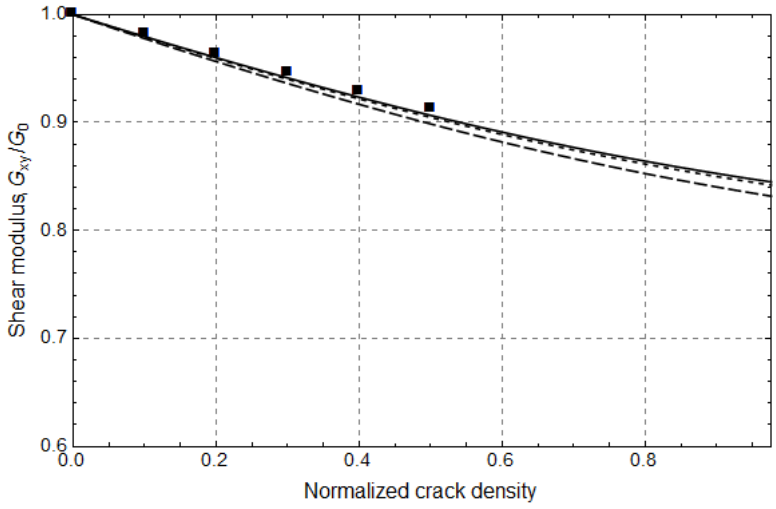

FIGURE 18: Normalized shear modulus of $[\pm 45/90_2]_S$ as a function of normalized crack density. Bottom (dashed) line: no refinement; middle (dashed) line - each ply is split in two sub-plies, $n = 2$; top (solid) line - each ply is split in four sub-plies, $n = 4$. Dots represent FE calculations of Katerelos et al.[15]

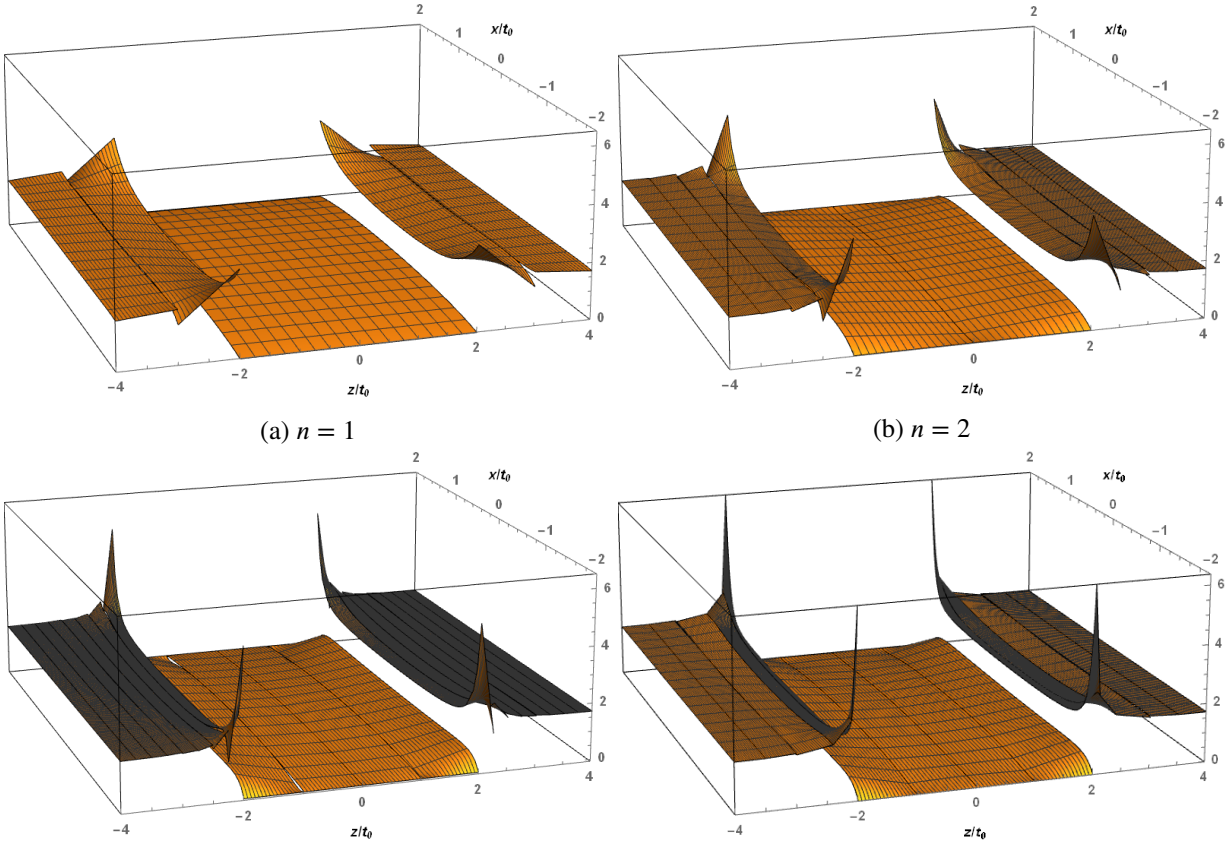

(a) $n = 1$ (b) $n = 2$

(c) $n = 4$ (d) compatibility

FIGURE 19: Effect of ply refinement on the shear stress distribution in $[\pm 45/90_2]_S$: (a) no ply refinement; (b) 2 sub-plies; (c) 4 sub-plies; (d) with compatibility constraints at the interfaces between the sub-plies.

contribution to the laminate compliance under axial tension than the shear component; when the cracks are closed, reduction in the Young's modulus is solely due to the relative sliding of the crack surfaces (zero shear stress on the closed crack surfaces). When the laminate is subjected to shear, the normal component of the crack opening plays a minor role, which is reflected in the similar values of the shear modulus in the two cases of open and closed cracks (Figure 20b).

For the $[\pm 45]_S$ laminate, Figure 21a, application of compressive loading and consequent crack closure has a minor effect on the Young's modulus reduction, mainly dominated by shear. The shear modulus of this laminate with closed cracks is predicted to be equal to the one of the laminate without any cracks (Figure 21b), since in the coordinate system associated with the fiber orientations, the cross-ply laminate experiences compression in the direction normal to the crack surfaces and tension along the crack surfaces, with no shear/sliding.

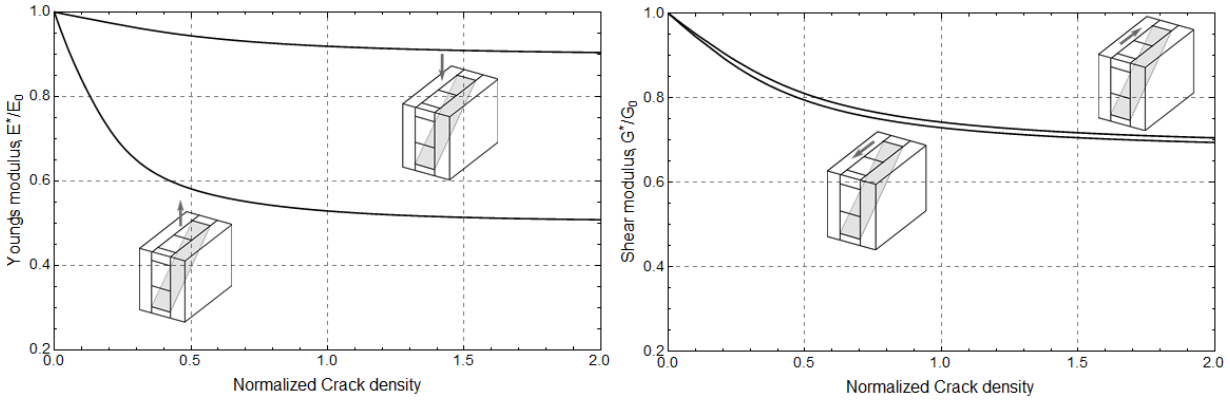

(a) (b)

FIGURE 20: Effect of crack closure on the effective Young's and shear moduli of $[\pm 75]_S$ GFRP.

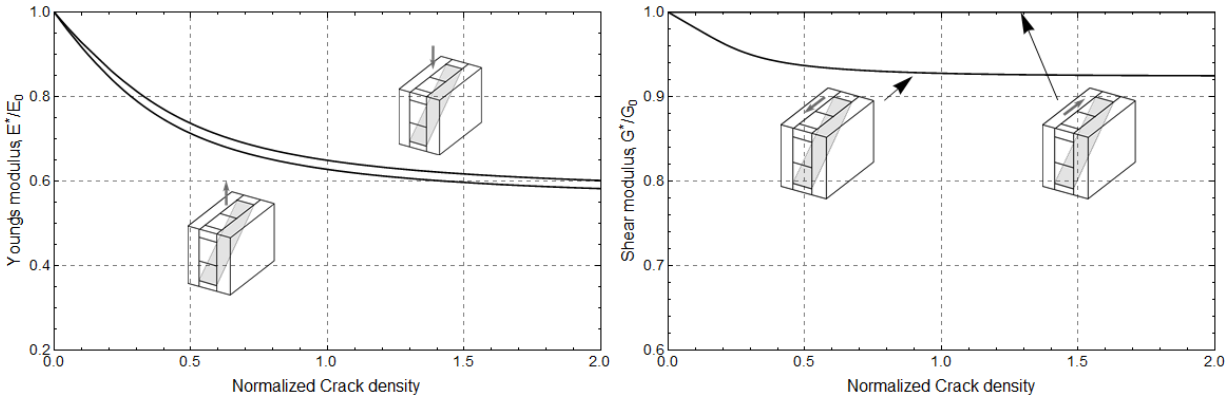

(a) (b)

FIGURE 21: Effect of crack closure on the effective Young's and shear moduli of $[\pm 45]_S$ GFRP.

Since the method is not limited to the case of in-plane membrane forces, analysis of crack closure due to bending can also be performed. The problem was looked at by Kuriakose and Talreja [16], who used a variational analysis, assuming crack opening over one half thickness of the transverse ply of $[0/90]_S$. In the following exercise, a GFRP cross-ply $[0/90_2]_S$ having a normalized transverse crack density of $c = 2x_0/t_{90^\circ} = 1$ is analyzed (Figure 22a). When the cracks are present, application of a bending moment causes partial crack closure on the compressed side of the laminate. Within the framework of the model, the transverse ply has to be split into two plies (or groups of plies), assuming different boundary conditions: zero traction should be imposed on

the plies with the open cracks, while only the shear components of traction should set to zero in the plies with the closed cracks, assuming frictionless contact. Since the problem can be viewed as an elastic contact between two adjacent fragments, the contact pressure should be continuous and equal to zero at the point of transition between the open and closed crack regions. Therefore, it is possible to determine the length of the open crack by varying the location of the interface between plies with open and closed cracks, searching for the location that corresponds to zero contact pressure σ_1 at the left tip of the closed crack (Figure 22a). Indeed, if the open crack is too long or too short, the stress analysis would reveal either positive or negative stress concentration at the transition point. For the presented example, the ratio between the lengths of the open and closed crack regions, which corresponds to a zero pressure at the edge of the contact zone (no stress concentrations), is found to be around ~ 2.0. This value would vary with crack density. It should be noticed that this result is obtained with an approximate stress field, and although ply refinement was used in this example to demonstrate stress singularities in the 0° ply and some nonlinearity in the shape of the contact pressure distribution (Figure 22b), it might slightly deviate from the true/exact value. The transition point is indicated with an arrow in Figure 22b. The method developed herein can further be used to investigate the effects of the crack density, laminate layup, location of the cracked ply within the laminate and residual thermal stresses on the length of partially closed crack and corresponding laminate curvatures.

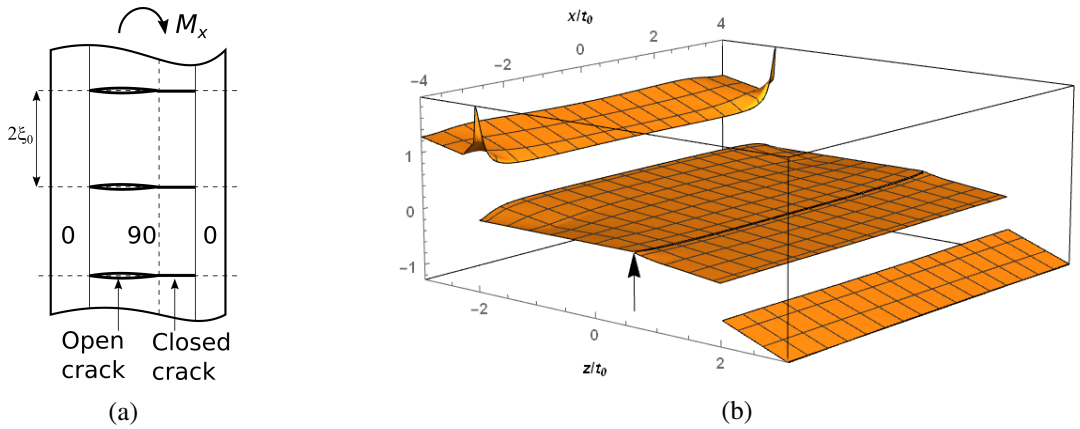

FIGURE 22: $[0/90_2]_S$ laminate under bending. (a) Schematic presentation of partial crack closure. (b) Stress $\sigma_{xx}(x, z)$. The arrow indicates the point between the open (to the left of the arrow) and closed (to the right of the arrow) crack surfaces.

8.3 | Extension to non-uniform crack distributions

Variational analysis of a symmetric laminate with non-uniform crack distribution has recently been looked at by Hajikazemi et.al.[33], where the perturbation stresses were assumed piece-wise constant in the z-direction. For some specific crack arrangements the authors also compared the resultant effective elastic properties and thermal expansions with FEM results and with a method of simplified account for non-uniform crack spacing, suggested by McCartney[34,12], and demonstrated agreement.

The method formulated in the present paper is not limited to symmetric laminates and can easily be extended to the case of non-uniform crack distribution (such as in Figure 2e). However, lack of periodicity requires modifications in both the complementary energy functional and boundary conditions. Whilst the eigenvalue problem formulated in Section 4 is independent of a particular crack distribution and results in the same set of eigenvalues and eigenvectors, determination of unknown constants should be carried out using minimization of the total complementary energy for the entire laminate. Periodicity conditions at the x-planes between adjacent fragments should be replaced with continuity conditions for the traction vector components at these planes.

Let the laminate under consideration comprise of n fragments of total normalized length L. The functional to be minimized is then

$$\mathcal{I} = \sum_{i=1}^{n} \mathcal{I}_k = \sum_{i=1}^{k} \mathbf{c}_k^{\mathrm{T}} \mathbf{W}_k(\tfrac{\xi^k}{\xi_0}) \mathbf{c}_k, \tag{107}$$

where ξ_0^k is the half length of fragment k. Since symmetry conditions do not necessarily hold in this case, the general expression (71) should be used, since it does not assume any specific boundary conditions. Then the matrix $\mathbf{W}_k$ for fragment k assumes the form

$$\mathbf{W}_k(\xi_0^k) = \left[\mathbf{U}^{\mathrm{T}}(\mathbf{M}^{11} - \mathbf{M}^{20} + \mathbf{M}^{02})\mathbf{U}' - \mathbf{U}^{\mathrm{T}}\mathbf{M}^{22}\mathbf{U}''' + \mathbf{U}'^{\mathrm{T}}\mathbf{M}^{22}\mathbf{U}''\right]_{-\xi_0^k}^{\xi_0^k}. \tag{108}$$

In the matrix form the functional can be presented as

$$\mathcal{I} = \mathbf{c}^{\mathrm{T}}\mathbf{W}\,\mathbf{c} = \begin{bmatrix}\mathbf{c}_1\\ \mathbf{c}_2\\ \vdots\\ \mathbf{c}_k\end{bmatrix}^{\mathrm{T}}\begin{bmatrix}\mathbf{W}_1(\xi_0^{(1)}) & \mathbf{0} & \dots & \mathbf{0}\\ \mathbf{0} & \mathbf{W}_2(\xi_0^{(2)}) & \dots & \mathbf{0}\\ \vdots & \vdots & \ddots & \vdots\\ \mathbf{0} & \mathbf{o} & \dots & \mathbf{W}_k(\xi_0^{(k)})\end{bmatrix}\begin{bmatrix}\mathbf{c}_1\\ \mathbf{c}_2\\ \vdots\\ \mathbf{c}_k\end{bmatrix}. \tag{109}$$

This functional is minimized subject to zero traction conditions on the crack surfaces described earlier, and traction continuity conditions for each ply m at the planes between two adjacent fragments k and $k+1$:

$$\begin{aligned}\sigma_1^{m,k}(\xi_0^k) - \sigma_1^{m,k+1}(-\xi_0^{k+1}) = 0\\ \sigma_6^{m,k}(\xi_0^k) - \sigma_6^{m,k+1}(-\xi_0^{k+1}) = 0\\ \sigma_5^{m,k}(\xi_0^k) - \sigma_5^{m,k+1}(-\xi_0^{k+1}) = 0\end{aligned} \tag{110}$$

$$\tag{111}$$

The continuity of stresses implies continuity of the mean stress terms and gradients for $\mathbf{f}_\alpha$ and $\mathbf{f}_\beta$, as well as the x-derivative of $\mathbf{f}_\alpha$:

$$\begin{aligned}\mathbf{f}_\alpha^k(\xi_0^k) - \mathbf{f}_\alpha^{k+1}(-\xi_0^{k+1}) = 0\\ \mathbf{f}_\beta^k(\xi_0^k) - \mathbf{f}_\beta^{k+1}(-\xi_0^{k+1}) = 0\\ \mathbf{f}_\alpha'^k(\xi_0^k) - \mathbf{f}_\alpha'^{k+1}(-\xi_0^{k+1}) = 0\end{aligned} \tag{112}$$

which should be applied to all independent plies ($m = 1, \dots, N_p - 1$). These conditions replace the symmetry conditions in (74) and with the zero traction boundary conditions for each crack plane form new matrices $\mathbf{B}_{\mathrm{bc}}$, $\mathbf{K}_{\mathrm{mech}}$ and $\mathbf{k}_{\mathrm{th}}$. These expanded matrices and the new $\mathbf{W}$ from (109) are used in (78) for evaluation of all the unknown constants. Calculation of the effective properties of the laminate follows (93)-(95), while replacing the length $2\xi_0$ with the total (normalized) length of the laminate

$$L = 2\sum_{i=1}^{n}\xi_0^k. \tag{113}$$

Figure 23 shows an illustration of such an analysis and results for stress distributions in a non-uniformly cracked laminate of layup $[90/\pm 45]_{\mathrm{S}}$. The assumed cracking scheme shown in Figure 23a divides the laminate into six fragments of different lengths, where the intralaminar cracks do not follow any specific pattern, neither symmetric nor staggered. The shear stress σ_{xz} does not vanish in the uncracked plies at the crack planes, but it is continuous between the fragments. The stress distributions in a particular fragment depend on the lengths of the adjacent/other fragments as well. It should be noticed that analysis requires an explicit cracking geometry, which in the case of different crack densities in different transverse plies requires an assumption regarding the actual crack locations. However, as demonstrated, once the cracking geometry is known, the method described above is straightforward and is not limited to a specific number of plies, laminate layup, materials, etc.

9 | SUMMARY

A variational approach is presented for analysis of cracked laminates with parallel arrays of intralaminar cracks. The in-plane stresses in the cracked laminate are assumed to be linear through the thickness functions in each ply, which allows analysis of non-symmetric laminates or laminates with non-symmetric crack distribution. Based on this assumption, an admissible stress filed was derived using equilibrium equations and continuity of tractions at the interfaces between plies. The functions that define the in-plane behavior of the stress tensor components were determined using the principle of minimum complementary energy.

The simpler form of the minimization problem leading to the effective thermoelastic moduli of a cracked laminate uses the Lagrange multipliers technique to incorporate boundary conditions for traction free surfaces. The solution steps can be summarized as follows:

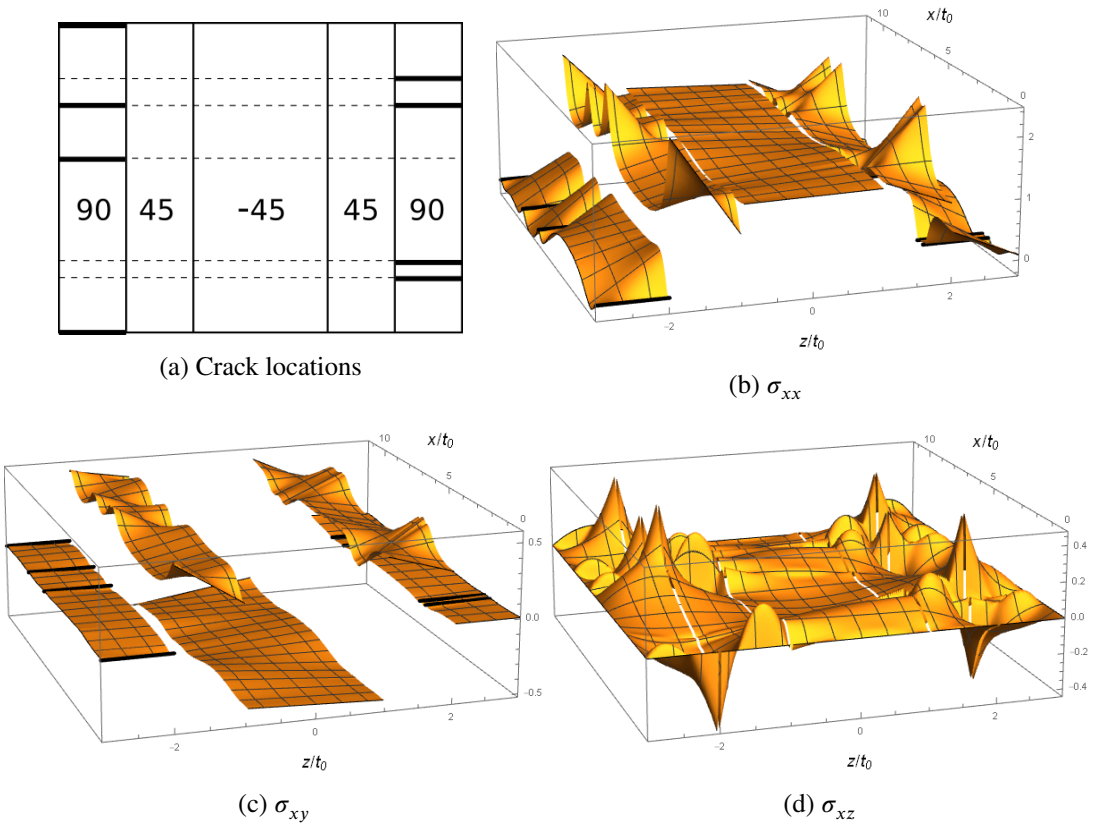

(a) Crack locations

(b) σ_{xx}

(c) σ_{xy}

(d) σ_{xz}

FIGURE 23: Crack locations (a) and corresponding stress distributions (b)-(d) in a non-symmetrically cracked laminate $[90/\pm 45]_S$. Thick black lines indicate the transverse crack locations.

1. For a laminate with a given layup and lamina material properties, calculate the elements of matrices $\mathbf{B}_{\text{eq}}$, $\mathbf{P}^{(m)}$ and $\mathbf{M}^{pq}$ using the expressions given in Appendix B and definition (19).
2. Solve the eigenvalue problem (69) for $6(N-1)$ nonzero eigenvalues and the corresponding eigenvectors, which are used to construct the general solution for the stress field (70).
3. For a curtain crack density (inter-crack spacing ξ_0), calculate matrix $\mathbf{W}(\xi_0)$ determined by (73) or its simplified variant (86).
4. For given crack arrays (e.g. aligned, staggered, etc.), assemble the matrix of boundary conditions $\mathbf{B}_{\text{bc}}$ (Section 3.2.1), stress concentration matrix $\mathbf{K}_{\text{mech}}$ and vector $\mathbf{k}_{\text{th}}$, as described in Appendix D.
5. Calculate the effective compliance $\mathbf{ABD}'$ (93), thermal expansions and curvatures $\boldsymbol{\alpha}$ (94) and specific heat c_p (95) of the cracked laminate.

The solution algorithm only requires several rather simple matrix operations, which makes it very convenient for implementation and potentially for incorporating into FE for a continuum damage type of analysis.

The extensive comparison to experimental data shown in Section 7 demonstrates the model's ability to accurately predict the effect of transverse cracks on the engineering elastic constants of laminates, independently on their layups. The potentials of the approach are complemented by its robustness, when all the thermoelastic properties of the cracked laminate are given by the corresponding entries in the effective compliance matrix and thermal expansions defined in Section 5, without the need for experimentally fitted parameters.

The ply refinement technique can be employed for laminates with thick plies or for comparison with FE results (Section 8.1). It allows subdivision of plies for a more accurate stress field estimation (at the cost of larger matrices one has to operate with). It has been shown that some compatibility constraints can also be taken into account for the interfaces between the sub-plies, which leads to a continuous stress transfer over the interfaces.

Adjustment of boundary conditions for the crack planes allows to employ the same mathematical formalism to analyze laminates with fully or partially closed cracks, Sections 8.2, as well as laminates with arbitrary spatial crack distribution along the laminate, Section 8.3.

It is worth noticing, that the derivation presented in Sections 4-5 is not limited to the assumed linear stress distribution. It will be valid for any in-plane perturbation stress expansion in the form

$$\sigma(x,z) = \sum_{i=1}^{n} f_i(x) g_i(z),$$

where $g_i(z)$ are explicit functions of z, as long as the expansion can satisfy the z-linear boundary conditions on the crack surfaces. If this approach is pursued instead of or in addition to ply refinement, the dimensions of the involved matrices and the corresponding number of eigenvalues should be adjusted accordingly.

ACKNOWLEDGMENT

The author would like to thank Prof Andrej Cherkaev of the University of Utah, whose lecture notes on Calculus of Variations served as an invaluable source of reference. The author is grateful to the referees for their helpful comments and suggestions.

References

1. Hashin Z. Analysis of Cracked Laminates: A Variational Approach. *Mechanics of Materials* 1985; 4(2): 121-136. doi: 10.1016/0167-6636(85)90011-0

2. Hashin Z. Analysis of Orthogonally Cracked Laminates under Tension. *Journal of Applied Mechanics* 1987; 54(4): 872-879. doi: 10.1115/1.3173131

3. Nairn JA. Matrix Microcracking in Composites. In: Kelly A, Zweben C., eds. *Comprehensive Composite Materials*. 2. Oxford: Pergamon. 2000 (pp. 403-432)

4. Hashin Z. Finite Thermoelastic Fracture Criterion with Application to Laminate Cracking Analysis. *Journal of the Mechanics and Physics of Solids* 1996; 44(7): 1129-1145. doi: 10.1016/0022-5096(95)00080-1

5. Vinogradov V, Hashin Z. Probabilistic Energy Based Model for Prediction of Transverse Cracking in Cross-Ply Laminates. *International Journal of Solids and Structures* 2005; 42(2): 365-392. doi: 10.1016/j.ijsolstr.2004.06.043

6. Nairn JA, Hu S. The Formation and Effect of Outer-Ply Microcracks in Cross-Ply Laminates: A Variational Approach. *Engineering Fracture Mechanics* 1992; 41(2): 203-221. doi: 10.1016/0013-7944(92)90181-D

7. Vinogradov V, Hashin Z. Variational Analysis of Cracked Angle-Ply Laminates. *Composites Science and Technology* 2010; 70(4): 638-646. doi: 10.1016/j.compscitech.2009.12.018

8. Katerelos DG, McCartney LN, Galiotis C. Effect of off – Axis Matrix Cracking on Stiffness of Symmetric Angle-Ply Composite Laminates. *International Journal of Fracture* 2006; 139(3-4): 529-536. doi: 10.1007/s10704-006-0100-9

9. Li S, Hafeez F. Variation-Based Cracked Laminate Analysis Revisited and Fundamentally Extended. *International Journal of Solids and Structures* 2009; 46(20): 3505-3515. doi: 10.1016/j.ijsolstr.2009.03.031

10. Hajikazemi M, Sadr MH, Hosseini-Toudeshky H, Mohammadi B. Thermo-Elastic Constants of Cracked Symmetric Laminates: A Refined Variational Approach. *International Journal of Mechanical Sciences* 2014; 89: 47-57. doi: 10.1016/j.ijmecsci.2014.08.008

11. Hajikazemi M, Sadr MH. A Variational Model for Stress Analysis in Cracked Laminates with Arbitrary Symmetric Lay-up under General in-Plane Loading. *International Journal of Solids and Structures* 2014; 51(2): 516-529. doi: 10.1016/j.ijsolstr.2013.10.024

12. McCartney L. Derivations of Energy-Based Modelling for Ply Cracking in General Symmetric Laminates. *Journal of Composite Materials* 2013; 47(20-21): 2641-2673. doi: 10.1177/0021998313492359

13. Hajikazemi M, McCartney LN. Comparison of Variational and Generalized Plane Strain Approaches for Matrix Cracking in General Symmetric Laminates. *International Journal of Damage Mechanics* 2018; 27(4): 507-540. doi: 10.1177/1056789516685381

14. Giannadakis K, Varna J. Potential of a Simple Variational Analysis in Predicting Shear Modulus of Laminates with Cracks in 90-Layers. *Journal of Composite Materials* 2014; 48(15): 1843-1856. doi: 10.1177/0021998313490976

15. Katerelos D, Krasnikovs A, Varna J. Variational Models for Shear Modulus of Symmetric and Balanced Laminates with Cracks in 90-Layer. *International Journal of Solids and Structures* 2015; 71: 169-179. doi: 10.1016/j.ijsolstr.2015.06.017

16. Kuriakose S, Talreja R. Variational Solutions to Stresses in Cracked Cross-Ply Laminates under Bending. *International Journal of Solids and Structures* 2004; 41(9): 2331-2347. doi: 10.1016/j.ijsolstr.2003.11.022

17. Hajikazemi M, Sadr MH, Talreja R. Variational Analysis of Cracked General Cross-Ply Laminates under Bending and Biaxial Extension. *International Journal of Damage Mechanics* 2015; 24(4): 582-624. doi: 10.1177/1056789514546010

18. Hajikazemi M, Sadr M, Varna J. Analysis of Cracked General Cross-Ply Laminates under General Bending Loads: A Variational Approach. *Journal of Composite Materials* 2017; 51(22): 3089-3109. doi: 10.1177/0021998316682364

19. Li S, Reid SR, Soden PD. A Finite Strip Analysis of Cracked Laminates. *Mechanics of Materials* 1994; 18(4): 289-311. doi: 10.1016/0167-6636(94)90041-8

20. Hashin Z. Thermal Expansion Coefficients of Cracked Laminates. *Composites Science and Technology* 1988; 31(4): 247-260. doi: 10.1016/0266-3538(88)90032-2

21. Levin VM. On the Coefficients of Thermal Expansion of Heterogeneous Materials. *Mekhanika Tverdogo Tela (in Russian)* 1967; 2: 88-94.

22. Joffe R, Krasnikovs A, Varna J. COD-Based Simulation of Transverse Cracking and Stiffness Reduction in [S/90n]s Laminates. *Composites Science and Technology* 2001; 61(5): 637-656. doi: 10.1016/S0266-3538(00)00172-X

23. Tsai CL, Daniel IM. The Behavior of Cracked Cross-Ply Composite Laminates under Shear Loading. *International Journal of Solids and structures* 1992; 29(24): 3251–3267. doi: 10.1016/0020-7683(92)90039-V

24. Kim RY, Crasto AS, Schoeppner GA. Dimensional Stability of Composite in a Space Thermal Environment. *Composites Science and Technology* 2000; 60(12): 2601-2608. doi: 10.1016/S0266-3538(00)00052-X

25. Varna J, Joffe R, Akshantala NV, Talreja R. Damage in Composite Laminates with Off-Axis Plies. *Composites Science and Technology* 1999; 59(14): 2139-2147. doi: 10.1016/S0266-3538(99)00070-6

26. Tong J, Guild FJ, Ogin SL, Smith PA. On Matrix Crack Growth in Quasi-Isotropic Laminates—I. Experimental Investigation. *Composites Science and Technology* 1997; 57(11): 1527-1535. doi: 10.1016/S0266-3538(97)00080-8

27. Schmitz A, Horst P. A Finite Element Unit-Cell Method for Homogenised Mechanical Properties of Heterogeneous Plates. *Composites Part A: Applied Science and Manufacturing* 2014; 61(Supplement C): 23-32. doi: 10.1016/j.compositesa.2014.01.014

28. Hoover JW, Kujawski D, Ellyin F. Transverse Cracking of Symmetric and Unsymmetric Glass-Fibre/Epoxy-Resin Laminates. *Composites Science and Technology* 1997; 57(11): 1513-1526. doi: 10.1016/S0266-3538(97)00082-1

29. Highsmith A, Reifsnider K. Stiffness-Reduction Mechanisms in Composite Laminates. In: Reifsnider K., ed. *Damage in Composite Materials: Basic Mechanisms, Accumulation, Tolerance, and Characterization*ASTM International. 1982 (pp. 103-117)

30. Knops M, Bögle C. Gradual Failure in Fibre/Polymer Laminates. *Composites Science and Technology* 2006; 66(5): 616-625. doi: 10.1016/j.compscitech.2005.07.044

31. Salavatian M, Smith L. A Novel Experimental Technique for Biaxial Testing of a Composite Laminate with Matrix Damage. *Journal of Composite Materials* 2016; 50(20): 2783-2792. doi: 10.1177/0021998315613125

32. Singh CV, Talreja R. A Synergistic Damage Mechanics Approach for Composite Laminates with Matrix Cracks in Multiple Orientations. *Mechanics of Materials* 2009; 41(8): 954-968. doi: 10.1016/j.mechmat.2009.02.008

33. Hajikazemi M, McCartney LN, Van Paepegem W, Sadr MH. Theory of Variational Stress Transfer in General Symmetric Composite Laminates Containing Non-Uniformly Spaced Ply Cracks. *Composites Part A: Applied Science and Manufacturing* 2018; 107: 374-386. doi: 10.1016/j.compositesa.2018.01.021

34. McCartney LN, Schoeppner GA. Predicting the Effect of Non-Uniform Ply Cracking on the Thermoelastic Properties of Cross-Ply Laminates. *Composites Science and Technology* 2002; 62(14): 1841-1856. doi: 10.1016/S0266-3538(02)00091-X

35. Rosen BW. Thermoelastic Energy Functions and Minimum Energy Principles for Composite Materials. *International Journal of Engineering Science* 1970; 8(1): 5-18. doi: 10.1016/0020-7225(70)90010-8

36. Rosen BW, Hashin Z. Effective Thermal Expansion Coefficients and Specific Heats of Composite Materials. *International Journal of Engineering Science* 1970; 8(2): 157-173. doi: 10.1016/0020-7225(70)90066-2

37. Lewiński T, Telega JJ. *Plates, Laminates, and Shells: Asymptotic Analysis and Homogenization*. Vol. 52 of *Series on Advances in Mathematics for Applied Sciences*. River Edge, NJ: World Scientific . 2000.

□

APPENDIX

A TRACTION ON EXTERNAL SURFACES

Consider equilibrium of stresses in coordinates without normalization. The differential equilibrium equations for the perturbation stresses have the form:

$$\begin{aligned}
\frac{\partial}{\partial x}\sigma_1(x,z) + \frac{\partial}{\partial z}\sigma_5(x,z) &= 0,\\
\frac{\partial}{\partial x}\sigma_6(x,z) + \frac{\partial}{\partial z}\sigma_4(x,z) &= 0,\\
\frac{\partial}{\partial x}\sigma_5(x,z) + \frac{\partial}{\partial z}\sigma_3(x,z) &= 0.
\end{aligned} \tag{A1}$$

The first two equations are integrated to get σ_5 and σ_4 taking into account that the stresses vanish on the free laminate surface $z = -h/2$:

$$\begin{aligned}
\sigma_5(x,z) &= -\int_{-h/2}^{z} \frac{\partial}{\partial x}\sigma_1(x,z)\,dz = -\frac{\partial}{\partial x}\int_{-h/2}^{z} \sigma_1(x,z)\,dz,\\
\sigma_4(x,z) &= -\int_{-h/2}^{z} \frac{\partial}{\partial x}\sigma_6(x,z)\,dz = -\frac{\partial}{\partial x}\int_{-h/2}^{z} \sigma_6(x,z)\,dz.
\end{aligned} \tag{A2}$$

At the external surface $z = h/2$ the above integrals become:

$$\begin{aligned}
\sigma_5(x,h/2) &= -\frac{d}{dx}\int_{-h/2}^{h/2} \sigma_1(x,z)\,dz = -\frac{d}{dx}N_1(x),\\
\sigma_4(x,h/2) &= -\frac{d}{dx}\int_{-h/2}^{h/2} \sigma_6(x,z)\,dz = -\frac{d}{dx}N_6(x),
\end{aligned} \tag{A3}$$

where N_1 and N_6 are the total perturbation membrane forces. The stress $\sigma_3(x, h/2)$ normal to the free surface is integrated using the third equilibrium equation in (A1):

$$\sigma_3(x,h/2) = -\int_{-h/2}^{h/2} \frac{\partial}{\partial x}\sigma_5(x,z)\,dz = \frac{d^2}{dx^2}\int_{-h/2}^{h/2}\int_{-h/2}^{z} \sigma_1(x,z')\,dz'\,dz. \tag{A4}$$

By changing the order of integration in the above integral,

$$\begin{aligned}\sigma_3(x,h/2) &= \frac{d^2}{dx^2}\int_{-h/2}^{h/2}\int_{z'}^{h/2} \sigma_1(x,z')\,dz\,dz' = \frac{d^2}{dx^2}\int_{-h/2}^{h/2}\left(h/2 - z'\right)\sigma_1(x,z')\,dz' \\ &= \frac{d^2}{dx^2}\left(\frac{h}{2}\int_{-h/2}^{h/2}\sigma_1(x,z)\,dz - \int_{-h/2}^{h/2} z\sigma_1(x,z)\,dz\right) = \frac{h}{2}\frac{d^2}{dx^2}N_1(x) - \frac{d^2}{dx^2}M_1(x),\end{aligned} \tag{A5}$$

where M_1 is the bending moment due to the perturbation stresses. Relations (A3) and (A5) were derived in Li and Hafeez[9] for piecewise constant through the thickness perturbation stress functions using their explicit integration. As shown herein, the relations hold for any arbitrary perturbation stress functions that independent of coordinate y. Since the total perturbation forces and moments should vanish, the traction vector on the external surface $z = h/2$ vanishes automatically.

B COEFFICIENTS

Indexes of the matrix elements below correspond to $\mathbf{f}(x)$ as shown in (15), such that functions that define the stresses in ply i are given by the following entries:

$$[f]_{6i-5} = \phi_1^{(i)}, \qquad [f]_{6i-3} = \phi_6^{(i)}, \qquad [f]_{6i-1} = \phi_2^{(i)},$$

$$[f]_{6i-4} = \psi_1^{(i)}, \qquad [f]_{6i-2} = \psi_6^{(i)}, \qquad [f]_{6i} = \psi_2^{(i)}.$$

For the matrices below only nonzero entries are shown with $S_{ij}^{(m)}$ being elements of the compliance matrix of ply m in the coordinate system of the problem (axis x is normal to the crack planes).

Elements of matrices $\mathbf{A}_p^{(m)}(\zeta)$, ($p = 0, 1, 2$, and $i = 1, 2, \ldots m-1$).

$$[A_0^{(m)}]_{1,6m-5} = [A_0^m]_{2,6m-1} = [A_0^m]_{6,6m-3} = 1, \qquad [A_0^{(m)}]_{1,6m-4} = [A_0^m]_{2,6m} = [A_0^m]_{6,6m-2} = \zeta,$$

$$[A_1^{(m)}]_{5,6i-5} = [A_1^m]_{4,6i-3} = -\lambda_i, \qquad [A_1^{(m)}]_{5,6m-5} = [A_1^m]_{4,6m-3} = -\tfrac{1}{2}\lambda_m(1+2\zeta),$$

$$[A_1^{(m)}]_{5,6m-4} = [A_1^m]_{4,6m-2} = \tfrac{1}{8}\lambda_m(1-4\zeta^2),$$

$$[A_2^{(m)}]_{3,6i-5} = \tfrac{1}{2}\lambda_i\left(\lambda_i + 2\sum_{j=i+1}^{m-1}\lambda_j + \lambda_m(1+2\zeta)\right), \qquad [A_2^{(m)}]_{3,6i-4} = -\tfrac{1}{12}\lambda_i^2,$$

$$[A_2^{(m)}]_{3,6m-5} = \tfrac{1}{8}\lambda_m^2(1+2\zeta)^2, \qquad [A_2^{(m)}]_{3,6m-4} = -\tfrac{1}{24}\lambda_m^2(1+2\zeta)^2(1-\zeta).$$

Elements of matrix $\mathbf{B}_{\text{eq}}$, ($i = 1, 2, \ldots, N$).

$$[B_{\text{eq}}]_{1,6i-5} = [B_{\text{eq}}]_{2,6i-1} = [B_{\text{eq}}]_{3,6i-3} = t_0\lambda_i,$$

$$[B_{\text{eq}}]_{4,6i-5} = [B_{\text{eq}}]_{5,6i-1} = [B_{\text{eq}}]_{6,6i-3} = \tfrac{1}{2}t_0^2\lambda_i\left(\sum_{k=1}^{i-1}\lambda_k - \sum_{k=i+1}^{N}\lambda_k\right),$$

$$[B_{\text{eq}}]_{4,6i-4} = [B_{\text{eq}}]_{5,6i} = [B_{\text{eq}}]_{6,6i-2} = \tfrac{1}{12}t_0^2\lambda_i^2.$$

Elements of matrix $\mathbf{P}_{00}^{(m)}$.

$$[P_{00}^{(m)}]_{6m-5,6m-5} = S_{11}^{(m)}, \qquad [P_{00}^{(m)}]_{6m-4,6m-4} = \tfrac{1}{12} S_{11}^{(m)},$$

$$[P_{00}^{(m)}]_{6m-1,6m-1} = S_{22}^{(m)}, \qquad [P_{00}^{(m)}]_{6m,6m} = \tfrac{1}{12} S_{22}^{(m)},$$

$$[P_{00}^{(m)}]_{6m-3,6m-3} = S_{66}^{(m)}, \qquad [P_{00}^{(m)}]_{6m-2,6m-2} = \tfrac{1}{12} S_{66}^{(m)},$$

$$[P_{00}^{(m)}]_{6m-5,6m-1} = [P_{00}^{(m)}]_{6m-1,6m-5} = S_{12}^{(m)}, \qquad [P_{00}^{(m)}]_{6m-4,6m} = [P_{00}^{(m)}]_{6m,6m-4} = \tfrac{1}{12} S_{12}^{(m)},$$

$$[P_{00}^{(m)}]_{6m-5,6m-3} = [P_{00}^{(m)}]_{6m-3,6m-5} = S_{16}^{(m)}, \qquad [P_{00}^{(m)}]_{6m-4,6m-2} = [P_{00}^{(m)}]_{6m-2,6m-4} = \tfrac{1}{12} S_{16}^{(m)},$$

$$[P_{00}^{(m)}]_{6m-3,6m-1} = [P_{00}^{(m)}]_{6m-1,6m-3} = S_{26}^{(m)}, \qquad [P_{00}^{(m)}]_{6m-2,6m} = [P_{00}^{(m)}]_{6m,6m-2} = \tfrac{1}{12} S_{26}^{(m)}.$$

Elements of matrix $\mathbf{P}_{02}^{(m)}$, $(i = 1, 2, \ldots, m-1)$, $\mathbf{P}_{20}^{(m)} = (\mathbf{P}_{02}^{(m)})^T$.

$$[P_{02}^{(m)}]_{6m-5,6i-5} = \tfrac{1}{2}\lambda_i \left(\lambda_i + 2 \sum_{k=i+1}^{m-1} \lambda_k + \lambda_m \right) S_{13}^{(m)}, \qquad [P_{02}^{(m)}]_{6m-5,6m-5} = \tfrac{1}{6}\lambda_m^2 S_{13}^{(m)},$$

$$[P_{02}^{(m)}]_{6m-1,6i-5} = \tfrac{1}{2}\lambda_i \left(\lambda_i + 2 \sum_{k=i+1}^{m-1} \lambda_k + \lambda_m \right) S_{23}^{(m)}, \qquad [P_{02}^{(m)}]_{6m-1,6m-5} = \tfrac{1}{6}\lambda_m^2 S_{23}^{(m)},$$

$$[P_{02}^{(m)}]_{6m-3,6i-5} = \tfrac{1}{2}\lambda_i \left(\lambda_i + 2 \sum_{k=i+1}^{m-1} \lambda_k + \lambda_m \right) S_{36}^{(m)}, \qquad [P_{02}^{(m)}]_{6m-3,6m-5} = \tfrac{1}{6}\lambda_m^2 S_{36}^{(m)},$$

$$[P_{02}^{(m)}]_{6m-5,6i-4} = -\tfrac{1}{12}\lambda_i^2 S_{13}^{(m)}, \qquad [P_{02}^{(m)}]_{6m-5,6m-4} = -\tfrac{1}{24}\lambda_m^2 S_{13}^{(m)},$$

$$[P_{02}^{(m)}]_{6m-1,6i-4} = -\tfrac{1}{12}\lambda_i^2 S_{23}^{(m)}, \qquad [P_{02}^{(m)}]_{6m-1,6m-4} = -\tfrac{1}{24}\lambda_m^2 S_{23}^{(m)}$$

$$[P_{02}^{(m)}]_{6m-3,6i-4} = -\tfrac{1}{12}\lambda_i^2 S_{36}^{(m)}, \qquad [P_{02}^{(m)}]_{6m-3,6m-4} = -\tfrac{1}{24}\lambda_m^2 S_{36}^{(m)},$$

$$[P_{02}^{(m)}]_{6m-4,6i-5} = \tfrac{1}{12}\lambda_i\lambda_m S_{13}^{(m)}, \qquad [P_{02}^{(m)}]_{6m-4,6m-5} = \tfrac{1}{24}\lambda_m^2 S_{13}^{(m)},$$

$$[P_{02}^{(m)}]_{6m,6i-5} = \tfrac{1}{12}\lambda_i\lambda_m S_{23}^{(m)}, \qquad [P_{02}^{(m)}]_{6m,6m-5} = \tfrac{1}{24}\lambda_m^2 S_{23}^{(m)}$$

$$[P_{02}^{(m)}]_{6m-2,6i-5} = \tfrac{1}{12}\lambda_i\lambda_m S_{36}^{(m)}, \qquad [P_{02}^{(m)}]_{6m-2,6m-5} = \tfrac{1}{24}\lambda_m^2 S_{36}^{(m)},$$

$$[P_{02}^{(m)}]_{6m-4,6m-4} = -\tfrac{1}{120}\lambda_m^2\lambda_i S_{13}^{(m)}, \qquad [P_{02}^{(m)}]_{6m,6m-4} = -\tfrac{1}{120}\lambda_m^2 S_{23}^{(m)},$$

$$[P_{02}^{(m)}]_{6m-2,6m-4} = -\tfrac{1}{120}\lambda_m^2 S_{36}^{(m)}.$$

Elements of matrix $\mathbf{P}_{11}^{(m)}$, $(i, j = 1, 2, \ldots, m-1)$.

$$[P_{11}^{(m)}]_{6i-5,6j-5} = \lambda_i\lambda_j S_{55}^{(m)},$$

$$[P_{11}^{(m)}]_{6m-5,6m-5} = \tfrac{1}{3}\lambda_m^2 S_{55}^{(m)},$$

$$[P_{11}^{(m)}]_{6i-5,6m-5} = [P_{11}^{(m)}]_{6m-5,6i-5} = \tfrac{1}{2}\lambda_i\lambda_m S_{55}^{(m)},$$

$$[P_{11}^{(m)}]_{6i-5,6m-4} = [P_{11}^{(m)}]_{6m-4,6i-5} = -\tfrac{1}{12}\lambda_i\lambda_m S_{55}^{(m)},$$

$$[P_{11}^{(m)}]_{6m-5,6m-4} = [P_{11}^{(m)}]_{6m-4,6m-5} = -\tfrac{1}{24}\lambda_m^2 S_{55}^{(m)},$$

$$[P_{11}^{(m)}]_{6m-4,6m-4} = \tfrac{1}{120}\lambda_m^2 S_{55}^{(m)},$$

$$[P_{11}^{(m)}]_{6i-3,6j-3} = \lambda_i\lambda_j S_{44}^{(m)},$$

$$[P_{11}^{(m)}]_{6m-3,6m-3} = \tfrac{1}{3}\lambda_m^2 S_{44}^{(m)},$$

$$[P_{11}^{(m)}]_{6i-3,6m-3} = [P_{11}^{(m)}]_{6m-3,6i-3} = \tfrac{1}{2}\lambda_i\lambda_m S_{44}^{(m)},$$

$$[P_{11}^{(m)}]_{6m-2,6m-2} = \tfrac{1}{120}\lambda_m^2 S_{44}^{(m)},$$

$$[P_{11}^{(m)}]_{6i-3,6m-2} = [P_{11}^{(m)}]_{6m-2,6i-3} = -\tfrac{1}{12}\lambda_i\lambda_m S_{44}^{(m)},$$

$$[P_{11}^{(m)}]_{6m-3,6m-2} = [P_{11}^{(m)}]_{6m-2,6m-3} = -\tfrac{1}{24}\lambda_m^2 S_{44}^{(m)},$$

$$[P_{11}^{(m)}]_{6i-3,6j-5} = [P_{11}^{(m)}]_{6i-5,6j-3} = \lambda_i\lambda_j S_{45}^{(m)},$$

$$[P_{11}^{(m)}]_{6m-3,6m-5} = [P_{11}^{(m)}]_{6m-5,6m-3} = \tfrac{1}{3}\lambda_m^2 S_{45}^{(m)},$$

$$[P_{11}^{(m)}]_{6i-3,6m-5} = [P_{11}^{(m)}]_{6m-3,6i-5} = [P_{11}^{(m)}]_{6i-5,6m-3} = [P_{11}^{(m)}]_{6m-5,6i-3} = \tfrac{1}{2}\lambda_i\lambda_m S_{45}^{(m)},$$

$$[P_{11}^{(m)}]_{6i-3,6m-4} = [P_{11}^{(m)}]_{6m-4,6i-3} = [P_{11}^{(m)}]_{6i-5,6m-2} = [P_{11}^{(m)}]_{6m-2,6i-5} = -\tfrac{1}{12}\lambda_i\lambda_m S_{45}^{(m)},$$

$$[P_{11}^{(m)}]_{6m-3,6m-4} = [P_{11}^{(m)}]_{6m-4,6m-3} = [P_{11}^{(m)}]_{6m-2,6m-5} = [P_{11}^{(m)}]_{6m-5,6m-2} = -\tfrac{1}{24}\lambda_m^2 S_{45}^{(m)},$$

$$[P_{11}^{(m)}]_{6m-2,6m-4} = [P_{11}^{(m)}]_{6m-4,6m-2} = \tfrac{1}{120}\lambda_m^2 S_{45}^{(m)}.$$

Elements of matrix $\mathbf{P}_{22}^{(m)}$, $(i, j = 1, 2, \ldots, m-1)$.

$$[P_{22}^{(m)}]_{6i-5,6j-5} = \tfrac{1}{12}\lambda_i\lambda_j\left[3\left(\lambda_i + 2\sum_{k=i+1}^{m-1}\lambda_k + \lambda_m\right)\left(\lambda_j + 2\sum_{k=j+1}^{m-1}\lambda_k + \lambda_m\right) + \lambda_m^2\right]S_{33}^{(m)}$$

$$[P_{22}^{(m)}]_{6i-5,6m-5} = [P_{22}^{(m)}]_{6m-5,6i-5} = \tfrac{1}{24}\lambda_i\lambda_m^2\left[2\left(\lambda_i + 2\sum_{k=i+1}^{m-1}\lambda_k + \lambda_m\right) + \lambda_m\right]S_{33}^{(m)},$$

$$[P_{22}^{(m)}]_{6m-5,6m-5} = \tfrac{1}{20}\lambda_m^4 S_{33}^{(m)},$$

$$[P_{22}^{(m)}]_{6i-4,6j-4} = \tfrac{1}{144}\lambda_i^2\lambda_j^2 S_{33}^{(m)},$$

$$[P_{22}^{(m)}]_{6i-4,6m-4} = [P_{22}^{(m)}]_{6m-4,6i-4} = \tfrac{1}{288}\lambda_i^2\lambda_m^2 S_{33}^{(m)},$$

$$[P_{22}^{(m)}]_{6m-4,6m-4} = \tfrac{13}{5040}\lambda_m^4 S_{33}^{(m)},$$

$$[P_{22}^{(m)}]_{6i-5,6j-4} = [P_{22}^{(m)}]_{6j-4,6i-5} = -\tfrac{1}{24}\lambda_i\lambda_j^2\left(\lambda_i + 2\sum_{k=i+1}^{m-1}\lambda_k + \lambda_m\right)S_{33}^{(m)},$$

$$[P_{22}^{(m)}]_{6i-5,6m-4} = [P_{22}^{(m)}]_{6m-4,6i-5} = -\tfrac{1}{240}\lambda_i\lambda_m^2\left[5\left((\lambda_i + 2\sum_{k=i+1}^{m-1}\lambda_k + \lambda_m\right) + 2\lambda_m\right]S_{33}^{(m)},$$

$$[P_{22}^{(m)}]_{6i-4,6m-5} = [P_{22}^{(m)}]_{6m-5,6i-4} = -\tfrac{1}{72}\lambda_i^2\lambda_m^2 S_{33}^{(m)},$$

$$[P_{22}^{(m)}]_{6m-5,6m-4} = [P_{22}^{(m)}]_{6m-4,6m-5} = -\tfrac{1}{90}\lambda_m^4 S_{33}^{(m)}.$$

C COMPLEMENTARY ENERGY OF A COMPOSITE PLATE IN THE THERMOELASTIC CASE

The following is an extension of the work of Levin[21], Rosen[35] and Rosen and Hashin[36] to the case of a laminate plate. Consider a heterogeneous thin plate in the xy plane of area A bounded by a closed contour $\mathcal{L}$. The plate is loaded by in-plane membrane forces $N_{\alpha\beta}$ and moments $M_{\alpha\beta}$ $(\alpha, \beta = x, y)$ and subjected to temperature change ΔT. one can represent the total stresses and strains as a superposition

$$\boldsymbol{\sigma} = \boldsymbol{\sigma}_{\mathrm{m}} + \boldsymbol{\sigma}_{\mathrm{th}}, \quad \boldsymbol{\varepsilon} = \boldsymbol{\varepsilon}_{\mathrm{m}} + \boldsymbol{\varepsilon}_{\mathrm{th}}, \tag{C6}$$

where the terms with the subscript 'm' correspond to fields induced by mechanical loads at the stress-free temperature, and the terms with subscript 'th' correspond to fields due to the temperature change and zero tractions on the external surfaces. Using the principle of virtual work, it can be shown that for any heterogeneous solid the following identities hold:

$$\begin{aligned}
&\int_V \boldsymbol{\sigma}_{\mathrm{th}}\boldsymbol{\varepsilon}_{\mathrm{m}} dV = \int_V \boldsymbol{\sigma}_{\mathrm{th}}\mathbf{S}\boldsymbol{\sigma}_{\mathrm{m}} dV = 0,\\
&\int_V \boldsymbol{\sigma}_{\mathrm{th}}\boldsymbol{\varepsilon}_{\mathrm{th}} dV = 0,\\
&\int_V \boldsymbol{\sigma}_{\mathrm{m}}\boldsymbol{\varepsilon}_{\mathrm{th}} dV = \int_V \boldsymbol{\sigma}_{\mathrm{m}}(\mathbf{S}\boldsymbol{\sigma}_{\mathrm{th}} + \boldsymbol{\alpha}\Delta T) dV = \int_V \boldsymbol{\sigma}_{\mathrm{m}}\boldsymbol{\alpha}\Delta T dV.
\end{aligned} \tag{C7}$$

Substitution of (C6) and (C7) into (87) yields

$$\mathcal{U}_C = \int_V \left(\frac{1}{2}\boldsymbol{\sigma}_{\mathrm{m}}\boldsymbol{\varepsilon}_{\mathrm{m}} + \boldsymbol{\sigma}_{\mathrm{m}}\boldsymbol{\varepsilon}_{\mathrm{th}} + \frac{1}{2}\boldsymbol{\sigma}_{\mathrm{th}}\boldsymbol{\alpha}\Delta T - \frac{1}{2}c_p\frac{\Delta T^2}{T_0}\right) dV. \tag{C8}$$

The last two terms are quadratic in ΔT and define the effective specific heat c_p^*. Using the principle of virtual work and the divergence theorem, work done by the mechanical stresses on any strain field can be expressed in terms of the in-plane forces and moments:

$$\begin{aligned}
\int_V \boldsymbol{\sigma}_{\mathrm{m}}\boldsymbol{\varepsilon}\, dV &= \oint_{\mathcal{L}} (N_{\alpha\beta}u_\alpha^0 + M_{\alpha\beta}u_{\alpha,z}^0)n_\beta\, d\mathcal{L} = N_{\alpha\beta}\oint_{\mathcal{L}} u_\alpha^0 n_\beta\, d\mathcal{L} + M_{\alpha\beta}\oint_{\mathcal{L}} u_{\alpha,z}^0 n_\beta\, d\mathcal{L}\\
&= N_{\alpha\beta}\int_A \varepsilon_{\alpha\beta}\, dA + M_{\alpha\beta}\int_A \varepsilon_{\alpha\beta,z}\, dA = (N_{\alpha\beta}\bar{\varepsilon}_{\alpha\beta} + M_{\alpha\beta}\bar{\kappa}_{\alpha\beta})A = \mathbf{t}^{\mathrm{T}}\bar{\boldsymbol{\varepsilon}}\, A.
\end{aligned} \tag{C9}$$

Here u^0 and $u_{,z}^0$ represent displacements and rotations of the plate edges, $\bar{\varepsilon}$ and $\bar{\kappa}$ are the average in-plane strains and curvatures of the plate, respectively, and the last equality utilizes the vector notations. The above expressions are valid for a cracked plate as well, since the surface integrals vanish over the crack planes due to zero tractions on the crack faces. For a mathematically rigorous introduction of the average curvature tensor for a general anisotropic plate, one can refer to Leviński and Telega[37].

Introducing the linear relation $\boldsymbol{\varepsilon}_{\mathrm{m}} = \mathbf{S}^*\mathbf{t}$ and recognizing that $\bar{\boldsymbol{\varepsilon}}_{\mathrm{th}} = \boldsymbol{\alpha}^*\Delta T$ where $\boldsymbol{\alpha}^*$ represent the thermally induced in-plane expansions and curvatures per unit temperature, the energy in (C8) can be written as

$$\mathcal{U}_C = \left(\frac{1}{2}\mathbf{t}^{\mathrm{T}}\mathbf{S}^*\mathbf{t} + \mathbf{t}^{\mathrm{T}}\boldsymbol{\alpha}^*\Delta T - \frac{1}{2}c_p^*\frac{\Delta T^2}{T_0}\right) A, \tag{C10}$$

which for a unit width of the composite plate reduces to (88) and (89).

D BOUNDARY CONDITIONS (CLASSICAL LAMINATE THEORY)

The solution of the Classical Laminate Theory is reformulated herein, using the principle of minimum complementary energy. This leads to both the effective thermoelastic properties of an uncracked laminate and stresses in each ply simultaneously in the

same format and in terms of the same matrices as for the cracked material, which simplifies assembly of matrices forming the boundary conditions on the crack surfaces.

Consider an uncracked laminate subjected to membrane forces and bending moments $\mathbf{t} = [N_x, N_y, N_{xy}, M_x, M_y, M_{xy}]^{\mathrm{T}}$ and temperature change ΔT. The in-plane stresses in each ply m, $m = 1, 2 \ldots N$, are linear functions of z and independent of x, implying that both the average in-plane stresses and the gradient terms are constants. The stresses can then be written using the expression (14):

$$\boldsymbol{\sigma}^m(\zeta) = \mathbf{A}_0^{(m)}(\zeta)\mathbf{f}, \tag{D11}$$

while the derivatives of $\mathbf{f}$ vanish. The matrix expression for the stresses is now substituted into the complementary energy expression (87):

$$\begin{aligned} \mathcal{U}_C^0 &= t_0 L \sum_m \lambda_m \int_{-\frac{1}{2}}^{\frac{1}{2}} \left(\frac{1}{2}\mathbf{f}^{\mathrm{T}}\mathbf{A}_0^{(m)^{\mathrm{T}}}\mathbf{S}^{(m)}\mathbf{A}_0^{(m)}\mathbf{f} + \mathbf{f}^{\mathrm{T}}\mathbf{A}_0^{(m)^{\mathrm{T}}}\boldsymbol{\alpha}^{(m)}\Delta T - \frac{1}{2}c_p\frac{\Delta T^2}{T_0} \right) d\zeta \\ &= t_0 L \left(\frac{1}{2}\mathbf{f}^{\mathrm{T}}\mathbf{M}^{00}\mathbf{f} + \mathbf{f}^{\mathrm{T}}\mathbf{b}_{\mathrm{th}}\Delta T - \frac{1}{2}\bar{c}_p\frac{\Delta T^2}{T_0} \right), \end{aligned} \tag{D12}$$

where $\mathbf{M}^{00}$ is the same matrix as in (19), $\boldsymbol{\alpha}^{(m)} = [\alpha_1^{(m)}, \alpha_2^{(m)}, 0, 0, 0, \alpha_6^{(m)}]^{\mathrm{T}}$, $\bar{c}_p = \sum_m \lambda_m c_p^{(m)}$, and vector $\mathbf{b}_{\mathrm{th}}$ is defined as

$$\mathbf{b}_{\mathrm{th}} = \sum_m \lambda_m \left[\int_{-\frac{1}{2}}^{\frac{1}{2}} \mathbf{A}_0^{(m)^{\mathrm{T}}}(\zeta)\, d\zeta \right] \boldsymbol{\alpha}^{(m)}. \tag{D13}$$

After integration of the elements of matrices $\mathbf{A}_0^{(m)}$ the vector $\mathbf{b}_{\mathrm{th}}$ becomes:

$$\mathbf{b}_{\mathrm{th}} = \begin{bmatrix} \mathbf{b}_{\mathrm{th}}^{(1)} \\ \mathbf{b}_{\mathrm{th}}^{(2)} \\ \vdots \\ \mathbf{b}_{\mathrm{th}}^{(N)} \end{bmatrix}, \quad \text{where} \quad \mathbf{b}_{\mathrm{th}}^{(m)} = \lambda_m \left[\alpha_1^{(m)},\ 0,\ \alpha_6^{(m)},\ 0,\ \alpha_2^{(m)},\ 0 \right]^{\mathrm{T}} \tag{D14}$$

The complementary energy is now minimized subject to the following equilibrium constraints

$$\mathbf{B}_{\mathrm{eq}}\mathbf{f} = \mathbf{t}, \tag{D15}$$

where $\mathbf{B}_{\mathrm{eq}}$ is introduced in (16). The minimization problem becomes:

$$\min_{\mathbf{f}} \left\{ F = \frac{1}{2}\mathbf{f}^{\mathrm{T}}\mathbf{M}^{00}\mathbf{f} + \mathbf{f}^{\mathrm{T}}\mathbf{b}_{\mathrm{th}}\Delta T \right\}, \tag{D16}$$

subject to constraints (D15). The term containing the specific heat is dropped, as it is independent of $\mathbf{f}$. Using the method of Lagrange multipliers, we add the constraints to the Lagrangian:

$$F = \frac{1}{2}\mathbf{f}^{\mathrm{T}}\mathbf{M}^{00}\mathbf{f} + \mathbf{f}^{\mathrm{T}}\mathbf{b}_{\mathrm{th}}\Delta T + \boldsymbol{\omega}^{\mathrm{T}}(\mathbf{B}_{\mathrm{eq}}\mathbf{f} - \mathbf{t}). \tag{D17}$$

The corresponding Euler-Lagrange equations are

$$\mathbf{M}^{00}\mathbf{f} + \mathbf{B}_{\mathrm{eq}}^{\mathrm{T}}\boldsymbol{\omega} = -\mathbf{b}_{\mathrm{th}}\Delta T, \tag{D18}$$

$$\mathbf{B}_{\mathrm{eq}}\mathbf{f} = \mathbf{t}, \tag{D19}$$

which are solved for vector $\mathbf{f}$, yielding

$$\mathbf{f} \equiv \mathbf{f}^0 = \mathbf{K}_{\mathrm{mech}}^0\mathbf{t} + \mathbf{k}_{\mathrm{th}}^0\Delta T, \tag{D20}$$

where

$$\mathbf{K}_{\mathrm{mech}}^0 = (\mathbf{M}^{00})^{-1}\mathbf{B}_{\mathrm{eq}}^{\mathrm{T}} \left(\mathbf{B}_{\mathrm{eq}}(\mathbf{M}^{00})^{-1}\mathbf{B}_{\mathrm{eq}}^{\mathrm{T}} \right)^{-1}, \tag{D21}$$

$$\mathbf{k}_{\mathrm{th}}^0 = -(\mathbf{M}^{00})^{-1}\mathbf{H}\,\mathbf{b}_{\mathrm{th}}, \tag{D22}$$

with matrix **H** defined in (68). Substitution of this into the expression for the complimentary energy (D12) and comparison with the corresponding terms in (88) leads to the effective thermoelastic properties of the laminate, which after some matrix manipulations obtain the following alternative forms:

$$\mathbf{S}^0 = t_0(\mathbf{K}^0_{\text{mech}})^{\text{T}}\mathbf{M}^{00}\mathbf{K}^0_{\text{mech}} = t_0\left(\mathbf{B}_{\text{eq}}(\mathbf{M}^{00})^{-1}\mathbf{B}^{\text{T}}_{\text{eq}}\right)^{-1}, \tag{D23}$$

$$\boldsymbol{\alpha}^0 = t_0(\mathbf{K}^0_{\text{mech}})^{\text{T}}\mathbf{b}_{\text{th}} = t_0\left(\mathbf{B}_{\text{eq}}(\mathbf{M}^{00})^{-1}\mathbf{B}^{\text{T}}_{\text{eq}}\right)^{-1}\mathbf{B}_{\text{eq}}(\mathbf{M}^{00})^{-1}\mathbf{b}_{\text{th}}, \tag{D24}$$

$$\frac{c^0_p}{T_0} = \frac{t_0\bar{c}_p}{T_0} + t_0(\mathbf{k}^0_{\text{th}})^{\text{T}}\mathbf{M}^{00}\mathbf{k}^0_{\text{th}} = \frac{t_0\bar{c}_p}{T_0} - t_0(\mathbf{k}^0_{\text{th}})^{\text{T}}\mathbf{b}_{\text{th}} = \frac{t_0\bar{c}_p}{T_0} + t_0\mathbf{b}^{\text{T}}_{\text{th}}(\mathbf{M}^{00})^{-1}\mathbf{H}\mathbf{b}_{\text{th}}, \tag{D25}$$

where $\mathbf{S}^0$ is the 6×6 compliance matrix $\mathbf{ABD}'$, and vector $\boldsymbol{\alpha}^0$ is a 6×1 vector of the effective in-plane thermal expansion coefficients and temperature induced curvatures per unit temperature change, $\boldsymbol{\alpha}^0 = \left[\alpha^0_1, \alpha^0_2\alpha^0_6, \kappa^0_1, \kappa^0_2, \kappa^0_6\right]^{\text{T}}$. The effective stiffness matrix **ABD** is then simply

$$\mathbf{ABD} = t_0^{-1}\mathbf{B}_{\text{eq}}(\mathbf{M}^{00})^{-1}\mathbf{B}^{\text{T}}_{\text{eq}}. \tag{D26}$$

The vector of stresses in an uncracked laminate $\mathbf{f}^0$ defined in (D20) has the same structure as for a cracked laminate and is expressed in terms of the same matrices $\mathbf{M}^{00}$ and $\mathbf{B}_{\text{eq}}$. The matrices (D21) and (D22) provide the stresses in all the plies of the uncracked laminate. Assembly of physical boundary conditions (43) and stress concentration matrices for calculation of the effective thermoelastic properties (93)-(95) of a cracked laminate, implies appending contributions from all the cracked plies. In other words, $\mathbf{K}_{\text{mech}}$ and $\mathbf{k}_{\text{th}}$ are formed by appending the rows of $\mathbf{K}^0_{\text{mech}}$ (D21) and $\mathbf{k}^0_{\text{th}}$ (D22) that correspond to $\mathbf{f}_\alpha$ and $\mathbf{f}_\beta$ of the cracked plies at the two ends of the fragment and zero rows for the derivatives of $\mathbf{f}_\alpha$ of any $N-1$ plies (the right hand side of (46)).